HEAT TRANSFER IN SMOOTH AND RIBBED RECTANGULAR TWO-PASS CHANNELS WITH A DEVELOPING FLOW ENTRANCE AT HIGH ROTATION NUMBERS

A Dissertation

by

MICHAEL HUH

Submitted to the Office of Graduate Studies of
Texas A&M University
in partial fulfillment of the requirements for the degree of

DOCTOR OF PHILOSOPHY

August 2009

Major Subject: Mechanical Engineering

HEAT TRANSFER IN SMOOTH AND RIBBED RECTANGULAR TWO-PASS CHANNELS WITH A DEVELOPING FLOW ENTRANCE AT HIGH ROTATION NUMBERS

A Dissertation

by

MICHAEL HUH

Submitted to the Office of Graduate Studies of
Texas A&M University
in partial fulfillment of the requirements for the degree of

DOCTOR OF PHILOSOPHY

Approved by:

Chair of Committee,	Je-Chin Han
Committee Members,	Sai Lau
	Hamn-Ching Chen
	Jorge Alvarado
Head of Department,	Dennis O'Neal

August 2009

Major Subject: Mechanical Engineering

ABSTRACT

Heat Transfer in Smooth and Ribbed Rectangular Two-Pass Channels with a Developing Flow Entrance at High Rotation Numbers. (August 2009)

Michael Huh, B.S., Texas Tech University;

M.S., The University of Texas at Arlington

Chair of Advisory Committee: Dr. Je-Chin Han

Cooling channels with a developing flow entrance condition and aspect ratios of 1:4 and 2:1 were studied. The range of the rotation number and buoyancy parameter for the selected AR channels was extended. The maximum Ro and Bo for the 1:4 channel was 0.67 and 1.9, respectively. For the 2:1 channel, these values were 0.45 and 0.85, respectively.

The effect of rib spacing and rib height on heat transfer in the 1:4 channel is investigated. Three rib spacing configurations were considered: P/e=2.5, 5, 10 with a constant e/D_h ratio of 0.078. To investigate the effect of rib height, a rib configuration with an e/D_h ratio of 0.156 and P/e ratio of 10 was considered. For the 2:1 channel, a smooth channel surface condition was studied. For each channel aspect ratio and surface condition, five Reynolds numbers were studied up to 40K. At each Re, five rotational speeds are considered up to 400 rpm.

The results of this research work indicate that rotation can cause a significant increase in heat transfer on the first pass trailing surface of both aspect ratio channels.

The leading surface in ribbed channels has shown a dramatic decrease in heat transfer with rotation in the first pass. Reductions in heat transfer by as much as 50% were observed. In the second pass, the leading and trailing surfaces with ribs showed very similar effects of rotation. Also, the effect of rotation seems to vary with the rib spacing. The strength of rotation showed to be greater in the tight rib spacing of P/e=2.5. The rib height in the 1:4 channel had minimal impact due to the large distance between the leading and trailing surfaces. The tip cap heat transfer for both channels showed large increases with rotation. This is very beneficial since tip cooling is an important part of maintaining the life a turbine blade. Finally, the buoyancy parameter proved to be very useful in predicting heat transfer in rotating conditions. The correlations developed showed very acceptable accuracy when compared to the experimental data.

DEDICATION

To my wife of 10 years, Christy; and my children, Ashley (9 yrs), Hayden (7 yrs), Paige (5 yrs), and Hannah (2 yrs)….the joys of my heart.

ACKNOWLEDGEMENTS

I'd like to thank Dr. Je-Chin Han for his guidance and for the opportunity to study in his group. Dr. S.C. Lau, Dr. Hamn-Ching Chen and Dr. Jorge Alvarado are also thanked for serving on my dissertation committee and for their time. Thanks also to my colleagues in the Turbine Heat Transfer Laboratory for their friendship and intellectual stimulation.

NOMENCLATURE

A_t	total heat transfer surface area for segment
A_p	projected surface area
A_h	total heater surface area
AR	channel aspect ratio, W:H
Bo_x	local buoyancy parameter, $(\Delta\rho/\rho_{b,x})Ro^2(R_x/D_h)$
c_p	specific heat at constant pressure
D_h	channel hydraulic diameter
e	rib height
H	channel height
h	regionally averaged heat transfer coefficient
i	designates a given region in the channel ($1 \leq i \leq 12$)
I	current
k	thermal conductivity of the coolant
L	length of the heated portion of the test section
m	mass flow rate
Nu	regionally averaged Nusselt number
Nu_s	stationary regionally averaged Nusselt number
Nu_o	Nusselt number for fully-developed turbulent flow in non-rotating smooth pipe
P	rib pitch
Pr	Prandtl number of the coolant

Q_{net}	net heat transfer
Q_{loss}	external heat loss
R	mean radius of rotation
R_x	local radius of rotation
Re	Reynolds number
Ro	Rotation number, $\Omega D_h/U_b$
$T_{w,x}$	regionally averaged wall temperature
$T_{b,x}$	local coolant bulk temperature
$T_{f,x}$	local film temperature
$T_{b,in}$	bulk fluid temperature at inlet of a given region
$T_{b,out}$	bulk fluid temperature at outlet of a given region
U_b	bulk velocity in streamwise direction
V	voltage
W	channel width
β	angle of channel orientation with respect to the axis of rotation
μ	viscosity of the coolant
$\rho_{b,x}$	local density of air based on local bulk air temperature
$\rho_{w,x}$	local density of air based on local wall temperature
$\Delta\rho/\rho_{b,x}$	local bulk-to-wall density ratio ($\Delta\rho=\rho_{b,x}$ -$\rho_{w,x}$)
Ω	rotational speed

TABLE OF CONTENTS

Page

Page

LIST OF FIGURES

FIGURE Page

FIGURE Page

FIGURE Page

FIGURE Page

LIST OF TABLES

1. INTRODUCTION

1.1 Internal Cooling Techniques for Gas Turbine Blades

The applications for gas turbines range from land based power generation to aircraft engines (commercial and military) to the oil and gas industry. Clearly, the efficiency and power production of gas turbines has a strong implication in many different areas. Numerous research studies have been conducted by industry, government agencies, and universities over the past several decades to improve the design of gas turbines with respect to heat transfer. As hot gases from the combustor pass over the blade, heat is transferred from the hot gases to the blade external surface and is then conducted through the blade wall. In the internal cooling channels, cooler air bled from the compressor stage, is circulated as to remove heat from the blade surface. Thus, high heat transfer on the walls of internal cooling channels is desirable. If insufficient heat is removed, the blade could be thermally stressed and possibly fracture.

The ability to increase the turbine inlet temperatures, which in turn increases efficiency and power, is partially due to the turbine blade cooling techniques developed through research. From **Figure 1,** it is seen that different heat transfer enhancement techniques are used for different portions of the gas turbine blade. In the internal cooling channel at the leading edge of the blade, jet impingement cooling is used. In the mid-portions of the blade, angled ribs are used to break the boundary layer and create angled secondary flows. Finally at the trailing edge of the blade, pin fin cooling is used. It is

---

This dissertation follows the style of ASME Journal of Heat Transfer.

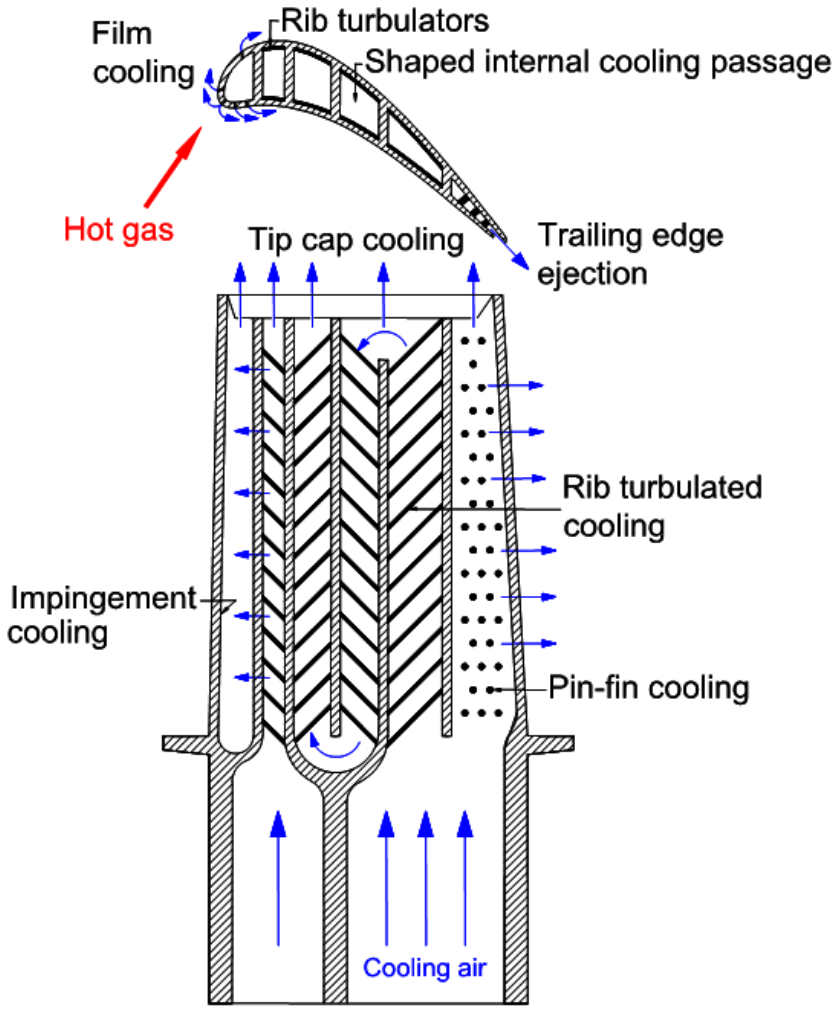

Figure 1: Typical heat transfer enhancement techniques for gas turbine blades.

also important to note that the internal cooling air is expelled or ejected through film cooling holes to the blade external surface. At the leading edge a shower head scheme provides maximum cooling for the blade. During rotation, some flow leaks over the blade tip and high velocities are experienced due to the clearance gap between the blade tip and turbine casing. Tip ejection is used to cool the blade tip. At the trailing edge, slot ejection is used to provide cooling. Han et al. [1] provides details of the different cooling techniques for gas turbine blades and vanes. The interested reader is encouraged to review that work.

1.2 Literature Review

1.2.1 Aspect Ratio Effects

Figure 2 shows that the cross-section of the internal cooling channels varies from the leading edge to the trailing edge of the gas turbine blade. Depending on the location of the internal cooling channel, the channel may be simulated by various geometrical cross-sections. The leading edge cooling passage of the gas turbine blade is typically modeled with equilateral triangular shaped channels. Near the leading edge of the blade, the internal cooling channel has a narrow aspect ratio (i.e. suction and pressure surfaces are separated by a large distance). Rectangular channels with an aspect ratio (AR=W/H) of 1:4 and 1:2 are used to simulate these channels. In the mid portions of the blade, the internal cooling channel is nearly square, thus channels with AR=1:1 are used to model this region of the gas turbine blade. Finally, near the trailing edge of the blade, the internal cooling channel has a wide aspect ratio (i.e. suction and pressure surfaces are separated by a short distance). Rectangular channels with AR= 2:1 and 4:1 or wedge

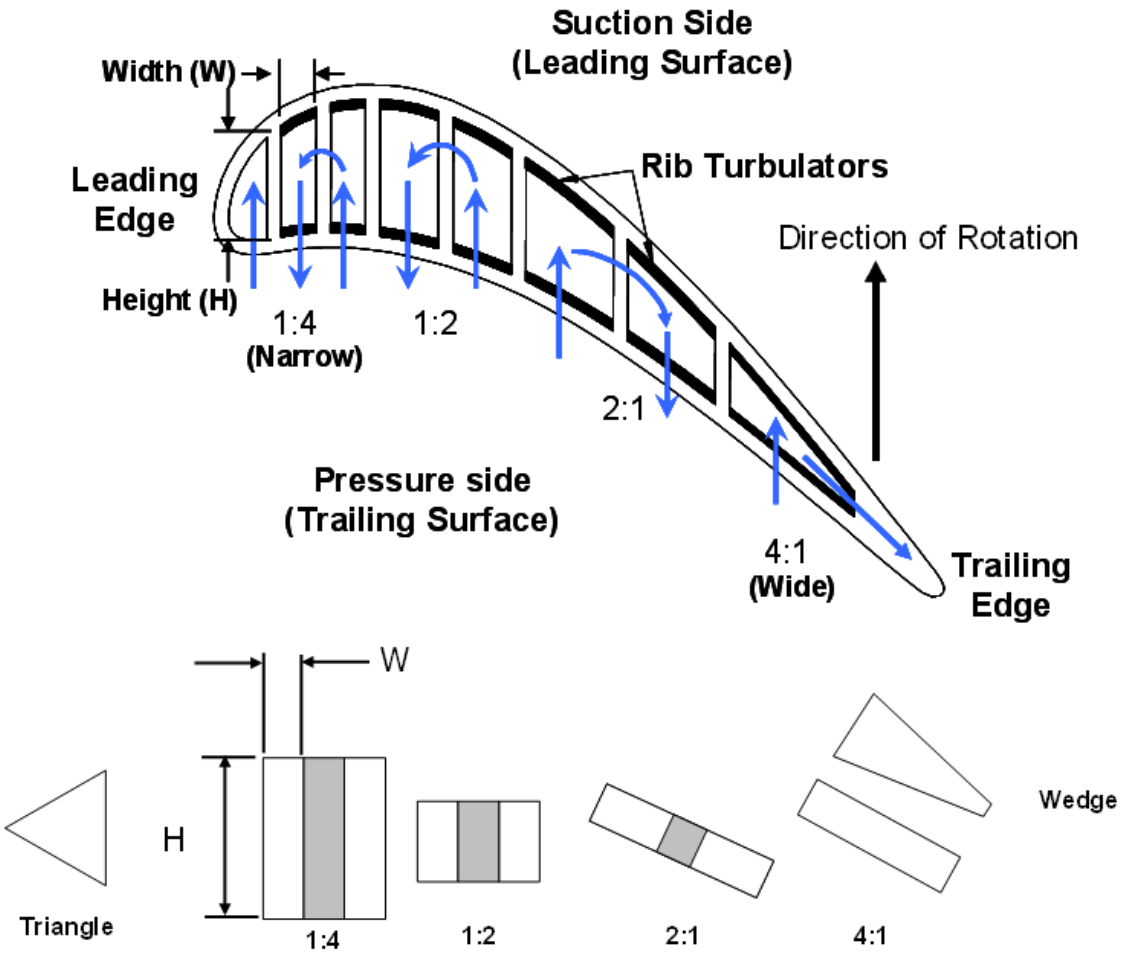

Figure 2: Geometries used in the simulation of gas turbine blade internal cooling channels.

shaped channels are used to model these cooling channels.

It has been shown that the heat transfer and fluid flow characteristics are dependent on the channel aspect ratio. Several studies, under stationary conditions, have been performed in order to understand how heat transfer varies in the different aspect ratio channels with smooth and ribbed walls. Han [2] studied the effect of the channel aspect ratio on heat transfer for five different channel aspect ratios (AR=1:4, 1:2, 1:1, 2:1, 4:1). He concluded that the local heat transfer in the narrow aspect ratio channel is higher than the wide aspect ratio channel. Han and Park [3] studied heat transfer performance in ribbed channels with aspect ratios of AR=1:1, 2:1, and 4:1. Heat transfer performance takes into consideration both heat transfer enhancement and the pressure drop. They concluded that the square channel (AR =1:1) provided better heat transfer performance than the wide aspect ratio channels (AR=2:1, 4:1). Park et al. [4] studied heat transfer and pressure drop in five different aspect ratio channels (AR=1:4, 1:2, 1:1, 2:1, and 4:1) with a rib angle of 60^{o}. The results showed that the pressure penalty was drastically different in each channel. The pressure drop increased between 2- to 18-times as the aspect ratio of the channel changed from narrow (AR=1:4) to wide (AR=4:1). They concluded that narrow aspect ratio channels provide a better heat transfer performance compared to wide aspect ratio channels.

1.2.2 Rotation Number Effects

One drawback to the stationary experiments is that the effects of the Coriolis and rotation induced buoyancy forces, which occur under rotating conditions in a heated channel, are not present. The flow field is strongly affected by rotation and thereby the

heat transfer. Guidez [5] studied a smooth duct with an aspect ratio of 1:2. In his study, the rotation number reached was 0.2 at a Reynolds number of 17,000. He showed that for radially outward flow, the Coriolis force induces secondary flows in a plane perpendicular to the mainstream flow. He showed that the trailing surface heat transfer increased with the rotation number while the leading surface heat transfer decreased. He attributed these effects to the distorted velocity and temperature profiles achieved under rotating conditions.

Around the same time period, Wagner et al. [6] studied a four pass smooth square channel model. The rotation number reached in their study was 0.48 at a Reynolds number of 25,000. Initially, only results for the radially outward flow (first pass) were presented. They showed that the trailing surface heat transfer increased significantly (3.5 times) as the rotation number increased. They postulated that the Coriolis force accelerates the cooler mainstream flow towards the trailing surface. The leading surface heat transfer initially decreased as the rotation number increased, and then began to increase with further increases in the rotation number. Thus, they had observed that a critical rotation number existed after which heat transfer trends changed on the leading surface. This change was attributed to the development of large scale Coriolis generated secondary flow cells that circulate along the passage length.

Later, Wagner et al. [7] presented results for the radially inward flow condition of the second pass. They showed that the leading surface heat transfer increased with the rotation number by approximately 50% over the stationary case. The trailing surface heat

transfer decreased by up to 30% as the rotation number increased. They noted that with a radially inward flow condition, the direction of the Coriolis force is reversed.

Johnson et al. [8] utilized the same experimental test section as Wagner et al. [6, 7] except with ribs. In their study, ribs were placed at an angle of 45^{o} to the mainstream flow on the leading and trailing surfaces. For the radially outward flow condition (first pass), heat transfer trends were similar to the smooth case; the leading surface heat transfer decreased with the rotation number while the trailing surface heat transfer increased with the rotation number. However, for the radially inward flow condition, the effect of the rotation number was not nearly as strong as in the smooth channel. Both the leading and trailing surfaces had similar levels of heat transfer. This was attributed to the secondary flow of the angled ribs.

Liou and Chen [9] performed an experimental heat transfer study in a smooth 5:4 aspect ratio channel using aluminum plates and thermocouples. They also measured the flow velocity profile with a Laser Doppler Velocimetry (LDV) system. The rotation number in their study was 0.44 at a Reynolds number of 5,000. They showed that in the first pass with radially outward flow, the velocity profile was skewed. Azad et al. [10] and Al-Hadhrami et al. [11] performed rotating experiments in a two-pass 2:1 ribbed channel with rotation numbers up to 0.11 at a Reynolds number of 10,000. The results from Azad et al. [10] and Al-Hadhrami et al. [11], confirmed the work of Wagner et al. [6, 7] with respect to the heat transfer characteristics of the leading and trailing surfaces in both the first and second pass.

Zhou et al. [12] studied a 4:1 aspect ratio channel with a rotation number of 0.6 at a Reynolds number of 10,000. They concluded that on the destabilized surfaces in the first passage (trailing) and second passage (leading), rotation enhances the heat transfer up to a certain Ro, beyond which the enhancement is flat or reduced. Fu et al. [13, 14] performed experiments in ribbed channels with AR=1:4, 1:2, 1:1, 2:1 and 4:1. The rotation number in their study was 0.15 at a Reynolds number of 10,000. They showed that for the 1:4 aspect ratio channel, the heat transfer for both the leading and trailing surface in the second pass (radially inward flow) was similar under rotating conditions. The heat transfer increased with an increase in the rotation number.

1.2.3 Sharp Turn Effects

In a gas turbine blade, a sharp 180^{o} turn is used to connect the first pass channel to the second pass channel. In the turn region, secondary flows are generated due to the turn geometry. This secondary flow augments the heat transfer, especially at the first part of the second passage. Han et al. [15] investigated heat/mass transfer around a sharp turn in a stationary smooth square channel. They showed that the mass transfer in the turn and after turn was much greater than before the turn. This was attributed to the secondary flow generated by the centrifugal force at the turn. In the same study previously mentioned that Liou et al.. [9] performed, they also investigated the 180º turn effects. They showed that the unsteadiness of separation bubbles downstream of the sharp turn significantly augments the heat transfer in the first part of the second passage. Liou et al. [16] also used LDV to measure the turbulent flow field inside a rotating two-pass square duct. The flow field and the kinetic energy distribution near the 180° turn

were measured. The rotation number was varied from 0.0 to 0.2. They concluded that as the rotation number is increased, the turbulence intensity level increases exponentially. The increased turbulence intensity then enhances the heat transfer in the turn region.

1.2.4 Entrance Effects

Many of the previous studies considered a fully developed entrance condition. However, in a gas turbine blade, the flow may be in the developing state, depending on the ratio of the channel length to channel hydraulic diameter. It is well known that heat transfer behavior is different for fully developed flow when compared to flow in the entrance region.

Kays and Crawford [17] reviewed the work of Boelter et al. [18]. They showed that the entrance length was dependent on the entrance geometry. They noted that the Nusselt number for a sudden contraction entrance was much greater than a fully developed entrance. Han [2], Han & Park [3], and Park et al. [4] considered various aspect ratio channels. These studies showed that Nusselt number decreases in streamwise direction from the entrance and reaches a constant value. In ribbed channels, the Nusselt number reached a fully developed value after approximately a distance of three hydraulic diameters down from entrance. Liou & Hwang [19] found that the first 12-18% of channel length is affected by entrance.

More recently, Wright et al. [20] performed experiments in channels with three different entrance geometries. They concluded that the entrance condition will enhance the heat transfer. They also pointed out that the effect of the entrance weakens as the rotation number increases. The influence of the entrance geometry also is stronger in the

smooth channel when compared to the ribbed channel. Wright et al. [21] showed that an entrance contraction will enhance heat transfer near the entry region of the channel.

1.2.5 Rib Spacing Effects

Not only is heat transfer enhanced by the entrance effect, but also by the ribs which are cast on the blade walls. Many considerations need to be taken into account before proceeding to include ribs in a turbine blade internal cooling channel design. One important question, among many, is how far apart should the ribs be placed apart? Generally speaking, as the mainstream flow enters an internal cooling channel, the hydrodynamic boundary layer begins to develop as a direct result of viscosity. Allowing the free growth of the boundary layer results in a decrease in the heat transfer until the boundary layers merge and the inviscid core is eliminated.

Adding ribs to the blade internal cooling channel wall, then serves two purposes. The first is to break the boundary layer. As the mainstream flow approaches a rib, the flow separates from the surface and reattaches at a location between the ribs. The distance between ribs (the rib pitch, P) then is an important parameter to consider. Placing the ribs to close together can possibly jeopardize this reattachment zone where high heat transfer is experienced due to mainstream flow impingement. If the ribs are placed to far apart, the boundary layer will possibly grow too much and thus reduce heat transfer. The second reason to include ribs in a blade design is to create secondary flows that develop as a result of the rib angle. This rib induced secondary flow further increases heat transfer and turbulence mixing. Warm fluid in contact with the hot blade wall is removed by the secondary flow and replaced with cooler mainstream flow.

Initially, studies considered orthogonal ribs. Han et al. [22] studied five rib pitch-to-rib height ratios (P/e) of 5, 7.5, 10, 15, 20 in a 12:1 aspect ratio stationary channel. Han [23] considered a square channel with P/e ratios of 10, 20 and 40. Han [2] considered five different aspect ratio channels AR=1:4, 1:2, 1:1, 2:1 and 4:1 with P/e ratios of 10 and 20. These studies all showed that the best heat transfer was obtained at a P/e ratio of 10. Later Taslim & Wadsworth [24] studied a square channel with P/e ratios of 5, 7.5, 8.5, & 10. In their study the P/e = 8.5 ratio produced the highest heat transfer coefficient. More recently, Liu et al. [25] studied the rib spacing in a 1:2 aspect ratio channel under rotating conditions. They considered four P/e ratios: 3, 5, 7.5, 10. They showed that the Nusselt number increases as P/e decreases. However, the friction factor also increases with decreasing P/e ratio until a P/e ratio of 5. As the P/e ratio further decreased to 3, the friction factor was reduced. Thus, the P/e=3 case showed the best thermal performance.

1.2.6 Rib Height Effects

The ratio of the rib height-to-channel hydraulic diameter (e/D_h) is also an important factor to consider. Han [23] considered three blockage ratios of 0.021, 0.042, and 0.063 in a square channel. He showed that as the blockage ratio increases, the friction factor and the Stanton number increase. Taslim et al. [26] also studied a square channel with three high blockage ratios of 0.133, 0.25, and 0.333. They showed that as the blockage ratio increases the Nusselt number (for fixed Re) increased due to higher level of mixing of air inside the passage. Later Taslim and Spring [27] studied numerous blockage ratios ranging from 0.15 to 0.285 in a 1:2 aspect ratio channel. They concluded

that as the blockage ratio increases, the sensitivity of the Nusselt number on P/e will decrease. Taslim and Lengkong [28] studied a square channel with blockage ratios of 0.133, 0.167 and 0.25. Their results indicated that the thermal performance decreases as the blockage ratio increases due to the increased frictional losses. More recently, Casarsa et al. [29] showed that in their square channel with $e/D_h = 0.30$ a strong acceleration of the flow over ribs occurred due to the reduced cross-section. Bailey and Bunker [30] considered an aspect ratio of 1:2.5 with three blockage ratios of 0.193, 0.263, and 0.333. They showed that heat transfer enhancement and friction increase with the blockage ratio.

1.3 Objectives

The previously reviewed studies clearly show that the aspect ratio, rotation number, entrance geometry, and rib configuration (P/e and e/D_h) have an impact on the heat transfer distribution in the internal cooling channel. Up to this point, only limited research has been presented for rotating channels at high rotation numbers, particularly in 1:4 and 2:1 aspect ratio channels. Fu et al. [13, 14] presented data for a 1:4 channel but the rotation number was limited to 0.15. Their study considered a fully developed flow at the entrance. Azad et al. [10] and Al-Hadhrami et al. [11] presented results for an AR = 2:1 channel, but the rotation number was only 0.1. These two studies also considered a fully developed flow. Extending the range of the rotation number and buoyancy parameter for both of these aspect ratio internal cooling channels is important. By extending the range of these two relevant parameters, correlations can be developed thereby showing that Ro and Bo are useful for predicating heat transfer in rotating

channels. In order to model the AR = 1:4 and AR = 2:1 channels more like a gas turbine blade, the entrance design of the 1:4 aspect ratio channel and the 2:1 aspect ratio channel will provide a developing flow entrance condition. Including ribs on the pressure and suction inner walls of the gas turbine blade has been shown to increase heat transfer. However, detailed investigations on the rib configuration (P/e and e/D_h) is lacking for the 1:4 aspect ratio channel under rotating conditions. This study will provide a detailed investigation on the effects ribs on heat transfer in the 1:4 aspect ratio channels. In summary, the objectives of the current study are:

1. Extend the range of the rotation number and buoyancy parameter in the 1:4 and 2:1 aspect ratio channels. The target Ro and Bo parameter for the 1:4 AR channel is 0.67 and 1.9 respectively. For the 2:1 aspect ratio channel, the target Ro and Bo parameter are 0.45 and 0.80, respectively.
2. Determine the effects that the high rotation number and buoyancy parameter have on heat transfer in both smooth and rib roughened leading and trailing surfaces in the first and second pass of the 1:4 and 2:1 AR channels.
3. Provide new information on the effects of the high rotation number on heat transfer in the tip portion of the 1:4 and 2:1 aspect ratio channels.
4. Develop correlations to predict the heat transfer enhancement in the 1:4 and 2:1 aspect ratio channels using Bo.

5. Investigate the effects of the inlet geometry (re-directed sharp bend) on heat transfer with both smooth and rib roughened surfaces in the 1:4 aspect ratio channel. A sharp bend entrance, that turns the flow 90^o twice, prior to entering the heated region of the test channel, is used to create a developing flow region in the first pass. A sudden expansion entrance from a circular cross-section to a rectangular channel is used for the 2:1 aspect ratio channel.
6. Investigate the effects of rib pitch-to-rib height ratio (P/e) and rib height-to-channel hydraulic diameter ratio (e/D_h) on the heat transfer coefficient in a two pass 1:4 aspect ratio channel. To accomplish this task, three rib spacing configurations are considered: P/e = 2.5, 5, and 10 with a constant e/D_h ratio of 0.078. To investigate the effect of rib height, a rib configuration with an e/D_h ratio of 0.156 and P/e ratio of 10 is considered. A smooth channel surface condition is also studied and serves as a reference. For the 2:1 channel, a smooth channel surface condition is studied. The angle of the ribs in all experiments involving ribs is held constant at 45^o.

2. EXPERIMENTAL SETUP

Typical rotation numbers for aircraft engines are near 0.25 with Reynolds numbers in the range of 50,000. One method to achieve similar conditions for the large rotation number in the laboratory is to use air at high pressures. As the pressure of the air increases so will the density. For a fixed mass flow rate and hydraulic diameter, an increase in density will result in a decrease in velocity. A lower velocity will in turn increase the rotation number. In order to achieve larger rotation numbers at higher Reynolds numbers, the experiments for the present study are conducted with air at a pressure of 620 kPa-abs (90 psia). In this study, the rotation number is controlled by varying the rotational speed and the flow velocity. **Figure 3** provides an overview of the flow Reynolds number, rotational speeds, and the corresponding rotation numbers and buoyancy parameters achieved in this study for both the 1:4 and 2:1 aspect ratio channels. It is worth noting that the maximum rotation numbers for the AR = 2:1 channel is lower that the 1:4 AR channel due to the decreased hydraulic diameter of the test section.

2.1 Rotating Facility

Figure 4 shows the rotating arm assembly used to conduct the experiments for the current study. A steel table is used as the support structure. A 25 hp electric motor is used to drive the shaft which in turn spins the arm. Counterweights, located opposite of the test section housing, are used to balance the arm so that minimal vibrations are

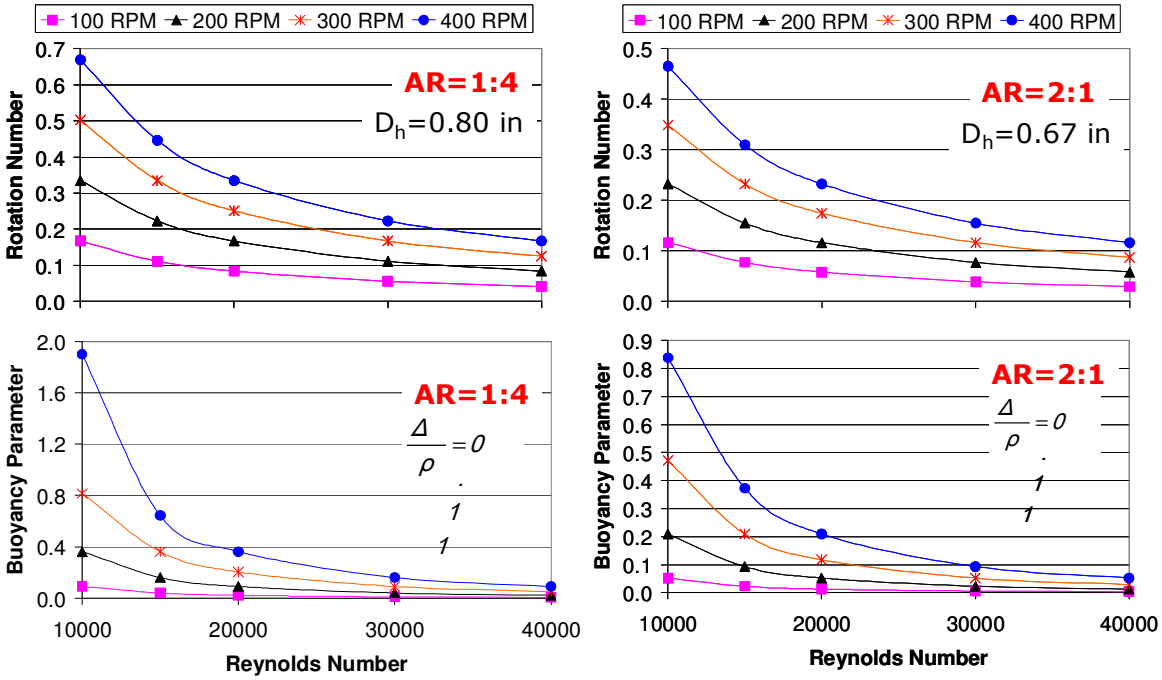

Figure 3: Buoyancy parameters and rotation numbers at various combinations of Reynolds number and rotational speeds for the 1:4 and 2:1 aspect ratio internal cooling channels.

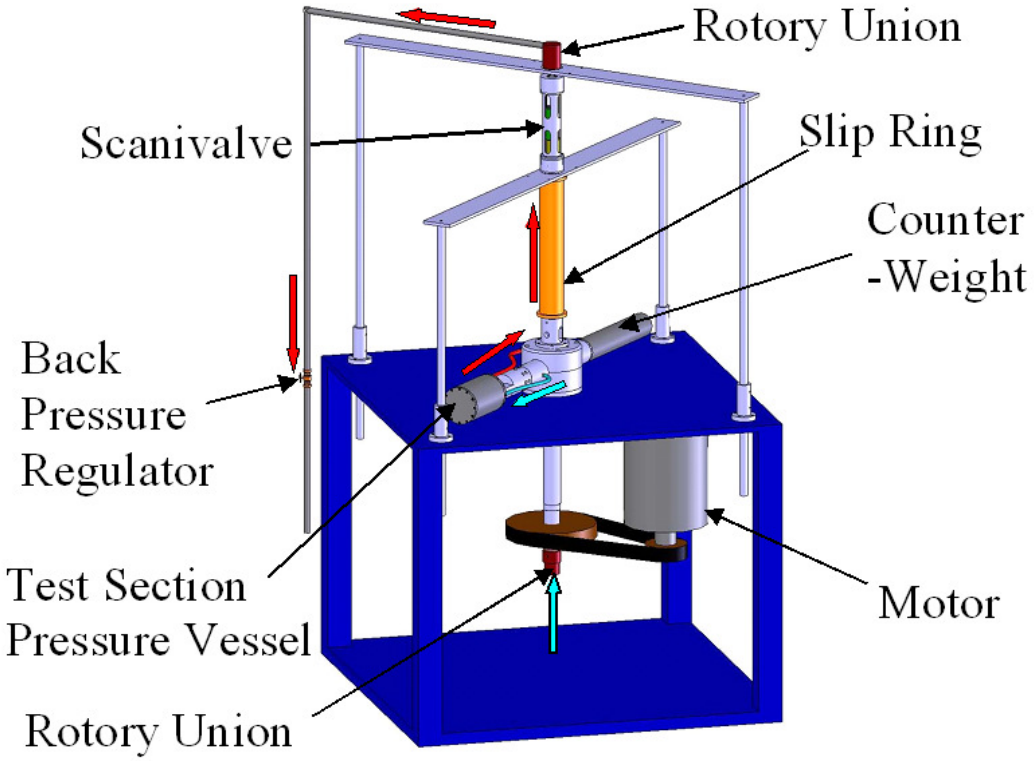

Figure 4: Rotating arm assembly used for performing rotating heat transfer experiments.

experienced during rotation. The air from the compressor enters an ASME square-edge orifice meter (not shown) where the mass flow rate is measured. Air enters the rotating assembly at the bottom of the shaft via a rotary union. The air then passes through the hub and into the bore of the arm. A rubber hose is used to direct the flow from the arm to the test section housing. After the air flows through the test section, it exits the housing. The hot exhaust air is then directed, by means of a rubber hose, to the slip ring. A ½-inch copper tube, which passes through the bore of the slip ring, is used to direct the air to the top rotary union. Steel pipe is connected to the top rotary union and a valve is used to adjust the back pressure of the system.

2.2 Data Acquisition

Signals from the 37 thermocouples that were installed in the test section, pass through the 100 channel slip ring. The thermocouple wires from the slip ring stationary side, are connected to two 32 channel (National Instruments) NI SCXI-1303 modules. These modules are coupled with two 32 channel NI SCXI-1102 thermocouple amplifiers that are housed in NI SCXI-1000 chassis. The chassis passes data to a LabView program where temperature measurements are displayed. The program collects data at a rate of 100 scans/sec. Temperatures are recorded when steady state is achieved. Steady state is considered to have been reached once all temperature changes are less than 0.5 ^{o}C per hour.

2.3 Test Section AR = 1:4

For the present study, the both test sections (AR=1:4 and AR=2:1) were oriented 90^{o} to the direction of rotation. The test section consists of two passes. The flow in the

first passage is radially outward, and after a 180º turn, the flow is radially inward. These two passes are separated by an inner wall with a thickness of 11.95 mm.

The entrance geometry with a re-directed sharp bend sudden contraction is shown in **Figure 5**. The air passes through a 9.525 mm diameter inlet hose and enters the curved plenum region. After direct impingement on the plenum region, the flow is turned 90^{o} twice before entering the heated portion of the test section. This entrance design provides a developing hydrodynamic boundary layer due to a sudden contraction. A screen is placed prior to the first copper plate region of the test section to help spread the flow at the entrance and thus provide a more uniform velocity profile at the inlet. The wire diameter of the screen is 0.015 mm.

A nylon substrate, with a low thermal conductivity, is used to support the copper plates and heaters. Brass screws are used to attach the copper plates to the nylon test section. Between each copper plate is a strip of insulation material which prevents conduction between copper plates and also helps to create a smooth surface between adjacent copper plates. The thickness of all copper plates is 3.175 mm. The copper plates on the leading and trailing walls are rectangular in shape and measure 23.81 mm x 11.11 mm. The outer and inner wall copper plates are square and measure 23.81 mm x 23.81 mm. The tip copper plates are rectangular with dimensions of 23.81 mm x 17.46 mm.

The flow channel height (distance between leading and trailing) is 50.8 mm and has a width of 12.70 mm, resulting in a hydraulic diameter (D_h) of 20.32 mm as seen in **Figure 6.** The minimum thickness of the inner wall is 5.60 mm.

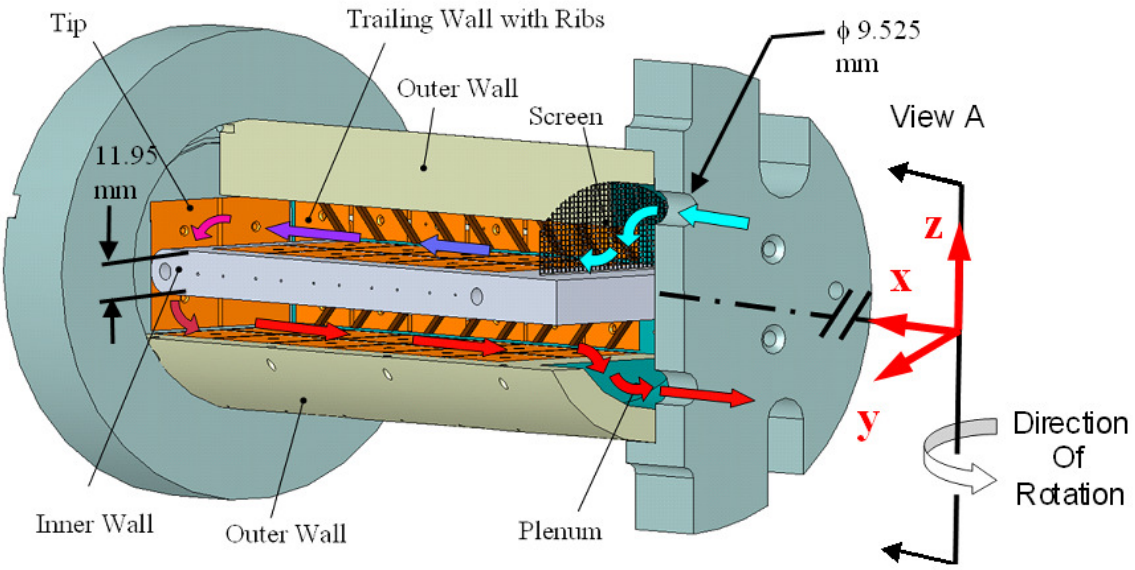

Figure 5: Drawing showing the flow channel geometry of the 1:4 aspect ratio test section.

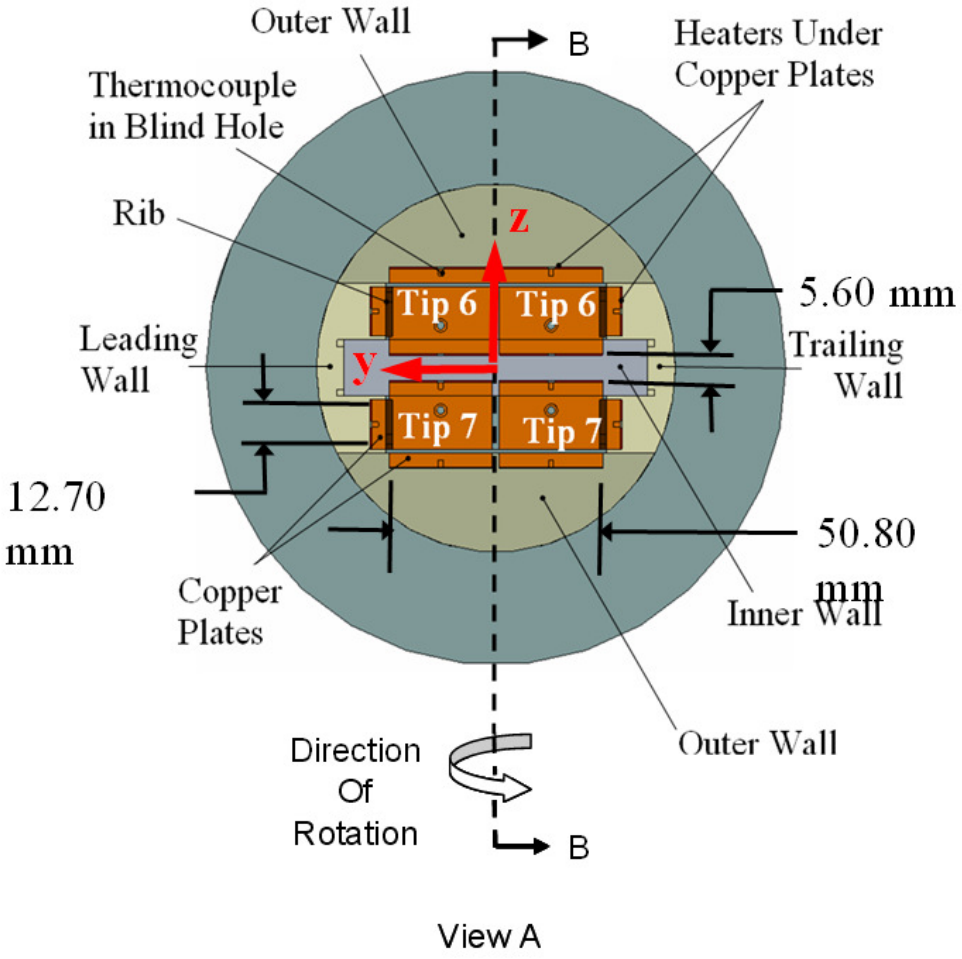

Figure 6: Test section (1:4) tip view showing location of heaters and wall naming convention.

As the air passes through the test section, it is heated using pre-fabricated silicone rubber heaters that are placed beneath the copper plates. A total of 12 heaters are used for the outer, inner, leading and trailing walls. An additional heater is used for the tip. Thermally conductive paste is used between the heaters and the copper plates in order to reduce contact resistance. Blind holes, with a diameter of 1.59 mm, are drilled 1.59 mm deep on the backside of each copper plate. Thermocouples are placed inside of the blind holes of the copper plates and are affixed to the copper plates using highly conductive epoxy.

Figure 7 shows that each passage is divided into six regions. There are a total of twelve regions in the test section. The overall test section length is 190.50 mm. The heated channel length of each passage is 154.50 mm and the plenum length is 19.05 mm. One thermocouple is placed at the inlet to measure the air temperature as it enters the test section. At the exit of the test section, two thermocouples are used to measure the air temperature. Temperature measurements were taken on all of the leading, trailing and tip cap copper plates, resulting in a subtotal of 28 thermocouples. On the outer and inner walls, only the temperatures of the copper plates at regions four and ten were measured due to limited slip ring channels giving a subtotal of 8 thermocouples measurements. Thus, a total of 36 thermocouple measurements are made on the heated walls of the test section.

Figure 8 shows details of the smooth and rib roughened surface of the test section. In all rib roughened experiments, the brass ribs were placed on the leading and trailing walls of both passes in a parallel configuration. A very thin layer of thermally

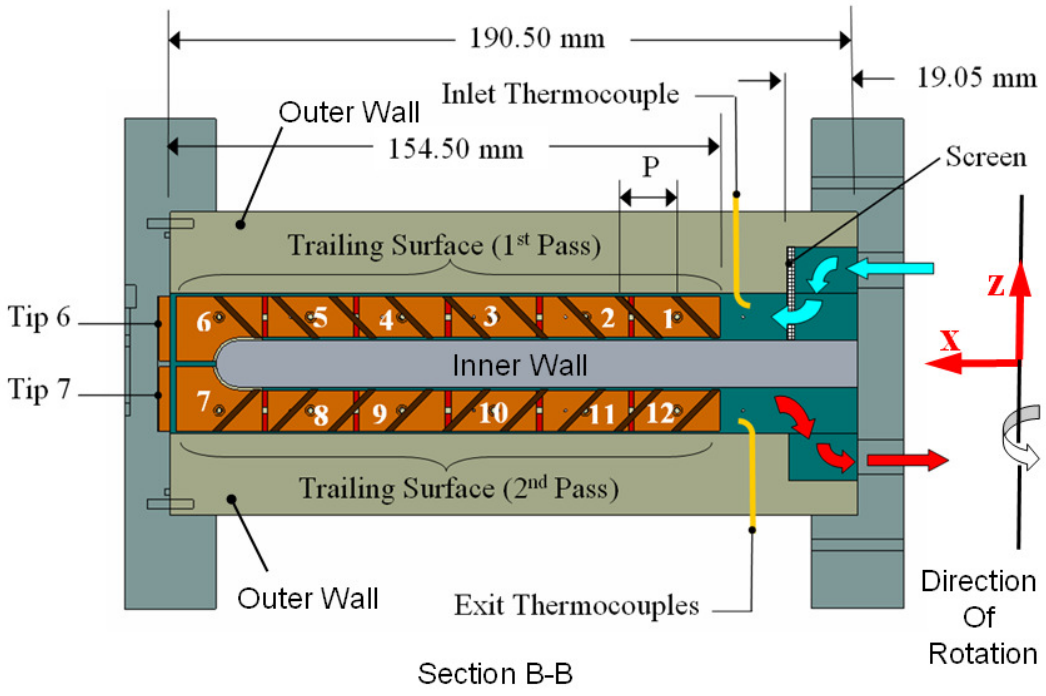

Figure 7: Test section (1:4) view showing the copper plate region numbering convention.

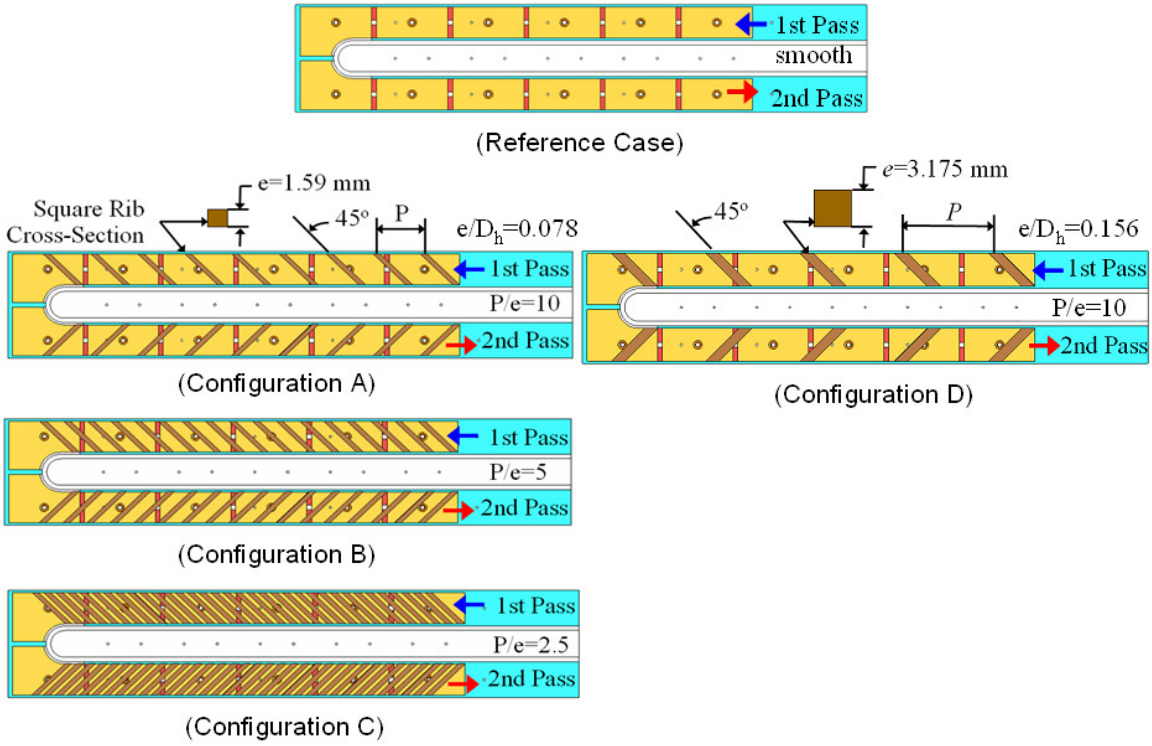

Figure 8: Surface conditions for the 1:4 aspect ratio channel.

conductive glue is used to affix the ribs to the surface of the copper plates. The ribs are placed at a 45^{o} angle relative to the mainstream flow. In order to investigate the effect of rib spacing, three different rib pitch-to-rib height (P/e) ratios were tested: P/e = 2.5, 5, and 10. For those experiments the ribs had a square cross-section measuring 1.59 mm x 1.59 mm. The blockage ratio (e/D_h) is held constant and for this rib height $e/D_h = 0.078$. In order to determine the effects of the rib height an additional rib configuration is considered as seen in **Figure 8.** Configuration D also utilizes ribs with a square cross-section but the rib height is doubled compared to the three other rib configurations (A, B, and C). For configuration D, the rib height is 3.175 mm, resulting in a rib blockage ratio of $e/D_h = 0.156$. The rib pitch-to-rib height (P/e) ratio is 10.

2.4 Test Section AR=2:1

The 2:1 aspect ratio test section, with a sudden expansion entrance, is shown in **Figure 9**. The test section consists of two passes. The flow in the first passage is radially outward, and after a 180º turn, the flow is radially inward in the second pass. The air enters the test section through a 9.525 mm diameter circular inlet hose and then expands to the rectangular cross- section of the test section passage shown in **Figure 10**. Two screens were placed prior to the first copper plate region of the test section, to help spread the flow at the entrance. The wire diameter of the screen is 0.015 mm. A nylon substrate, with a low thermal conductivity, is used to support the copper plates and heaters. Between each copper plate is a strip of insulation material which prevents conduction between copper plates and also helps to create a smooth surface between adjacent copper plates. The copper plates on the leading and trailing walls are square in

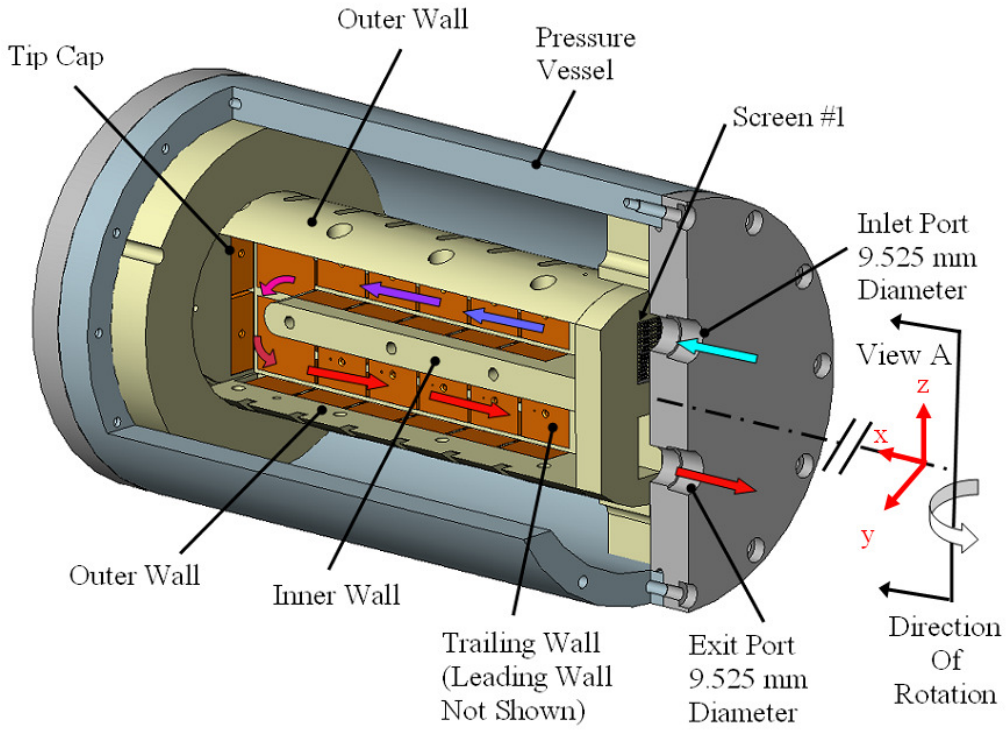

Figure 9**:** Drawing showing the flow channel geometry of the 2:1 aspect ratio test section.

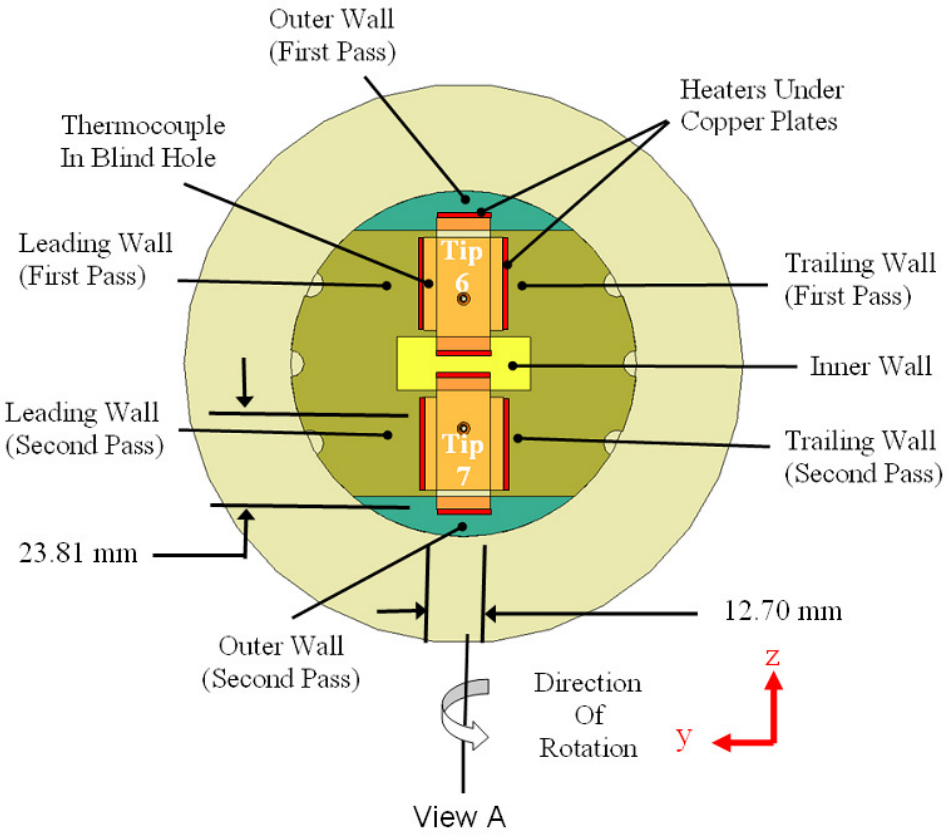

Figure 10**:** Test section (2:1) tip view showing location of heaters and wall naming convention.

shape and measure 23.81 mm x 23.81 mm. The outer and inner wall copper plates are rectangular and measure 23.81 mm x 12.70 mm. The tip copper plates are rectangular with dimensions of 29.37 mm x 12.70 mm. The thickness of all copper plates is 3.175 mm. The flow channel height (H) is defined as the distance between the leading and trailing surfaces. The channel in this study had a height of 12.70 mm and a width (W) of 23.81 mm, resulting in a hydraulic diameter (D_h) of 16.93 mm.

As the air passes through the test section, it is heated using pre-fabricated heaters that are placed beneath the copper plates as can be seen in **Figure 10**. A total of 9 heaters are used for the outer, inner, leading and trailing walls. An additional heater is used for the tip. Thermally conductive paste is used between the heaters and the copper plates in order to reduce contact resistance. Blind holes, with a diameter of 1.59 mm, are drilled 1.59 mm deep on the backside of each copper plate. Thermocouples are placed inside of the blind holes of the copper plates and are affixed to the copper plates using highly conductive epoxy.

There are a total of twelve regions in the test section. Each passage consists of six regions as shown in **Figure 11**. The overall length of each passage is 203.0 mm. The heated channel length of each passage is 157.0 mm and the unheated entrance length is 46.0 mm. One thermocouple is placed at the inlet to measure the air temperature as it enters the test section. At the exit of the test section, two thermocouples are used to measure the air temperature. Temperature measurements were made on all of the leading, trailing, outer, inner and tip cap copper plates. Thus, a total of 48 temperature measurements were made from copper plates. **Figure 12** shows the surface conditions

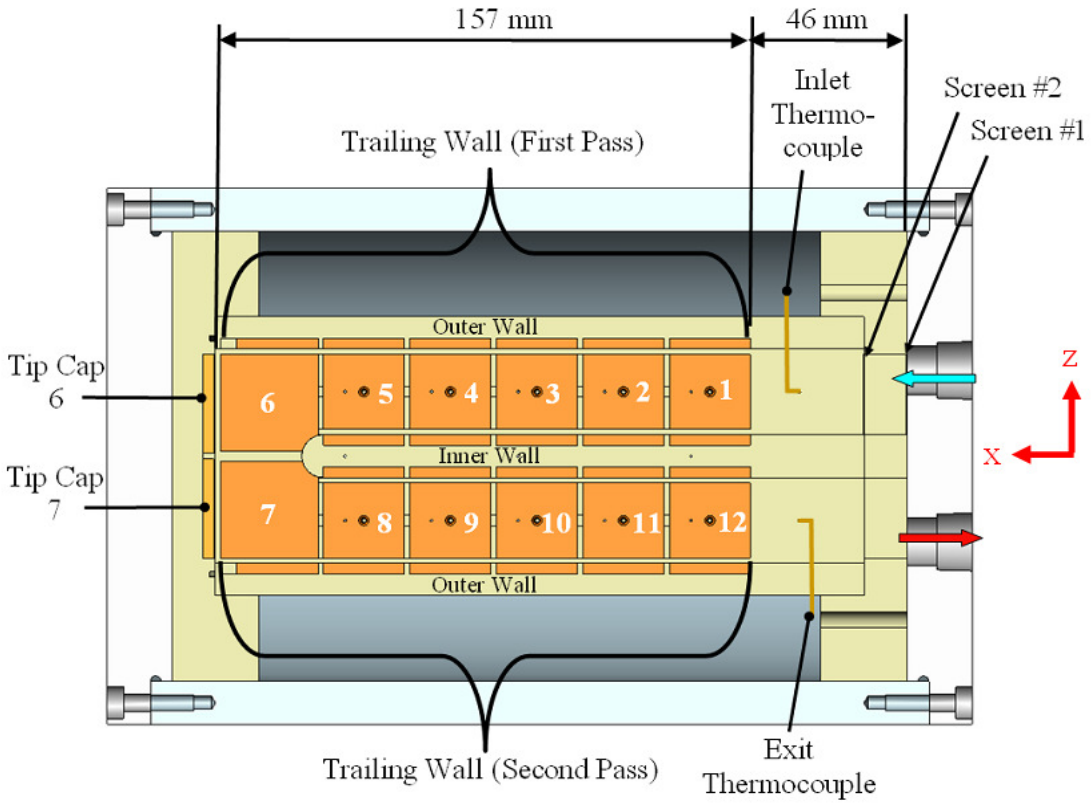

Figure 11: Test section (2:1) view showing the copper plate region numbering convention.

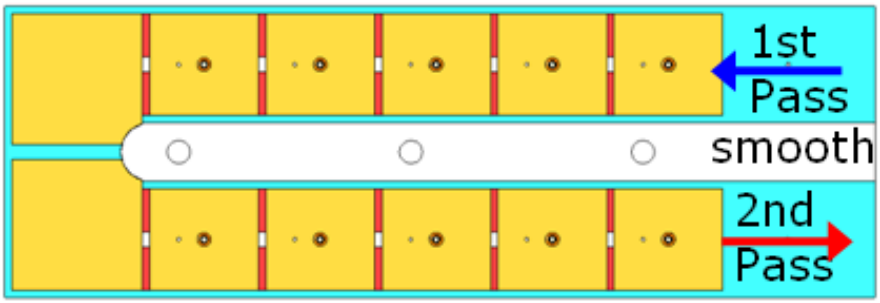

Figure 12**:** Surface conditions for the 2:1 aspect ratio channel**.**

tested in the 2:1 aspect ratio channel. A smooth surface condition is studied.

2.5 Testing Matrix

An exhaustive testing matrix is undertaken. A total of six cases were considered. These were: (AR=1:4) smooth, ribbed configurations A, B, C, D; (AR=2:1) smooth. The air pressure was maintained at 620 kPa-abs (90 psia) for all cases studied. For each case, the Reynolds numbers tested were 10000, 15000, 20000, 30000, and 40000. At each Reynolds number, the rotational speed was varied from 0 to 400 rpm with an increment of 100 rpm. The testing matrix is summarized in **Table 1**.

Table 1**:** Testing Matrix for Current Study

Aspect Ratio	**Surface Condition**		**Rotational Speed (RPM) for Each Surface Condition**	**Reynolds Number for Each Rotational Speed**
1:4	Smooth	Ribbed (α=45^o)	0, 100, 200, 300, 400	10K, 15K, 20K, 30K, 40K
		P/e=2.5, 5, 10 (e/D_h=0.078) P/e=10 (e/D_h=0.156)		
2:1	Smooth			

3. DATA REDUCTION

The experimental test sections used in this study utilizes copper plate segments with thermocouples placed in a blind hole that is drilled to a depth equal to one-half of the plate thickness. Since the copper plate segments are relatively thin (3.175 mm) and copper has a high thermal conductivity (W/mK), the typical Biot number for a copper plate segment is much smaller than unity. With this, the temperature of a given copper plate segment is expected to be uniform throughout. Thus, it is assumed that the temperature reading from the thermocouple is equal to the surface temperature of the copper plate segment. The thermocouple measurement reading is then referred to as a regionally averaged wall temperature measurement.

As such, this study investigates the regionally averaged convection heat transfer coefficient (h) at various locations within a rotating duct. A constant heat flux wall boundary condition is used in the experiments. During the experiments, a wall temperature of 65°C in the circumferential direction is maintained on all copper plate segments at regions 4 and 10 by supplying the proper amount of power to the heaters. The density ratio, based on the wall temperature (65 °C) and the temperature of the air at the inlet (23 ^{o}C), is 0.11.

3.1 Heat Transfer Coefficient

In the current study, the regionally averaged heat transfer coefficient (h) is calculated from Newton's law of cooling by considering the net heat transferred to the air from the heated copper plate segment (Q_{net}), the total heat transfer surface area (A_t = smooth area between ribs plus the area of 3 rib sides) for each copper plate segment, the

regionally averaged wall temperature of the copper plate ($T_{w,x}$), and the local bulk mean temperature of the air flowing in the channel ($T_{b,x}$). Therefore, the regionally averaged convection heat transfer coefficient is given as

$$h = \frac{Q_{net}}{A_t\left(T_{w,x} - T_{b,x}\right)} \tag{1}$$

The net heat transfer is calculated as

$$Q_{net} = \left(V \cdot I\right)\left(\frac{A_p}{A_{heater}}\right) - Q_{loss} \tag{2}$$

The voltage (V) is measured with a multi-meter and the current (I) is supplied to each heater by variac transformers. The power input to each heater is multiplied by the ratio of the copper plate segment projected heat transfer area (A_p) to the total heater area (A_{heater}).

In order to determine the external heat losses for a given copper plate segment (Q_{loss}) escaping from the test section during the experiment, two heat loss calibration tests are performed. In the first heat loss calibration test, the proper amount of power is supplied to the heaters so that the temperatures of all copper plate segments in regions 4 and 10 are at a temperature of 50 ^{o}C. Similarly, a second heat loss calibration test is performed at a temperature of 75 ^{o}C. During the heat loss calibration tests, the wall temperature is maintained by supplying power to each heater with the variac transformers. A successful heat loss calibration test is achieved when the total power input to the test section reaches equilibrium with the environment (i.e. the wall temperature reaches a steady state condition). The heat loss which occurs during the

experiment is then determined by interpolating between the two sets of heat loss data. It is noted that heat loss calibration tests were performed at all rotational speed conditions considered in the present study and the stationary case as well. In order to minimize natural convection effects during the heat loss calibration tests, an insulating material was placed inside of the flow channel.

One thermocouple at the inlet of the test section and two thermocouples at the outlet of the test section measure the inlet and outlet bulk air temperatures, respectively. The bulk air temperature at any location in the test section can be calculated using linear interpolation. The results presented in this study are based on the linear interpolation method.

Although linear interpolation was chosen for determining the air temperature at various locations in the channel, the bulk air temperature can also be calculated using the conservation of energy principle. For the present study, both methods compare very well. The energy balance shown in equation (3) can be used to determine the regional average bulk air temperature. For a given region i ($1 \le i \le 12$) the energy balance equation is:

$$\sum_{i} Q_{net} = \dot{m} c_p \left(T_{b,out,i} - T_{b,in,i} \right) \tag{3}$$

In equation (3), the left side term is the summation of the net heat transferred to the air, from all surfaces (leading, trailing, inner, and outer walls) at region *i*. The mass flow rate of air passing through the region is $\dot{m}$ and c_p is the specific heat at constant pressure. Also in equation (3), $T_{b,in,i}$ is the bulk air temperature at the inlet of region *i*

and $T_{b,out,i}$ is the bulk air temperature at the exit of region *i*. Solving for $T_{b,out,i}$ in equation (3) yields

$$T_{b,out,i} = T_{b,in,i} + \frac{\sum_{i} Q_{net}}{\dot{m} c_p} \tag{4}$$

Thus, for the first region at the channel inlet (region i=1), $T_{b,in,1}$ is the actual measured temperature of the air using the channel inlet thermocouple. Heat is added to the air in region i=1 from all four walls. This results in a bulk air temperature increase at the exit of region i=1. At the exit of region i=1, the bulk air temperature is $T_{b,out,1}$ which is also the inlet temperature for region i=2, $T_{b,in,2}$. The local bulk air temperature $T_{b,x}$ in region i is then determined as the average of $T_{b,in,i}$ and $T_{b,out,i}$ from equation (5)

$$T_{b,x} = \frac{T_{b,out,i} + T_{b,in,i}}{2} \tag{5}$$

3.2 Nusselt Number Ratios

The Nusselt number for fully developed turbulent flow through a smooth stationary pipe (Nu_o) is calculated by equation (6) and is known as the Dittus-Boelter/McAdams correlation for heating.

$$Nu_o = 0.023 \cdot Re^{0.8} \cdot Pr^{0.4} \tag{6}$$

Equation (6) is used in this study to provide a basis of comparison. Therefore, the heat transfer enhancement (Nu/Nu_o) is given as:

$$Nu/Nu_o = \left(\frac{hD_h}{k_{air}} \right) \left(\frac{1}{0.023 \cdot Re^{0.8} \cdot Pr^{0.4}} \right) \tag{7}$$

where Nu is the regionally averaged Nusselt number based on the regionally averaged convection heat transfer coefficient h. Thus, the term Nu is obtained experimentally and is either the stationary Nusselt number or the Nusselt number from rotating experiments. All air properties are taken based on the channel averaged bulk air temperature with a Prandtl number (Pr) for air of 0.71.

3.3 Rotating Parameters

Rotation causes a difference in the heat transfer between the leading and trailing walls as mentioned previously. The effect of rotation is evaluated by the rotation number (Ro). The rotation number is defined as the ratio of the Coriolis force to the inertial force {Han et al. [1]} as shown in equation (8)

$$\mathrm{Ro} = \frac{\Omega D_h}{U_b} \tag{8}$$

The combined effect of rotation and temperature difference is evaluated by the local buoyancy parameter (Bo_x). For the radial outward flow in the first pass, the inertial force is in the same direction as the centrifugal force. The centrifugal force opposes the inertial force in the second pass because the flow direction is reversed. The buoyancy parameter, as defined by Wagner et al. [6, 7], is used to present the combined effects of the Coriolis and rotation induced buoyancy forces.

$$\mathrm{Bo}_x = \left(\frac{\Delta\rho}{\rho_{b,x}}\right)(\mathrm{Ro})^2\left(\frac{R_x}{D_h}\right) \tag{9}$$

This local buoyancy parameter can be re-written by incorporating the measured wall and bulk air temperatures as shown in equation (10).

$$Bo_x = \left(\frac{T_{w,x} - T_{b,x}}{T_{w,x}} \right) (Ro)^2 \left(\frac{R_x}{D_h} \right) \tag{10}$$

In the current study, to more accurately determine the local buoyancy parameter, the local wall temperature in the denominator of equation (10) is replaced by the local film temperature ($T_{f,x}$). The local film temperature is the average of the local wall and the local bulk temperatures as shown in equation (11).

$$T_{f,x} = (T_{w,x} + T_{b,x})/2 \tag{11}$$

3.4 Uncertainty

An uncertainty analysis was performed based on the method described by Kline and McClintock [31]. The estimated uncertainty for the temperature instrumentation is 0.5°C. The uncertainty of the Nu/Nu_o ratio is approximately 6% for the highest Reynolds number. For the lowest Reynolds number (Re=10000), the maximum uncertainty is approximately 10%.

4. RESULTS AND DISCUSSION

4.1 Heat Transfer in Smooth and Ribbed 1:4 Aspect Ratio Channels

4.1.1 Smooth Surface

4.1.1.1 *Stationary Nusselt Numbers and Entrance Geometry Effects*

Before explaining the rotating results, the stationary flow behavior inside the channel needs to be discussed. The cooling air enters the plenum and then is re-directed into the 1:4 test section. This re-directed sharp bend entrance significantly alters the heat transfer, especially in the regions near the plenum. **Figure 13** shows the stationary Nusselt number (Nu_s) in the in the different regions. The data for the fully developed turbulent flow in a smooth circular tube (Nu_o) is also plotted for comparison. The non-dimensional Nusselt number is chosen to study the heat transfer enhancement. The results are the average of the leading and trailing surfaces only.

Near the entry region of the channel, the Nusselt number is higher than the fully developed flow case in the smooth tube. It decreases along the streamwise direction from region 1 to region 4 as shown in **Figure 13(a)**. In **Figure 13(b)** and **Figure 13(c)**, the regions near the 180° turn portion are shown. The direct impingement in the tip region produces the highest Nusselt number.

In the second pass as shown in **Figure 13(d)**, although the stationary Nusselt number is still higher than the smooth tube, the magnitude of the heat transfer enhancement is smaller than the first pass and the turn region. The difference between

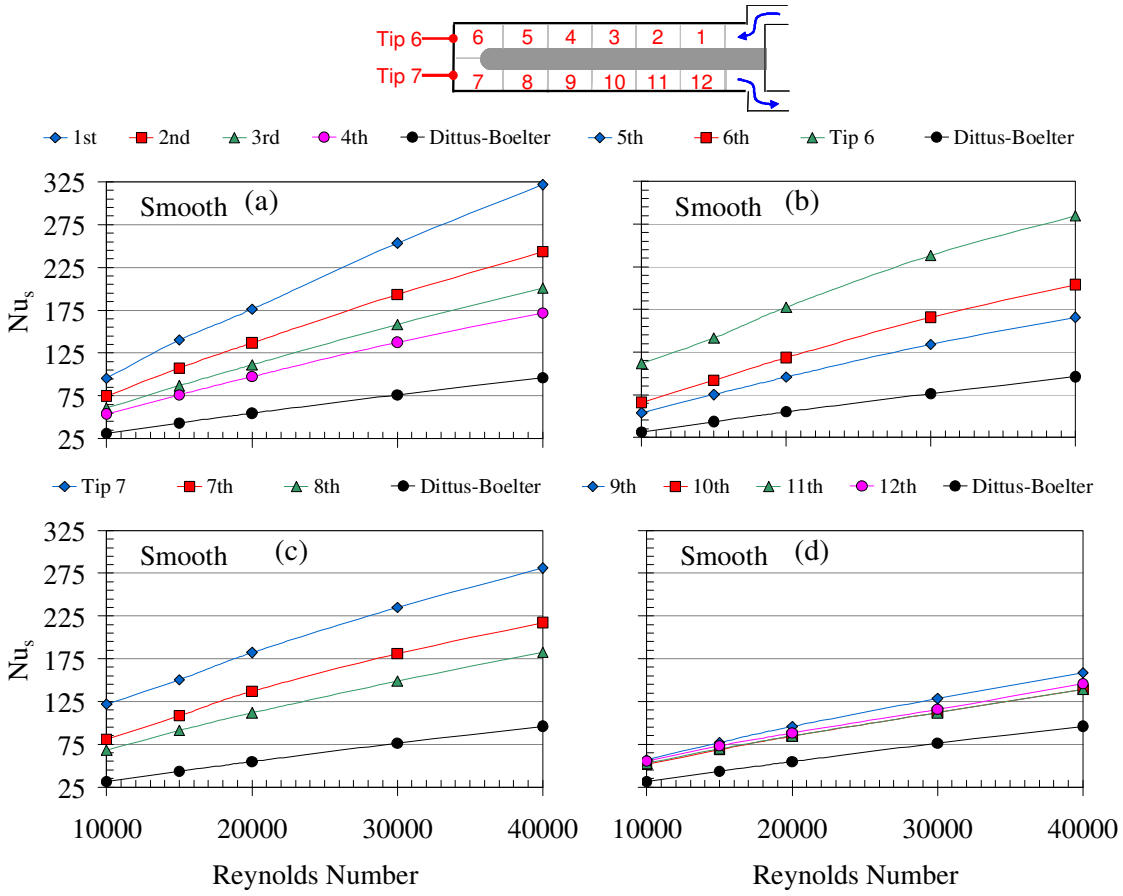

Figure 13: Stationary Nusselt number distribution in each region of the 1:4 smooth channel.

the four regions is also smaller which indicates that the flow is approaching the fully developed condition.

Figure 14 shows the Nu ratio comparisons inside the stationary channel from several open literature sources. The Nu ratio has been considered in order to eliminate the Reynolds number effects. Only the first few points of the current study, in the first passage with the re-directed sharp bend, are compared to eliminate the effects from the 180° turn. The sharp-bend geometry presented by Kays et al.. [32] in the circular tube and the re-direction partial sudden contraction geometry by Wright et al.. [20] in the 4:1 channel clearly show that the entrance geometry significantly augments the Nu ratio, especially when x/D_h is small. The fully-developed flow inside a 1:4 stationary channel by Fu et al.. [14] shows the lowest Nu ratio. As x/D_h increases, the Nu ratios of the four curves converge along the streamwise direction. The flow does not achieve the fully-developed flow behavior in the first passage because the passage is short (L/D_h=7.6).

4.1.1.2 *Rotating Streamwise Nusselt Number Ratios*

When there is no rotation, Coriolis and rotation induced buoyancy forces are not present, and thus the flow can be considered to be symmetric. Heat transfer enhancement is therefore similar on the leading and trailing surfaces in each respective passage. As the Reynolds number increases, the magnitude of the heat transfer (Nu) will increase, however the magnitude of the enhancement (Nu/Nu_o) decreases because a ratio is being considered. The conceptual view of the rotation induced secondary flow in a smooth channel is shown in **Figure 15(a)**. In the first passage, the rotation induced secondary flow impinges onto the trailing surface, and the rotation induced centrifugal

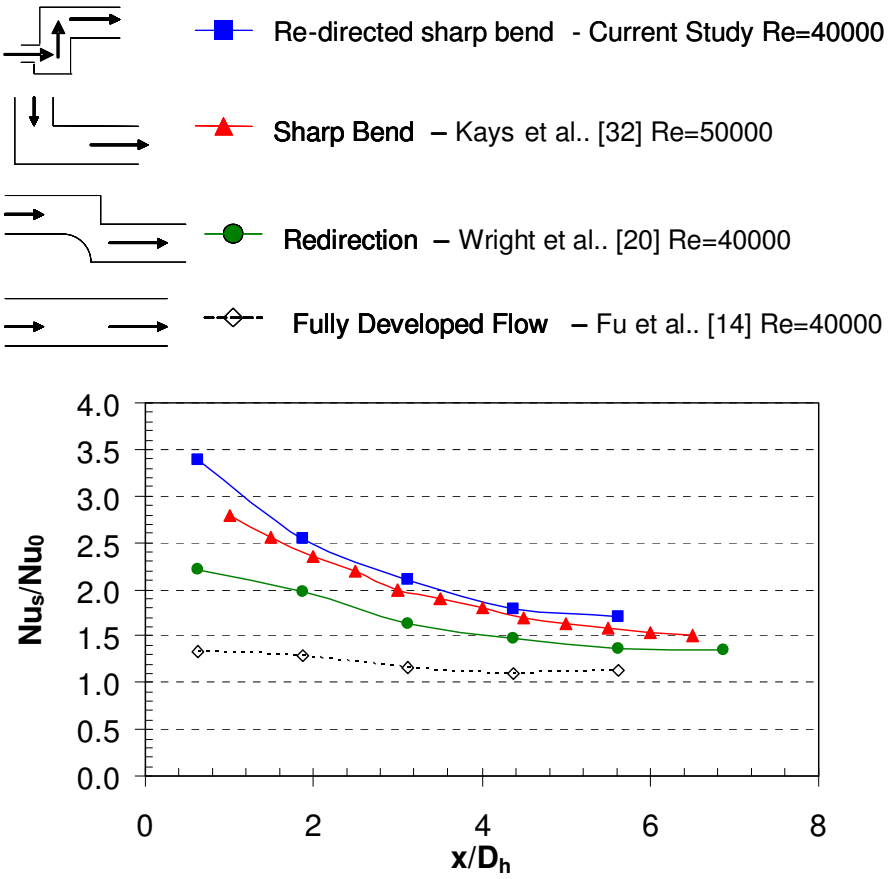

Figure 14: Comparisons of entrance geometries in the smooth 1:4 channel.

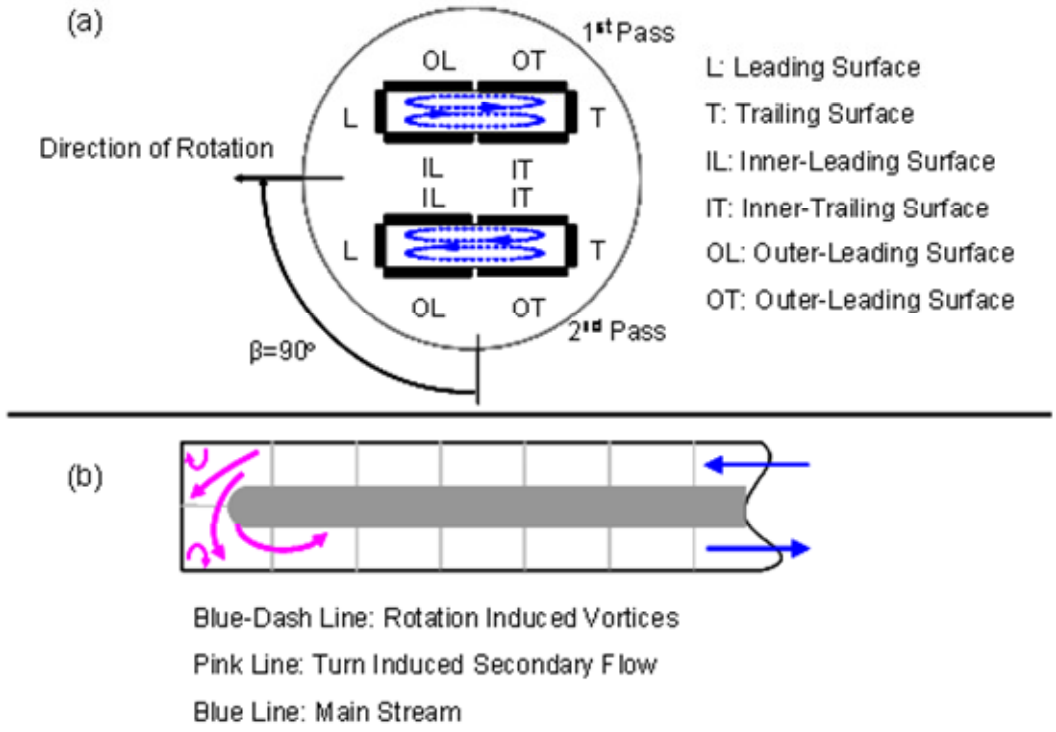

Figure 15: Conceptual view of (a) rotation induced secondary flow inside a two-passage rectangular channel (AR=1:4), (b) turn induced secondary flow.

force further thins the boundary layer on the trailing surface. In the second passage, the Coriolis force changes direction, due to radially inward flow, and impingement occurs on the leading surface. This secondary flow behavior has been predicted by the Su et al.. [33].

In general, in the first passage, the heat transfer enhancement begins to decrease due to the boundary layer growth along the streamwise direction. At the turn region, the heat transfer enhancement increases because of the turn induced secondary flow as shown in **Figure 15(b)**. The main flow impinges onto the tip. As the flow is redirected into the second passage, the flow impinges on the outer wall. Small vortices develop in the corner regions of the turn. The flow separates on the inner wall in the second passage near the turn region, but reattaches further downstream. In the second passage, the boundary layer begins to grow once again, and thus the heat transfer decreases in the streamwise direction.

The regionally averaged Nusselt number ratio (Nu/Nu_o) distribution in the streamwise direction of the smooth two-pass 1:4 aspect ratio flow channel is shown in **Figure 16**. At constant rotational speed, increasing the Reynolds number will decrease the effect of rotation. The heat transfer enhancement is greater on the trailing surface in the first passage under rotating conditions when compared to the stationary case. This is due to the combined effect of the rotation induced buoyancy forces, bulk inertia force and the Coriolis force. As the rotation number decreases, the enhancement begins to approach the stationary case because the bulk inertia force is increasing, and thus reducing the effects of rotation. From **Figure 16**, it is seen that the heat transfer

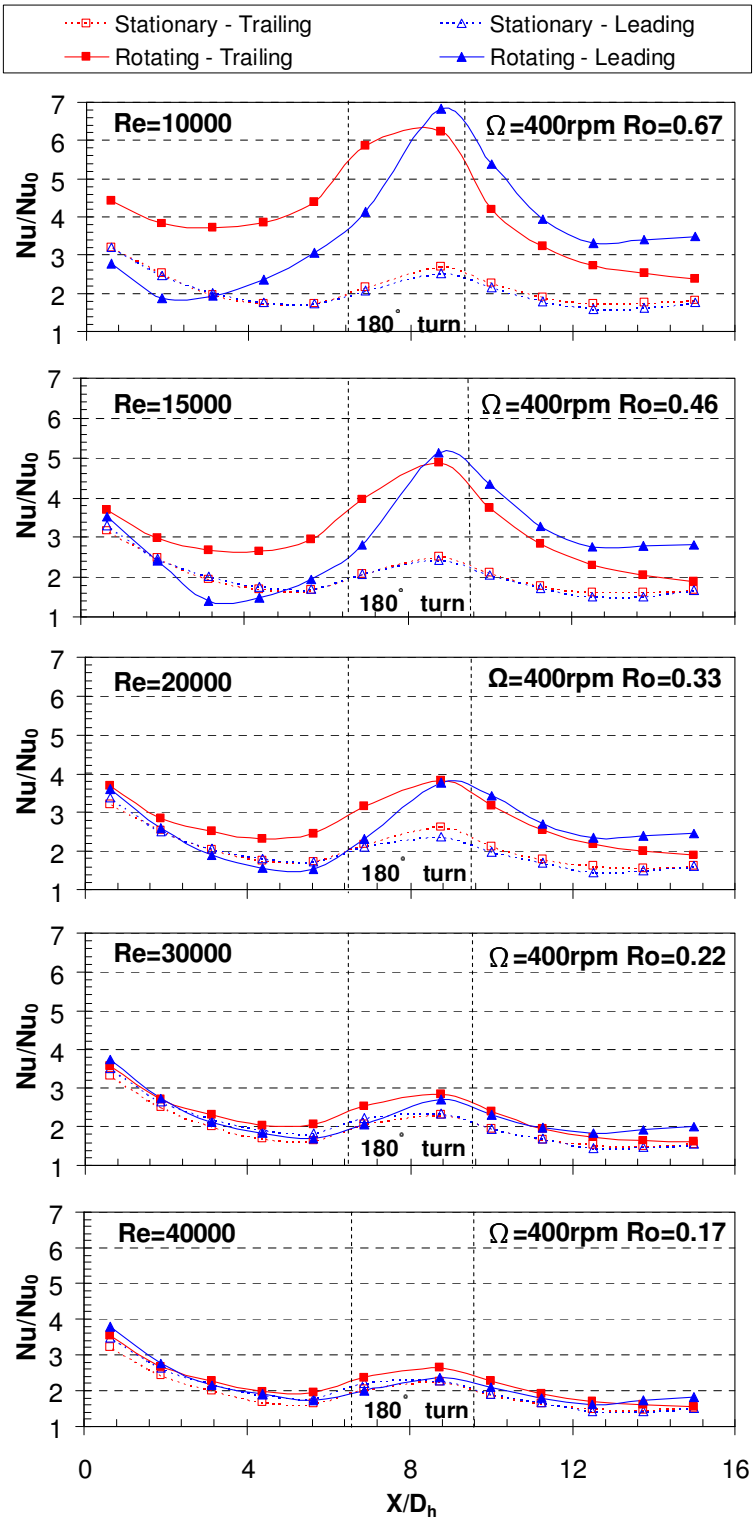

Figure 16: 1:4 Smooth streamwise Nu ratio distribution at different Reynolds numbers.

enhancement at the entrance is large. The large enhancement is due to a strong entrance effect. In the first passage, at a Reynolds number of 10000, it is seen that the enhancement near the entrance, on the leading surface, is lower for the rotating case when compared to the stationary case. This is due to the coolant being shifted towards the trailing surface. In the turn region, at a rotation number of 0.67, the Nu ratio reaches a maximum of 6.8, which is 2-3 times more than the stationary case. In the second passage, at low Reynolds numbers and under rotating conditions, the leading surface heat transfer enhancement is greater than the trailing. This is because the flow is radially inward and thus the rotation induced secondary flow impinges onto the leading surface. The cooler core flow is shifted towards the leading surface due to the Coriolis forces. However, both the leading and trailing surfaces in the second passage under rotation have higher Nu ratios than the stationary case.

Figure 17 shows the heat transfer enhancement at various rotational speeds at a Reynolds number of 10000 and 20000. The effect of increasing the rotational speed is observed. The effect of rotation near the entrance, on the leading surface is clearly shown in **Figure 17**. At a Reynolds number of 10000, as the rotation number increases, it is seen that the effect of rotation becomes stronger than the entrance effect. The leading surface exhibits degradation (decrease below the stationary case) at smaller x/D_h values with increasing rotation number. This behavior has been observed in a square channel by Wagner et al.. [6, 7]. For example, at a rotation number of 0.34, degradation begins to occur at an x/D_h greater than 4.375. For a rotation number of 0.67, degradation occurs at x/D_h=1.875. However, at a Reynolds number of 20000, near the entrance

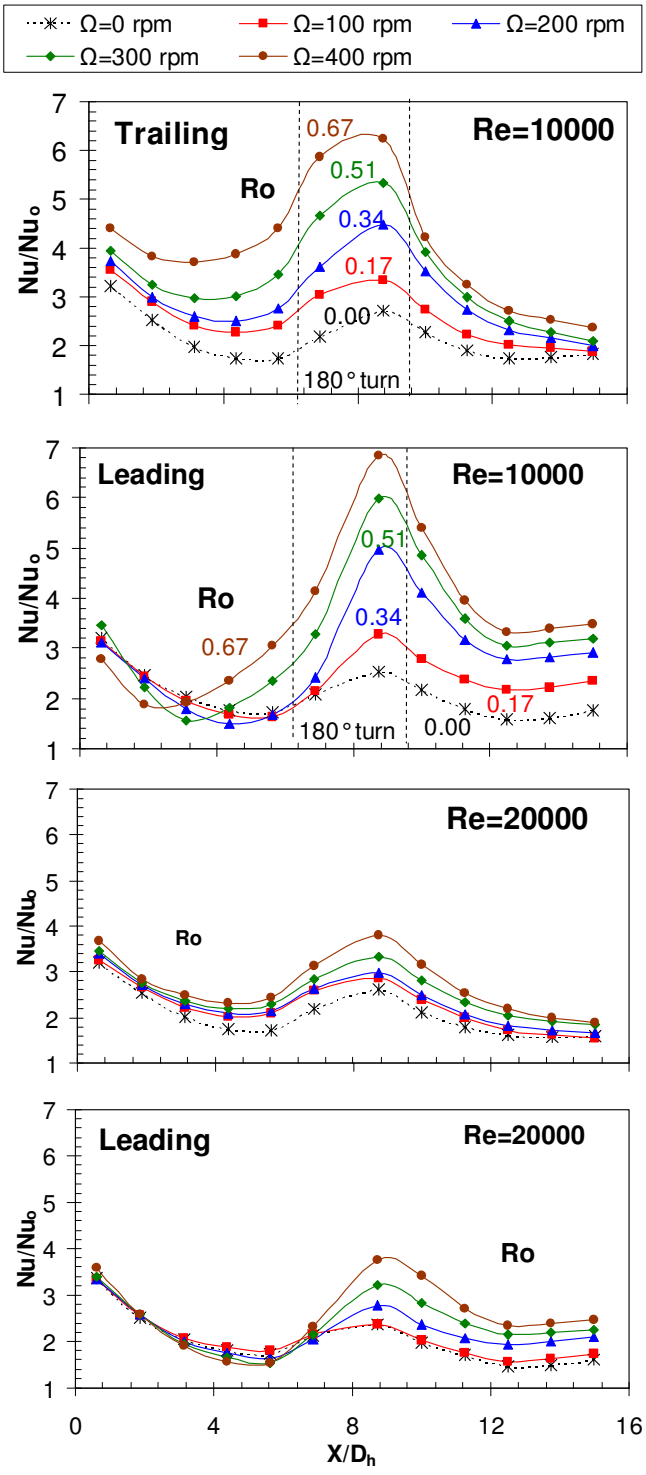

Figure 17: 1:4 Smooth streamwise Nu ratio distributions for different rotational speeds.

region, the entrance effect is larger than the rotation effect. The heat transfer enhancement for the rotating case is similar to the stationary case near the entrance.

4.1.1.3 *Rotation Induced Secondary Flow Effect on Circumferential Heat Transfer*

Figure 18 shows the circumferential distribution of the Nu ratio in region 4 in the first passage and region 10 in the second passage. These two regions were selected because the entrance effects and the turn effects are at a minimum at these locations. For the stationary case, at both Reynolds numbers, the Nu ratio in the first passage is slightly higher than the second passage. In the first passage, the boundary layer is thinner than the boundary layer in the second passage. For all rotating cases, the Nu ratio on the trailing surface is higher than the leading surface in the first passage for both Reynolds number cases. The maximum Nu ratio of 3.87 occurs at a rotation number of 0.67.

The difference between the leading surface and trailing surface will be larger when the rotation number is increased. The rotation induced secondary flow causes turbulence enhancement on the trailing surface and turbulence decay on the leading surface in the first passage. A thicker boundary layer develops on the leading surface, thus the decrease in heat transfer. The rotation induced secondary flow behavior becomes stronger as the rotation number increases. The difference between the inner/outer leading surface and the inner/outer trailing surface is small. The rotation induced vortices do not impinge on the inner/outer surfaces because the channel orientation is 90°. In the second passage, the rotation induced secondary flow has the reverse trend as in the first passage. The effect of rotation is smaller than in the first

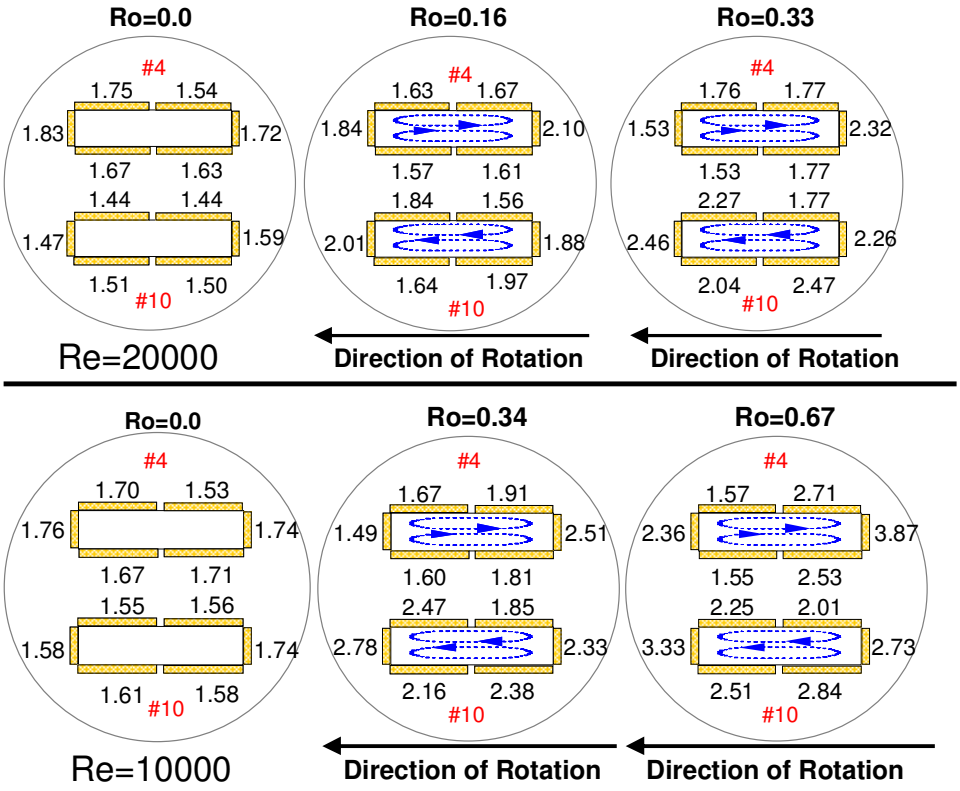

Figure 18: Circumferential Nu ratio distributions for region 4 and region 10 of the smooth 1:4 channel.

passage because the centrifugal force opposes the inertial force. Thus, the difference between leading and the trailing surfaces is smaller.

4.1.1.4 *Rotation Number Effects*

The rotation number is a relative measure of the rotational Coriolis force and bulk flow inertia force. In the current study, the rotation number is varied by the Reynolds number and the rotational speed. The rotation number in this study varied from 0 to 0.67. The data presented here are based on the wall temperature of 65°C (the inlet density ratio = 0.10). **Figure 19(a)** shows the effect of the rotation number on the Nu ratio (Nu/Nu_s) in the first passage at region 4. The stationary Nusselt number is chosen as the denominator of the Nu ratio (Nu/Nu_s) so that the effect of rotation on heat transfer can be compared. In the first passage, the Coriolis forces push the core coolant toward the trailing surface. The Nu ratio increases on the trailing surface as the rotation number increases. On the leading surface, the Nu ratio decreases up to a rotation number of 0.3. The Nu ratio then increases with the rotation number up to Ro=0.67. The increase of the Nu ratio is due to the development of large-scale reverse flow cells (Wagner et al.. [6, 7]). However, in a square channel (AR=1:1), the heat transfer ratio continues to decrease until the rotation number is 0.2 at the downstream location in the first passage as reported by Wagner et al.. [6, 7].

The Nu ratio on the inner/outer trailing surfaces also increases with increasing rotation number as shown in **Figure 19(c)** and **Figure 19(e)**. The heat transfer enhancement due to rotation in the inner and outer regions is smaller because of the

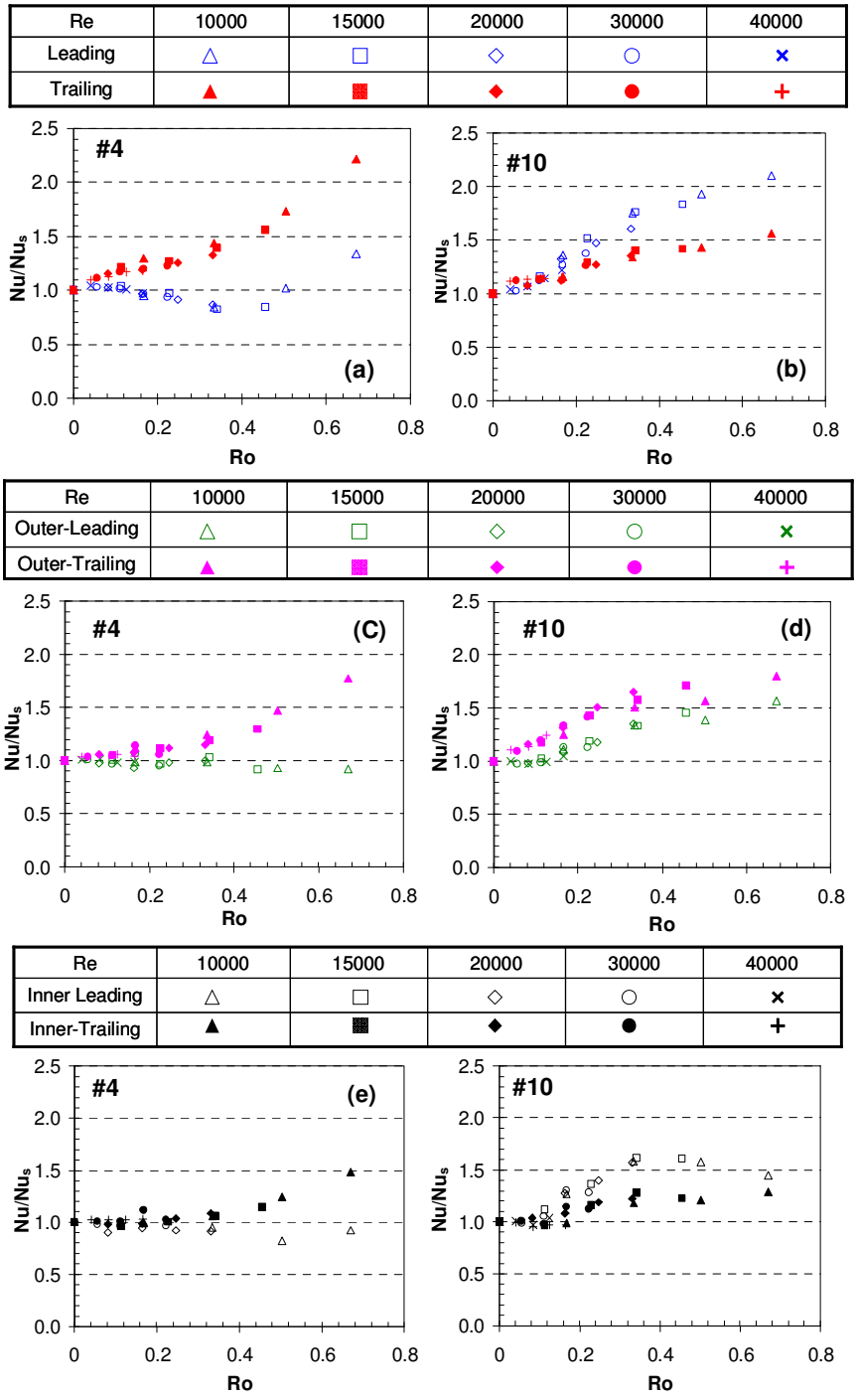

Figure 19: Nu ratio distribution with respect to the rotation number in regions 4 and 10 in the 1:4 smooth channel.

orientation of the rotating channel. The effect of the rotation induced secondary flow pattern on these regions is weaker.

The radially inward flow in the second passage reverses the direction of the Coriolis forces. **Figure 19(b)** shows the effect of rotation on the Nu ratio in region 10. No significant difference in Nu ratios for the leading and trailing surfaces is observed when rotation number is smaller than 0.12. Afterwards, the leading surface Nu ratios are greater than the trailing. At outer region 10 in **Figure 19(d)**, it is interesting to note that the outer trailing surface has greater heat transfer than the outer leading surface. The Nu ratios at inner region 10 on the leading and trailing surfaces increase up to a rotation number of 0.33 as shown in **Figure 19(f)**. Afterwards, the trailing surface Nu ratios remain level at approximately an Nu ratio of 1.2. The Nu ratio on the leading surface begins to decrease after a rotation number of 0.3.

The tip region is located at the end of the test section, where the 180° turn connects the first passage and the second passage. The incoming flow impinges on the tip region and creates the highest heat transfer throughout the entire channel. Impingement of the mainstream flow occurs on both tip regions 6 and 7, and enhances the heat transfer significantly in the tip region. The Nu ratio distribution with respect to the rotation number for the tip region is shown in **Figure 20**. Rotation also enhances the heat transfer in the tip region. The heat transfer enhancement in this region is due to the combined effects of Coriolis force and the turn induced secondary flow. The largest Nu ratio of 2.2 for tip 6 occurs on the trailing surface at a rotation number of 0.67. At tip 7, the largest Nu ratio of approximately 2.7, occurs at a rotation number of 0.67. The heat

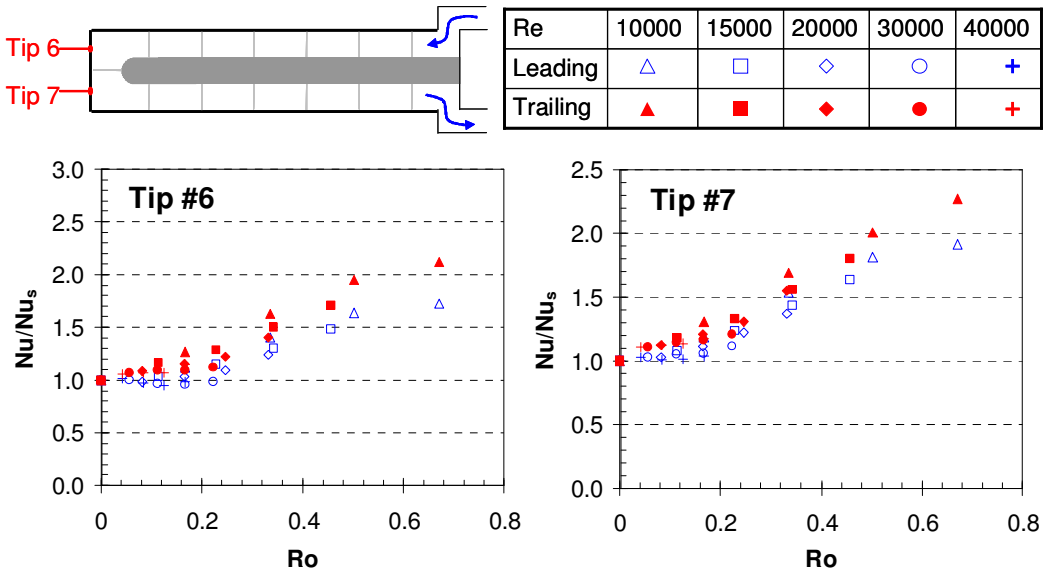

Figure 20: Nu ratio with respect to the rotation number in the tip region for smooth 1:4 channel.

transfer on the trailing surface is higher than the leading surface in the tip region. Liou et al.. [16] reported that as the rotation number increases, the magnitude of the secondary-flow velocity increases linearly and the magnitude of turbulence intensity level increases exponentially in the 180° turn region. This explains why the heat transfer ratio also enhances in the tip region.

4.1.1.5 *Buoyancy Parameter Effects*

Five Reynolds numbers, each at four rotational speeds, are presented at corresponding buoyancy parameters. In addition to the inlet density ratio of 0.10, the results of two additional density ratios of 0.14 and 0.16 are also presented. The rotation buoyancy effects, on the Nu ratio (Nu/Nu_s), caused by the radially outward flow in the first passage are shown in **Figure 21**. In the first passage, the Nu ratio on the trailing surface increases with an increase of the buoyancy parameter. In region 1, the entrance effects dominate over the rotation effects and the Nu ratios are close to 1.1. The Nu ratio on the leading surface continues to decrease in region 1 and region 2 because of the turbulence decay near the wall. However, the large-scale development of the recirculation flow will enhance the heat transfer at high buoyancy parameters. Therefore, region 3 and region 4 show the Nu ratio on the leading surface decreases, and then increases with an increase of the buoyancy parameter. The recirculation flow starts to develop near a buoyancy parameter of 0.8 in region 3 and region 4. Fu et al.. [14] showed a similar trend but at a buoyancy parameter of 0.08. The recirculation effect enhances the heat transfer ratio on the leading surface above that of the stationary case in

region 4. The heat transfer ratio is about 2.2 times higher than the stationary case at a buoyancy

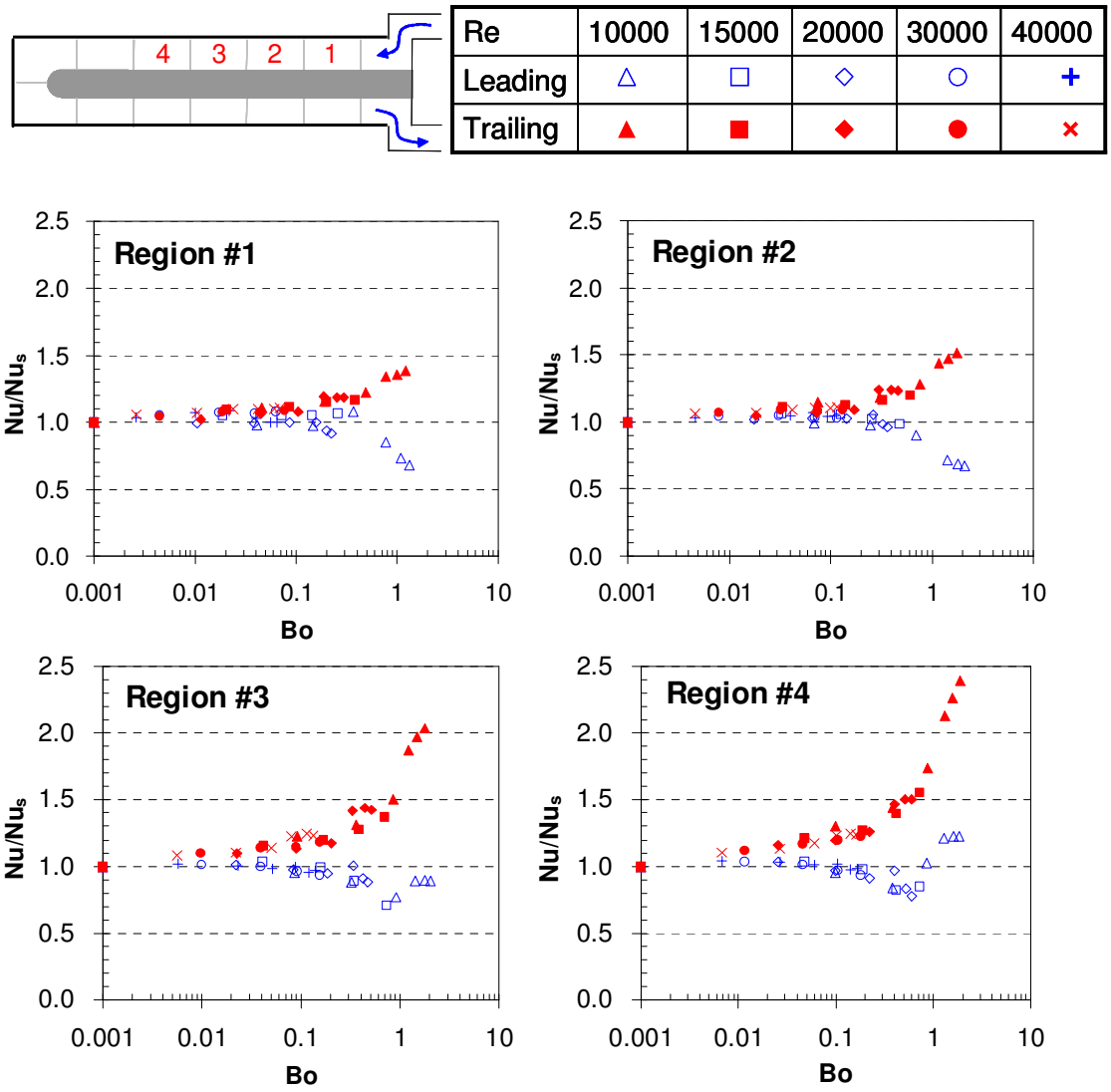

Figure 21: Nu ratios with respect to buoyancy parameter from region 1 to region 4 for smooth 1:4 channel.

parameter of 1.9 in region 4. The Nu ratio difference between the leading surface and trailing surface is small until the buoyancy parameter is larger than 0.3 in region 1. However, the Nu ratio difference between the leading surface and trailing surface becomes larger when the buoyancy parameter is larger than 0.01 in region 4. This shows that the entrance effect decreases along the streamwise direction.

Figure 22 shows the effect of the buoyancy parameter on the Nu ratio (Nu/Nu_s) in the regions near the 180° sharp turn in the test section. In region 5, the heat transfer ratio on the leading surface decreases slightly up to a buoyancy parameter of 0.3, where then it begins to increase. In region 6, the heat transfer increases as the buoyancy parameter increases on both the leading and trailing surfaces. The heat transfer enhancement on the trailing surface in region 6 is about 2.7 times greater than the stationary case. The trailing surface experiences higher heat transfer augmentation than the leading surface in all regions in the first passage.

At tip 6 and tip 7, the radially outward flow directly impinges on the surface. In this region, the heat transfer is considerably higher than any other surfaces in the test section. However, the heat transfer ratio is smaller when compared to region 6 and region 7. This shows that the rotation effect is smaller due to the flow impingement. The heat transfer increases when the buoyancy parameter increases. At low buoyancy parameters, the strong turbulence mixing near the turn dominates over the rotation effects. The heat transfer ratio in the tip region is slightly greater on the trailing surface than the leading surface. Region 7 and region 8 are strongly affected by the turn induced

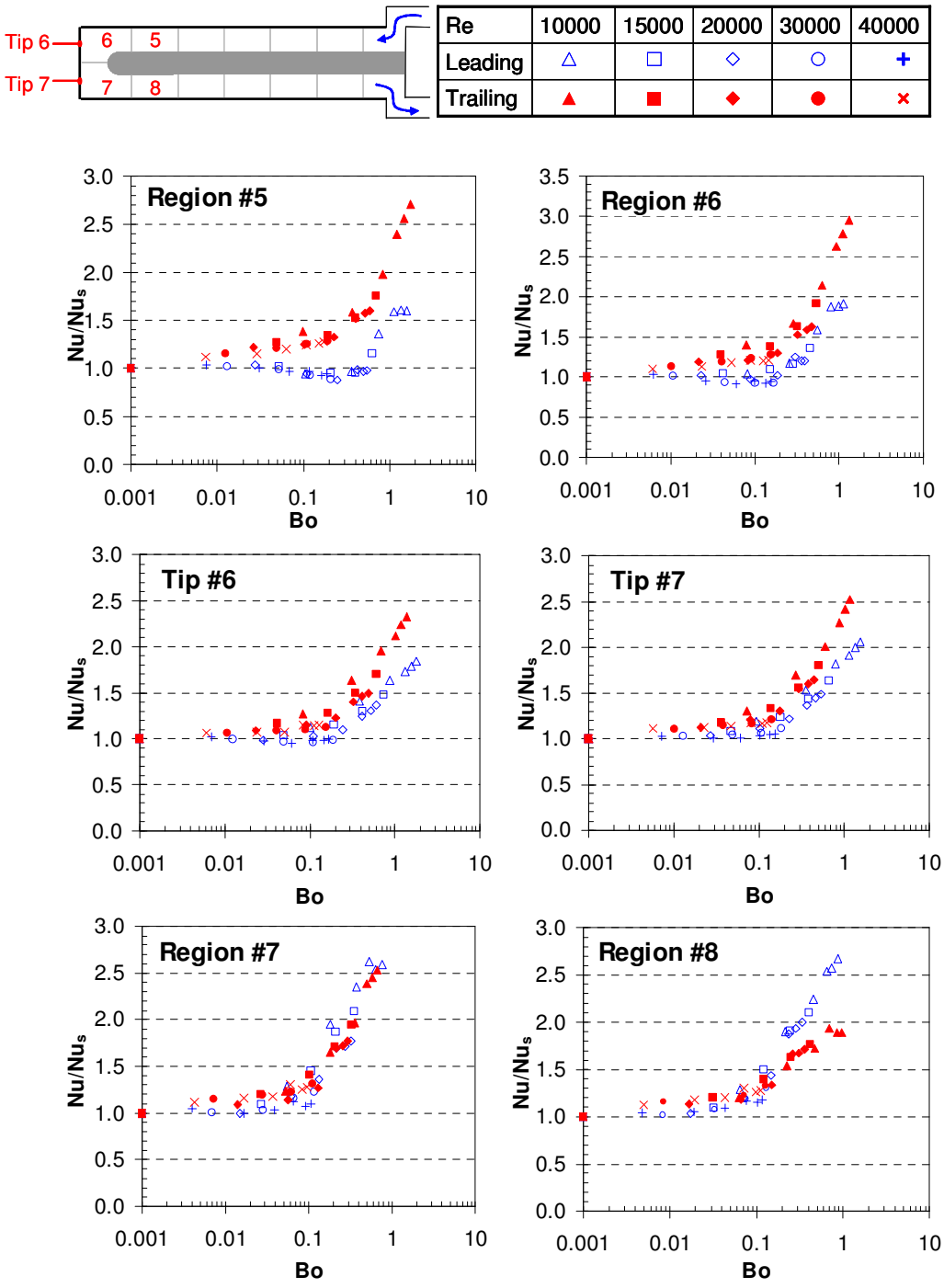

Figure 22: Nu ratios against buoyancy parameter from region 5 to region 8 in the smooth 1:4 channel.

secondary flow and the radially inward flow in the second passage. The Nu ratio is slightly higher on the leading surface than the trailing surface for both region 7 and region 8 at higher buoyancy parameters.

Figure 23 shows the effect of the buoyancy parameter on the Nu ratio in regions 9 through 12 in the second passage. In these four regions, radially inward flow moves the core coolant toward the leading surface. Therefore, higher Nu ratios are observed on the leading surface when compared to the trailing surface. Heat transfer increases with the buoyancy parameter on both the leading and trailing surfaces. Close to the exit of the channel, the effects of the 180° turn are reduced. The difference in heat transfer ratios between the leading and trailing surfaces increases in the streamwise direction.

4.1.1.6 *Pass Averaged Nusselt Number Ratios with Rotation Number and Buoyancy Parameter Correlations*

The average Nu ratios (Nu/Nu_s) in the first passage are presented in **Figure 24**. The results are based on the six copper plates on the leading surface and the six copper plates on the trailing surface. Results from the current study show a smaller enhancement on the trailing surface and smaller degradation on the leading surface than that of the fully-developed flow. The data from Fu et al.. [14] is with an unheated entrance length to provide a hydrodynamically fully developed flow condition. The effect of rotation in the current study is greatly reduced because of the entrance geometry with re-directed sharp bend in the first passage. The two sets of data show similar trends and the heat transfer ratio on the trailing surface is higher than the leading

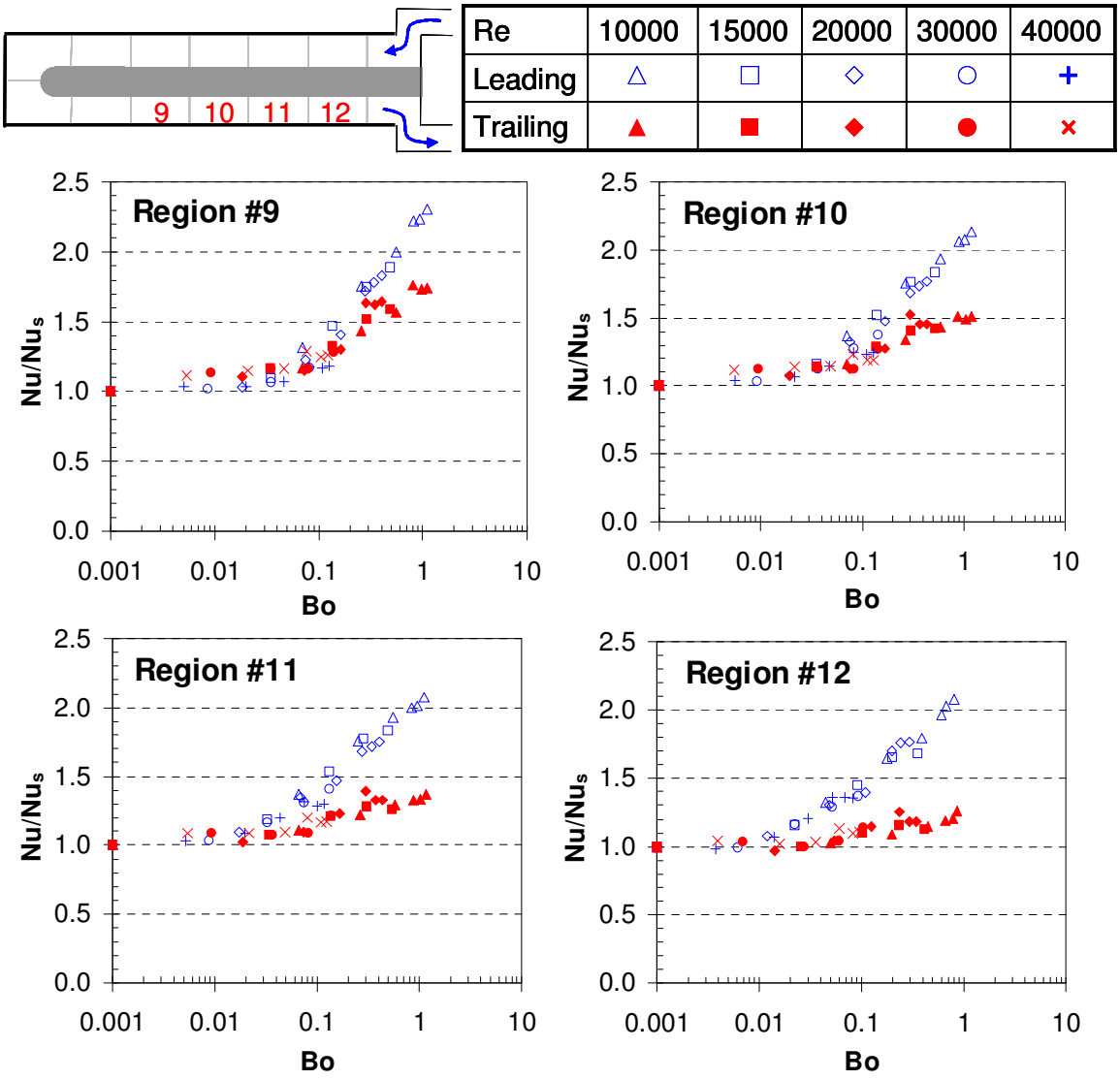

Figure 23: Nu ratios with buoyancy parameter from region 9 to region 12 in the smooth 1:4 channel.

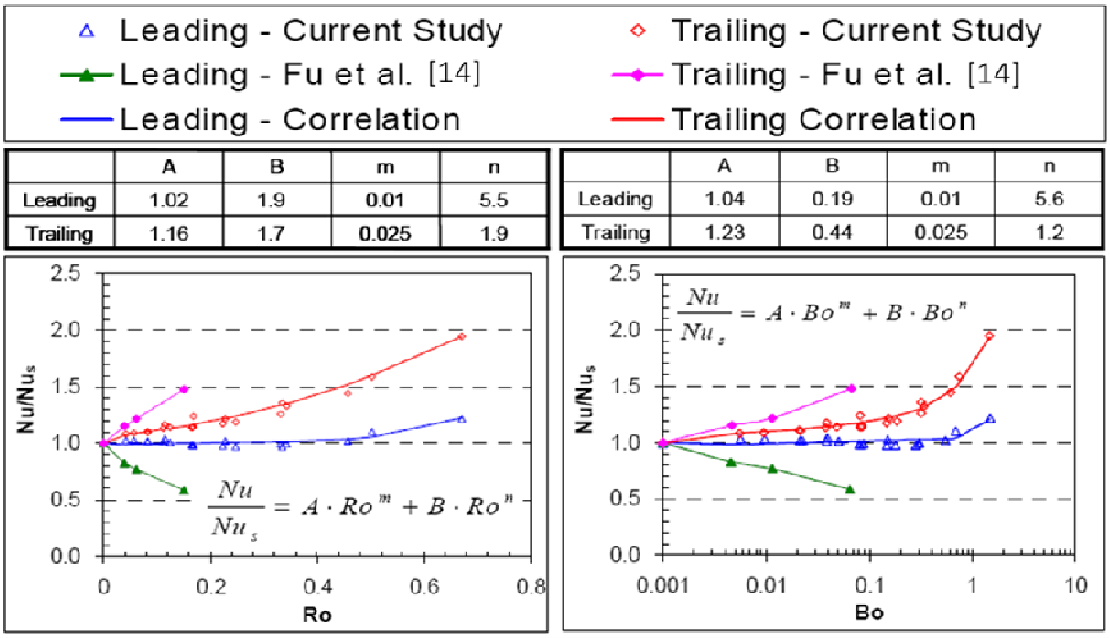

	A	B	m	n
Leading	1.02	1.9	0.01	5.5
Trailing	1.16	1.7	0.025	1.9

	A	B	m	n
Leading	1.04	0.19	0.01	5.6
Trailing	1.23	0.44	0.025	1.2

Figure 24: Average Nu ratios in the first pass for 1:4 smooth channel.

surface. The average Nu ratio on the trailing surface from Fu et al. [14] and the current study increases with the rotation number and buoyancy parameter. For the current study, the maximum average Nu ratio of 1.95 occurs at rotation number of 0.67 and buoyancy parameter of approximately 1.2 on the trailing surface in the first passage. The Nu ratio is correlated to both the rotation number and buoyancy parameter with a power-law function. The experimental Nu ratio results are within $\pm$10% of the correlation curve for both the rotation number and buoyancy parameter.

In **Figure 25**, the average Nu ratio for the second passage is presented. The average Nu ratios on both the leading and trailing surface increase with the rotation number and the buoyancy parameter. The results of the current study and those of Fu et al. [14] in the second passage have similar trends and levels because both of them have the same 180^{o} sharp turn. The experimental results can be correlated by a power-law function and the discrepancy is about $\pm$12%. The average heat transfer ratios on the leading and trailing surfaces increase with the rotation number as well as the buoyancy parameter. The maximum Nu ratio of 2.3 occurs at a rotation number of 0.67 and buoyancy parameter 1.0 on the leading surface in the second passage. The above results show that the rotation number can be used to correlate the data from different rotational speeds and Reynolds numbers. The buoyancy parameter is capable of quantifying the effects of rotation even with the contribution from different density ratios, rotational speeds, and Reynolds numbers.

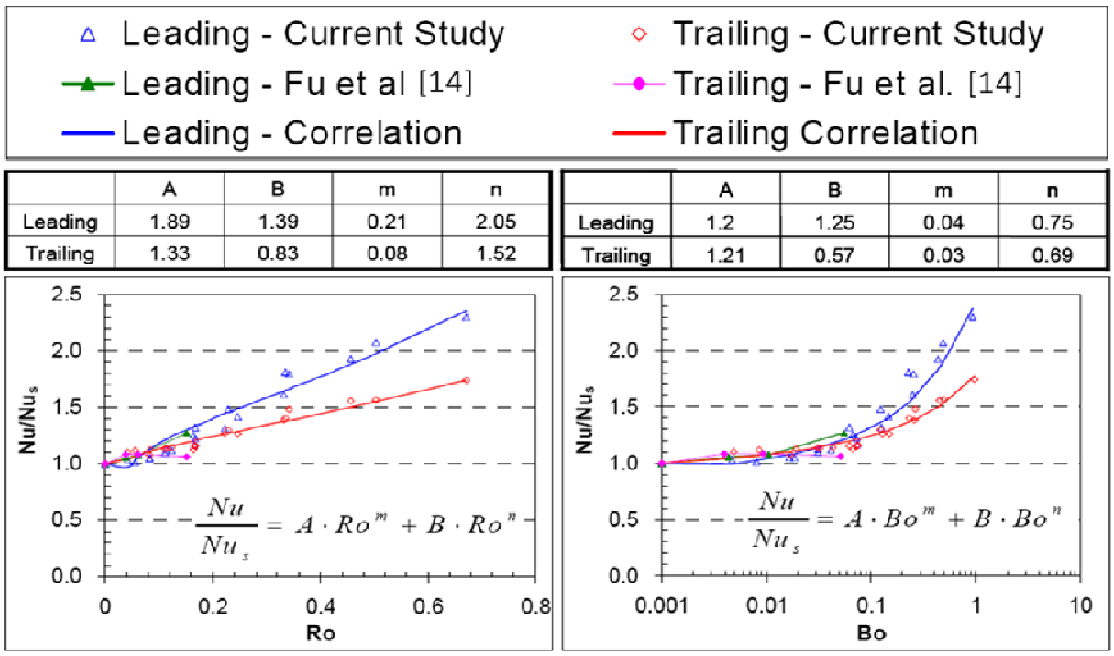

	A	B	m	n
Leading	1.89	1.39	0.21	2.05
Trailing	1.33	0.83	0.08	1.52

	A	B	m	n
Leading	1.2	1.25	0.04	0.75
Trailing	1.21	0.57	0.03	0.69

Figure 25: Average Nu ratios in the second pass for 1:4 smooth channel.

4.1.1.7 *Conclusions*

This portion of the study further increases the understanding of the effects of the entrance geometry and rotation on heat transfer in a smooth two-pass rotating 1:4 aspect ratio channel. The range of the rotation number and buoyancy parameter was extended to values above those in current open literature sources. The rotation and buoyancy parameters in this study reached 0.67 and 1.9, respectively. Previous studies reported results for the leading and trailing walls of the flow channel. However, important heat transfer information at the tip regions is lacking. This study has provided new insight to the heat transfer behavior in the tip region of the flow channel along with furthering the understanding of heat transfer on the leading and trailing walls. Listed below are the important findings from the research work performed.

1. The rotation effect on heat transfer on the leading and trailing surfaces in the first passage is dramatically reduced by the re-directed sharp bend entrance. As the rotation number increases, the rotation effect begins to dominate over the entrance effect in the first passage. The effect of the entrance geometry is diminished in the second passage due to the strong 180^{o} turn effect.

2. Heat transfer increases on the trailing surface in the first passage as the rotation number increases. On the leading surface, in the first passage (x/D_h of 4.375) the heat transfer initially decreases but begins to increase when the rotation number reaches a critical value of 0.3. This phenomenon is due to the formation of large scale rotating buoyancy generated reverse flow cells.

3. The increased range of the buoyancy parameter and rotation number, reached in this study, can be used to predict the heat transfer enhancement from different rotational speeds, Reynolds numbers, and density ratios.

4. The tip region experiences the highest heat transfer ratio over the entire channel because of the direct impingement of the main flow, 180^o sharp turn induced secondary flow, and rotation. Rotation increases the heat transfer (Nu/Nus) by 2-2.5 times in the tip portion. The largest Nu ratio (Nu/Nu_0) observed was between 6.0 and 8.0 in the tip region.

5. As the rotation number increases, the heat transfer increases on both the leading and trailing surfaces in the second passage. This trend is different from both the square (AR=1:1) and AR=2:1 channels. The difference is attributed to the geometrical effects of the 1:4 aspect ratio channel with 180^o sharp turn on the Coriolis induced secondary flow in the second passage.

A fundamental understanding of heat transfer for the 1:4 aspect ratio channel at high rotation numbers and buoyancy parameters is needed. The results of the current study provide this fundamental understanding. The valuable data obtained from the current work serves as a baseline comparison to ribbed wall heat transfer.

4.1.2 Rib Spacing Effects

4.1.2.1 *Flow Field Behavior in Ribbed Channels*

Before discussing the experimental results for the two pass 1:4 aspect ratio channel with angled ribs, it is necessary to understand the flow behavior inside the channel. The orientation of the ribs has a significant impact on the level of heat transfer

enhancement. Skewed ribs yield significantly higher heat transfer enhancement than orthogonal ribs. This is due to the additional secondary flow induced by the angle of the ribs. Rib turbulators are also widely known as "trip strips" as they simply trip the boundary layer in the internal channel. After the boundary layer is disturbed, redevelopment begins, and high heat transfer is associated with the thin boundary layer.

Figure 26 presents conceptual views of the most notable characteristics of the effects of ribs on the mainstream flow. As shown in **Figure. 26(a)**, as the mainstream flow near the surface of the channel wall passes over the rib, it separates from the surface due to the rib. Two zones of recirculation develop immediately upstream and downstream of the rib. In these two areas of recirculation, hot fluid cells cause the heat transfer to be low. However, when the mainstream flow reattaches to the surface (between two ribs), this is an area of relatively high heat transfer due to impingement of the mainstream flow on the surface. This pattern of separation, recirculation, and reattachment continues throughout the channel along with the repeated pattern of the rib design. In addition to flow separation and reattachment, the rib turbulators increase turbulent mixing. The relatively hot fluid near the surface is continuously mixing with the relatively cooler core fluid near the center of the channel. This mixing also serves to increase the heat transfer from the channel wall.

The ideal rib spacing is large enough for the mainstream flow to reattach to the surface between the ribs (high heat transfer), but not so large that the boundary layer is allowed to develop freely. By allowing the mainstream flow to develop freely, the advantage of the thin boundary layer is lost. It has been shown that the ideal spacing for

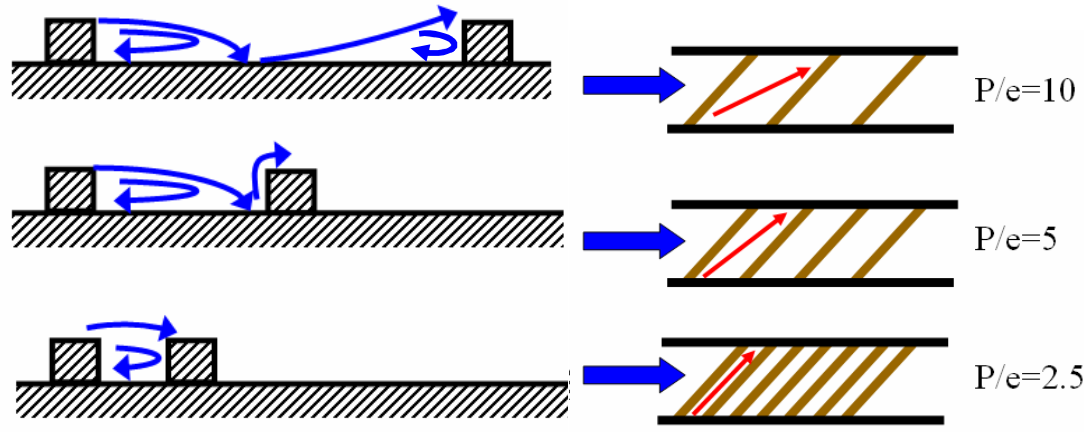

Figure 26: Effects of rib spacing on (a) mainstream flow separation and reattachment and (b) angled rib induced secondary flow.

orthogonal ribs is approximately P/e = 10. As conceptually shown in **Figure 26(a)**, with a P/e = 10 ratio, sufficient space is given between the ribs for reattachment of the flow between the ribs. However, as the ribs continue to move closer together, the reattachment area becomes jeopardized. After separation, the flow may impinge on the next downstream rib (P/e = 5), or the flow may completely pass over the next rib (P/e = 2.5), completely eliminating the desired flow behavior.

Ribs skewed to the mainstream flow are preferred to orthogonal ribs because they induce an angled secondary flow. The fluid near the surface follows the angle of the rib. This angled rib induced secondary flow creates a set of counter-rotating vortices in the channel. The secondary flow follows the rib until it impinges on the side wall as can be seen in **Figure 26(b)**. After impingement on the side wall, the rib induced angled secondary flow returns to the other side wall, creating a vortex. This behavior is identical on both the leading and trailing surfaces, so two counter rotating vortices form in the channel. Because the ribs are skewed to the mainstream flow, regardless of how closely the ribs are spaced, the angled rib induced secondary flow is expected to be present, as shown in **Figure 26(b)**. Unlike with 90° ribs, the fluid that is trapped between closely spaced angled ribs, is expected to travel along the length of the ribs, and create the counter rotating vortices. Predictions from Su et al. [33] for a non-rotating channel with angled ribs (P/e = 10), show the angled rib induced, counter-rotating vortices are not limited to areas close to the rib roughened walls; each vortex occupies nearly half of the channel cross-section. If this trend is present, regardless of the rib

spacing, the coolant between the ribs is moving (as opposed to being trapped), and additional heat transfer enhancement will occur.

The level of heat transfer enhancement in the two pass channel with angled ribs is altered by the sharp 180° turn which connects the first pass to the second pass, by rotation, and by rotational induced buoyancy forces**.** **Figure 27** shows the secondary flows induced by angled ribs, the 180° turn and rotation. The secondary flow induced by rotation, is a result of the Coriolis force. As conceptually shown in **Figure 27(a)**, with a 90° channel orientation, the Coriolis force induces a pair of vortices, which circulate toward the trailing wall for radial outward flow (first pass) and toward the leading wall for radial inward flow (second pass). This cross-stream secondary flow pattern significantly increases heat transfer on the trailing wall in the first pass and the leading wall in the second pass. However, the rotation induced secondary flow reduces heat transfer on the leading wall in the first pass and trailing wall in the second pass. In the current study, the secondary flow caused by the 45^{o} angled ribs that are located on the leading and trailing walls in the first pass, cause impingement of the flow onto the inner wall. In the second pass, the secondary flow due to the ribs cause impingement onto the outer wall as is shown in **Figure 27(a)**.

When the mainstream flow passes through the 180° turn, the flow impinges on the outer wall of the second pass, then reattaches on the inner wall in the second pass as is shown in **Figure 27(b)**. A circulation zone right after the turn near the inner wall in the second pass is created due to the sharp turn. Two additional circulation zones occur in the outer corners of the turn because of the geometry. These flow structures, due to

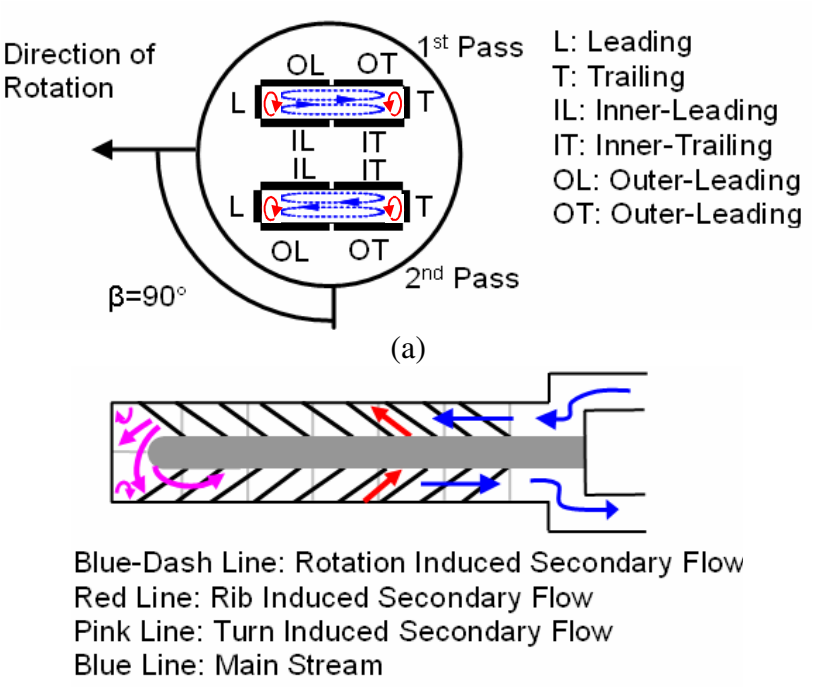

Figure 27: Conceptual view of (a) rib and rotation induced secondary flow inside a two-passage rectangular channel (AR=1:4), (b) rib and turn induced secondary flow.

the turn, result in different heat transfer enhancements inside the turn and after the turn. All of these secondary flows, induced by angled ribs, the 180° turn, and rotation, interact to make flow through a rib roughened serpentine passage very complex. The combination of these flows may result in further enhancement of the heat transfer, or they may have a negative impact on the heat transfer trend. The flow patterns previously described have been observed by previous studies (Han et al. [15], Han and Zhang [34], Ekkad and Han [35], Park and Lau [36], Park et al. [37], Liou et al. [38], and Liou and Chen [39]).

4.1.2.2 *Stationary Results with Entrance Effects*

All of the data involving ribs presented in the current study are based on the total area**.** A discussion on the effect of area in the determination of the Nu/Nu_o ratios is presented later. The entrance condition, whether fully developed or developing flow, has an effect on the heat transfer in the first pass. **Figure 28** shows the stationary streamwise average of the leading and trailing Nu_s/Nu_o ratios for smooth and ribbed (P/e = 10) walls in the first pass. The different entrance conditions of fully developed and sharp bend are compared at Reynolds numbers of 10000 and 40000. For the current study (P/e = 10 sharp bend), at Re=10000, the Nu_s/Nu_o ratio is the highest when compared to all cases until an $x/D_h = 3.125$, after which the P/e = 10 case with fully developed entrance has the highest Nu_s/Nu_o ratio. This is because Fu et al. [14] presented their data based on projected area and as such the additional rib area is not taken into consideration. At Re = 40000, comparing the P/e = 10 sharp bend with the smooth walled sharp bend results, it is seen that the effects of the ribs is not present in the first pass (both sets of data lie on

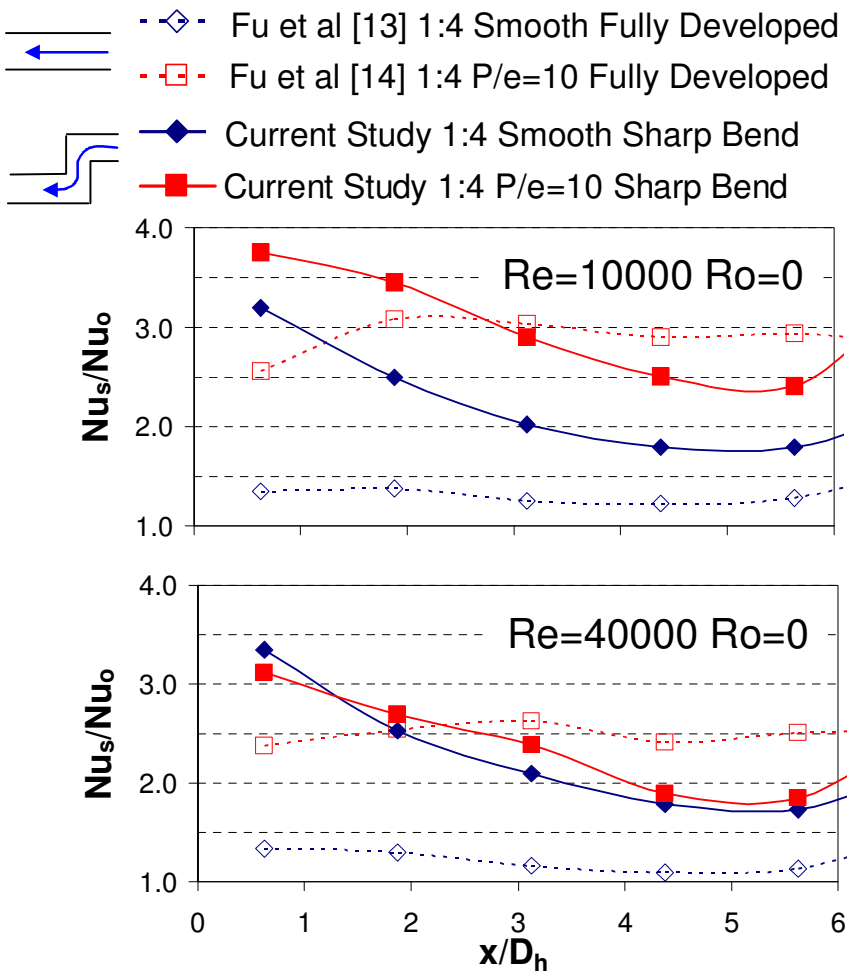

Figure 28: Comparison of stationary streamwise averaged Nu_s/Nu_o ratios with fully developed and sharp entrance condition with smooth and ribbed (P/e = 10) walls in the first pass of the 1:4 AR channel.

top of each other). Thus, the effect of the rib decreases with increasing Reynolds number.

4.1.2.3 *Channel Averaged Nusselt Number Ratios with Area Effects*

For a ribbed channel, when evaluating the heat transfer enhancement, the area used to perform the calculations can strongly impact the values of Nu/Nu_o ratios obtained. By adding ribs to the leading and trailing walls in the first pass and second pass, the total heat transfer area for the entire channel increases. In **Table 2**, the percent of area increase, due to the ribs, for each P/e ratio tested, is shown. For the case of P/e = 10, the total area for the entire channel is only 1.28 times greater than the smooth channel. However, for the case of P/e = 2.5, the total area for the ribbed channel is more than 2 times greater than the smooth channel.

Figure 29(a) shows the channel averaged (leading and trailing) Nu_s/Nu_o ratios for the 1:4 AR test section under stationary conditions at the Reynolds numbers tested. For the smooth channel, the channel averaged Nu_s/Nu_o ratio remains approximately constant for all Reynolds numbers at 2.0. For the ribbed cases, with the Nu_s/Nu_o ratio based on the total area, the Nu_s/Nu_o ratio increases with increasing P/e ratio. The P/e = 10 case shows the highest Nu_s/Nu_o ratios based on the total area. However, for all ribbed cases, as the Reynolds number increases, the effect of the ribs decreases, and thus the decrease in Nu_s/Nu_o ratios. When the projected area is considered, the Nu_s/Nu_o ratios for the ribbed cases are higher when compared to the total area Nu_s/Nu_o ratios. For the 1:4 AR channel in this study, when the projected area is considered, the close rib spacing of P/e = 2.5 case exhibits the highest heat transfer enhancement; although the P/e =5 case is

Table 2: Percentage of Area Increase due to Ribs for the Three P/e Ratios Tested for the Entire Channel

P/e	Area Increase
10	27.89%
5	52.68%
2.5	105.37%

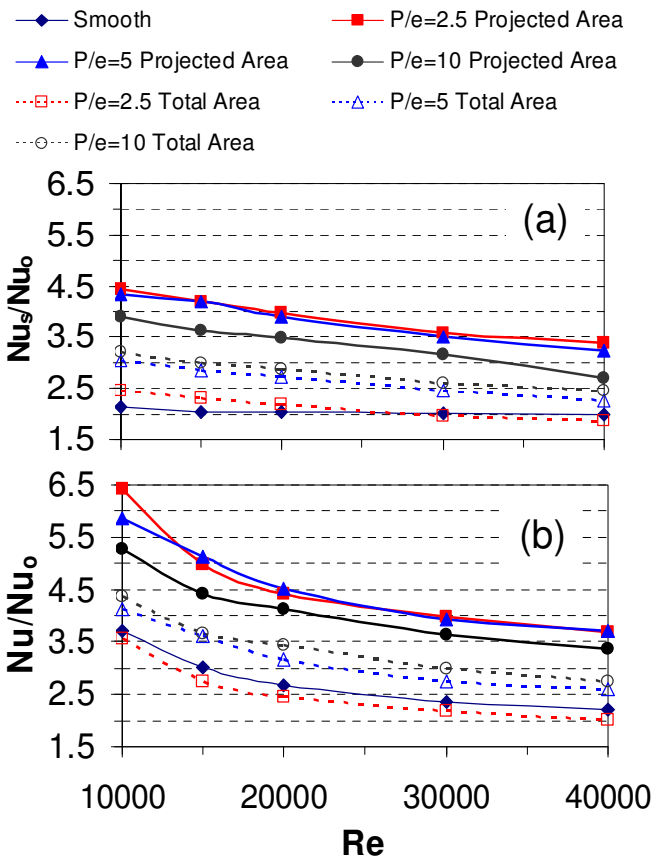

Figure 29: (a) Stationary and (b) rotating (RPM=400) channel averaged Nusselt number ratios as a function of Reynolds number for ribbed 1:4 channel.

only slightly less. Liu et al. [25] showed a similar result. In their study, (AR = 1:2), the close rib spacing of P/e = 3, showed the highest Nu_s/Nu_o ratios based on the projected area. For the rotating case, as shown in **Figure 29(b)**, similar trends are observed. It should be understood that when considering the rotating case, different rotation numbers are achieved at different Reynolds numbers since the rotational speed is held constant at 400 rpm.

4.1.2.4 *Rotating Streamwise Nusselt Number Ratios*

Figure 30 shows the effect of increasing the rotational speed on the streamwise Nu/Nu_o ratio distribution for the leading and trailing surfaces, with smooth and ribbed walls at a Reynolds number of 10000. From **Figure 30**, the effect of rotation in a ribbed channel is visible when compared to the smooth case. Consider the leading surface at $x/D_h = 3.125$; notice that for all P/e ratios, between 100 to 400 rpm, there are different values of Nu/Nu_o ranging from 1 to 3. For the smooth case at the same location, Nu/Nu_o is about 2 for all rotational speeds.

Also notice that for the leading surface when P/e = 10, for 0 to 200 rpm, the entrance effect is more apparent in that the Nu/Nu_o ratio continually decreases in the streamwise direction until $x/D_h = 5.625$ where an increase is experienced because of the turn. For the P/e = 2.5 and 5 cases, after $x/D_h = 3.125$, for rpm = 0 to 200, the Nu/Nu_o ratio remains approximately constant until $x/D_h = 5.625$ where an increase is experienced because of the turn. For example, consider P/e = 10, at 200 rpm, the Nu/Nu_o decreases from about 2 (at $x/D_h = 3.125$) to about 1 (at $x/D_h = 5.625$). For the P/e = 2.5 and 5 cases, at the same rpm and x/D_h range, the Nu/Nu_o ratio is constant at about 1. However, for an

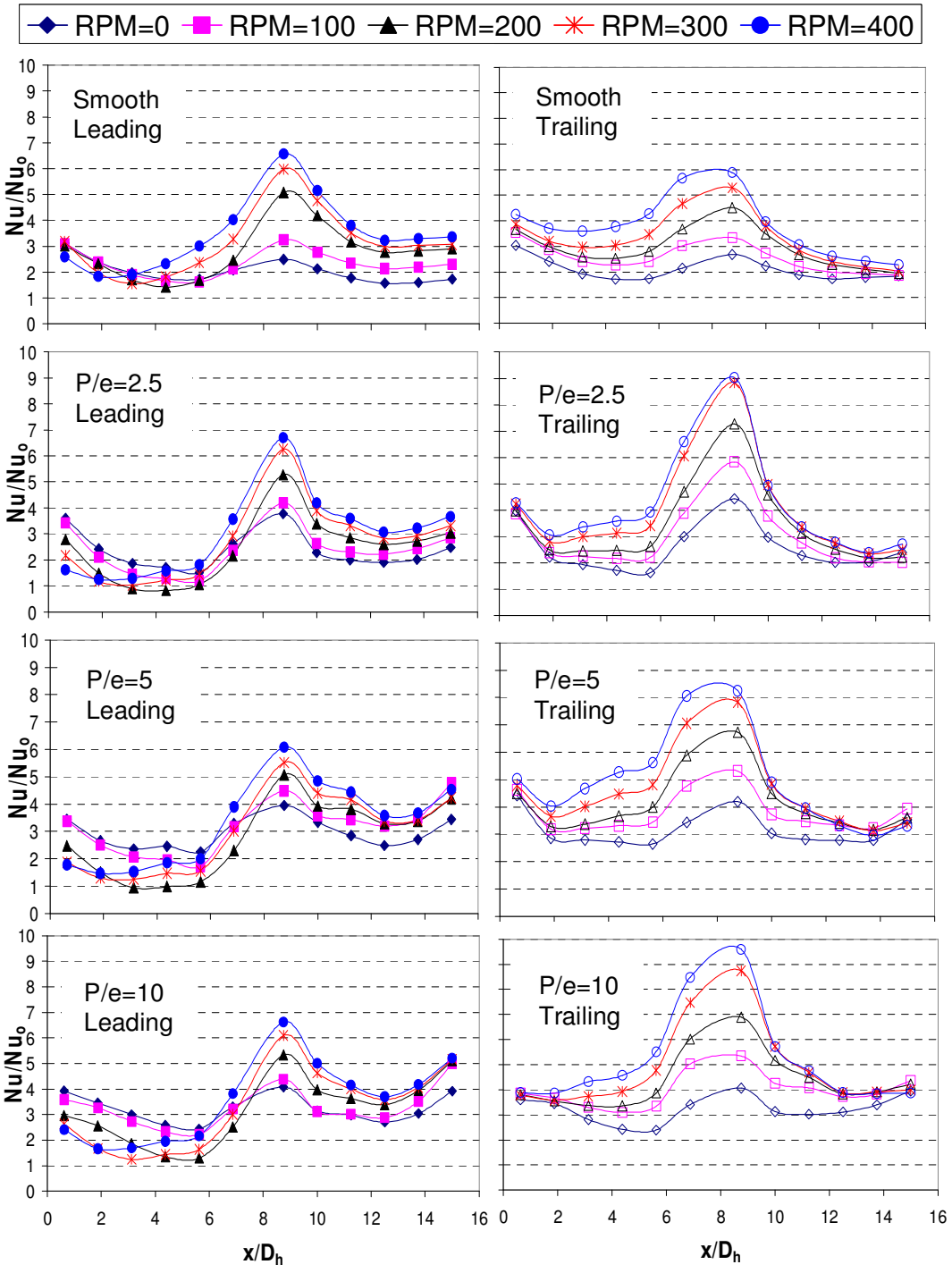

Figure 30: Streamwise Nu ratios (Nu/Nu_o) distribution at Re=10000 for the leading and trailing walls in ribbed 1:4 channel.

rpm value of 400, for all P/e ratios, the Nu/Nu_o ratio begins to increase after x/D_h = 1.875. This is similar to the smooth case and in a smooth square channel as observed by Wagner et al. [6]. For all P/e ratios studied, notice that in the first pass on the leading surface, as the rotational speed increases, the values of Nu/Nu_o fall below the stationary case. This is different from the smooth case. For all ribbed cases, on the leading surface for $x/D_h > 10$, the effect of rotation remains constant with increasing x/D_h, compared to the trailing surface.

On the trailing surface for $x/D_h > 10$, as x/D_h increases, the effect of rotation decreases. This is observed by noting that the differences in Nu/Nu_o for different rotational speeds decreases in the streamwise direction on the trailing surface. Finally, for the second pass trailing surface, at all P/e ratios, notice that rotation increases the Nu/Nu_o ratios above the stationary case. This trend is different than what Al-Hadhrami and Han [40] observed in a square channel.

4.1.2.5 *Rotation Number Effects*

The rotation number is a relative measure of the Coriolis force and bulk flow inertia force. In the current study, the rotation number is varied by the Reynolds number and the rotational speed. The rotation number in this study varied from 0 to 0.65. The data presented here are based on the total heat transfer area (3 times rib side area plus smooth area between ribs). **Figure 31** shows the Nu/Nu_s ratios, as a function of Ro, for the leading and trailing surfaces in regions 4 and 9. The stationary Nusselt number (Nu_s) is chosen as the denominator so that the effect of rotation on heat transfer can be compared.

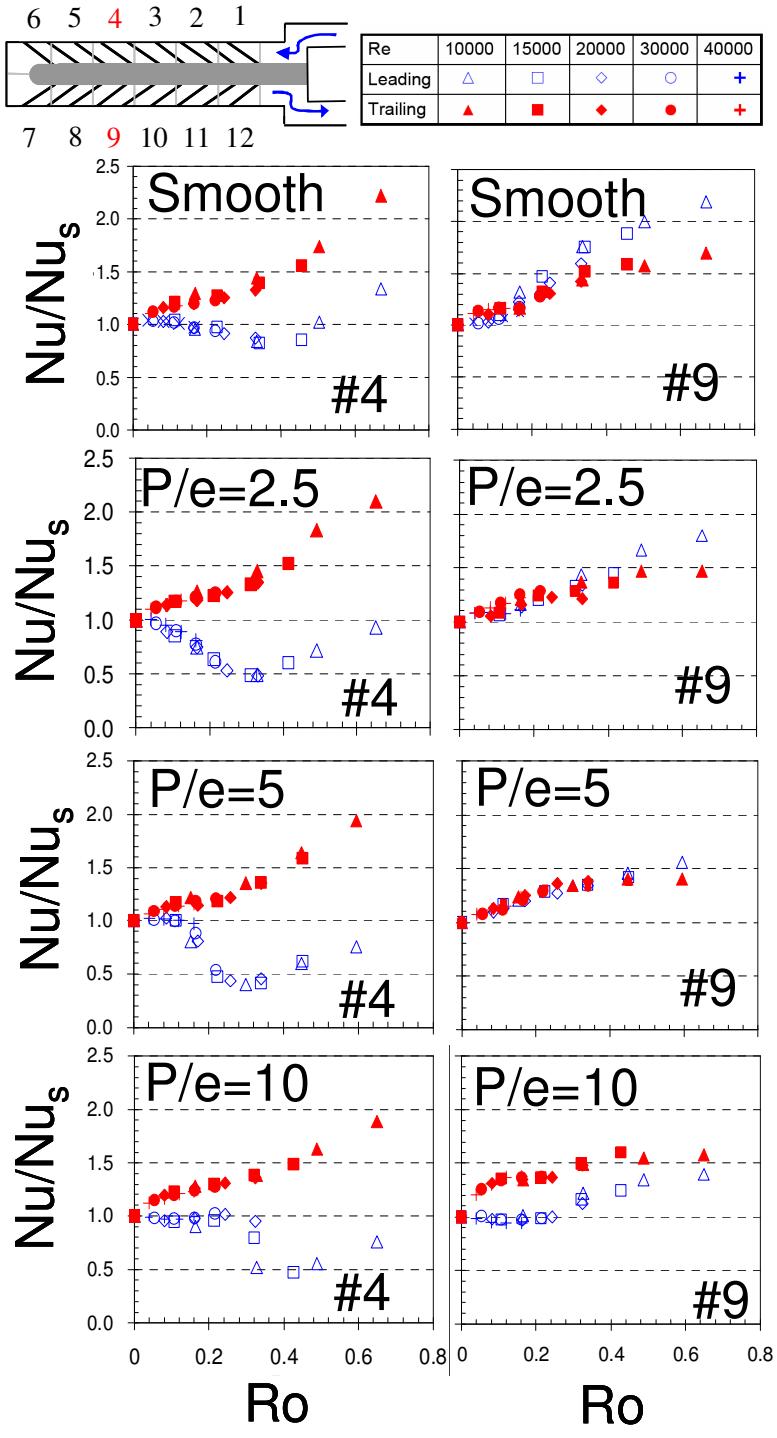

Figure 31: Nu/Nu_s ratio distribution on the leading and trailing surfaces with respect to the rotation number in regions 4 and 9 for smooth and all ribbed cases.

In the first passage, the Coriolis force pushes the core coolant toward the trailing surface. For all cases (ribbed and smooth) in region 4 on the trailing surface, the Nu/Nu_s ratio increases in a similar manner as the rotation number increases. However, as P/e increases, the maximum Nu/Nu_s ratio decreases at the maximum Ro of 0.65. For P/e = 2.5, Nu/Nu_s is approximately 2.1wheras for P/e = 10, Nu/Nu_s is nearly 1.8.

On the leading surface, for the smooth case, the Nu/Nu_s ratio decreases to a value of 0.8 at a rotation number of 0.3. The Nu/Nu_s ratio then increases with the rotation number up to Ro = 0.65. However, for all ribbed cases, the Nu/Nu_s ratio decreases to a value of 0.5. Su et al. [33] showed that in the 1:4 aspect ratio channel, at a rotation numbers below the critical Ro, the secondary flow vortex due to the rib angle, is weakened near the leading surface and strengthened on the trailing surface. Notice also that the effect of rotation is strongest in the P/e = 2.5 case. Degradation on the leading surface occurs immediately with the onset of rotation. Whereas for the P/e = 5 case, degradation occurs at Ro = 0.15. Finally, for the P/e = 10 case, rotation effects are seen at Ro = 0.3, where a Reynolds number effect is also present. The increase of the Nu/Nu_s ratio on the leading surface after the critical Ro, in all cases (ribbed and smooth) in region 4, is due to the development of large-scale reverse flow cells as reported by Wagner et al. [6] and Su et al. [33].

In the second pass at region 9, the Coriolis force pushes the core coolant toward the leading surface because the flow is radially inward. Little difference is seen on the trailing surface between the smooth case and all ribbed cases. The trailing surface heat

transfer increases in a similar fashion for the smooth case and ribbed cases. At the highest rotation number of Ro = 0.65, all cases have an Nu/Nus ratio around 1.5.

The leading surface for the smooth case has the highest heat transfer enhancement due to rotation. As P/e increases, the effect of rotation on heat transfer on the leading surface in region 9, decreases. At the highest rotation number of Ro = 0.65, the Nu/Nu_s ratio for the smooth case is approximately 2.25. The Nu/Nu_s ratio steadily decreases (for fixed Ro = 0.65) to a value of approximately 1.4 for P/e = 10. This shows that the heat transfer enhancement is dominated by the rib spacing rather than rotation.

4.1.2.6 *Buoyancy Parameter Effects*

The buoyancy parameter (Bo) takes into account not only rotation, but the temperature difference between the heated wall and the cool mainstream flow. **Figures 32** and **33** show how the Nu/Nu_s ratio is affected by local Bo for all P/e ratios tested. **Figure 32** is for regions 1, 4, 6 and tip region 6 which are in the first pass. In region 1, for all ribbed cases, it is seen that the trailing surface Nu/Nu_s ratio remains constant at 1 as Bo increases. This implies that the effects of the entrance dominate over rotation on the trailing surface in region 1 regardless of rib spacing. The trailing surface for the smooth case shows a slight increase at high Bo numbers.

On the leading surface for the ribbed cases, the Nu/Nu_s ratio remains constant at 1 until a Bo value of 0.1, after which the Nu/Nu_s ratio begins to decrease to approximately 0.5. This trend is different than the smooth case in which a slight decrease on the leading surface is not seen until a Bo of 1. No increase in heat transfer is seen on the leading surface because buoyancy forces are weak at this point.

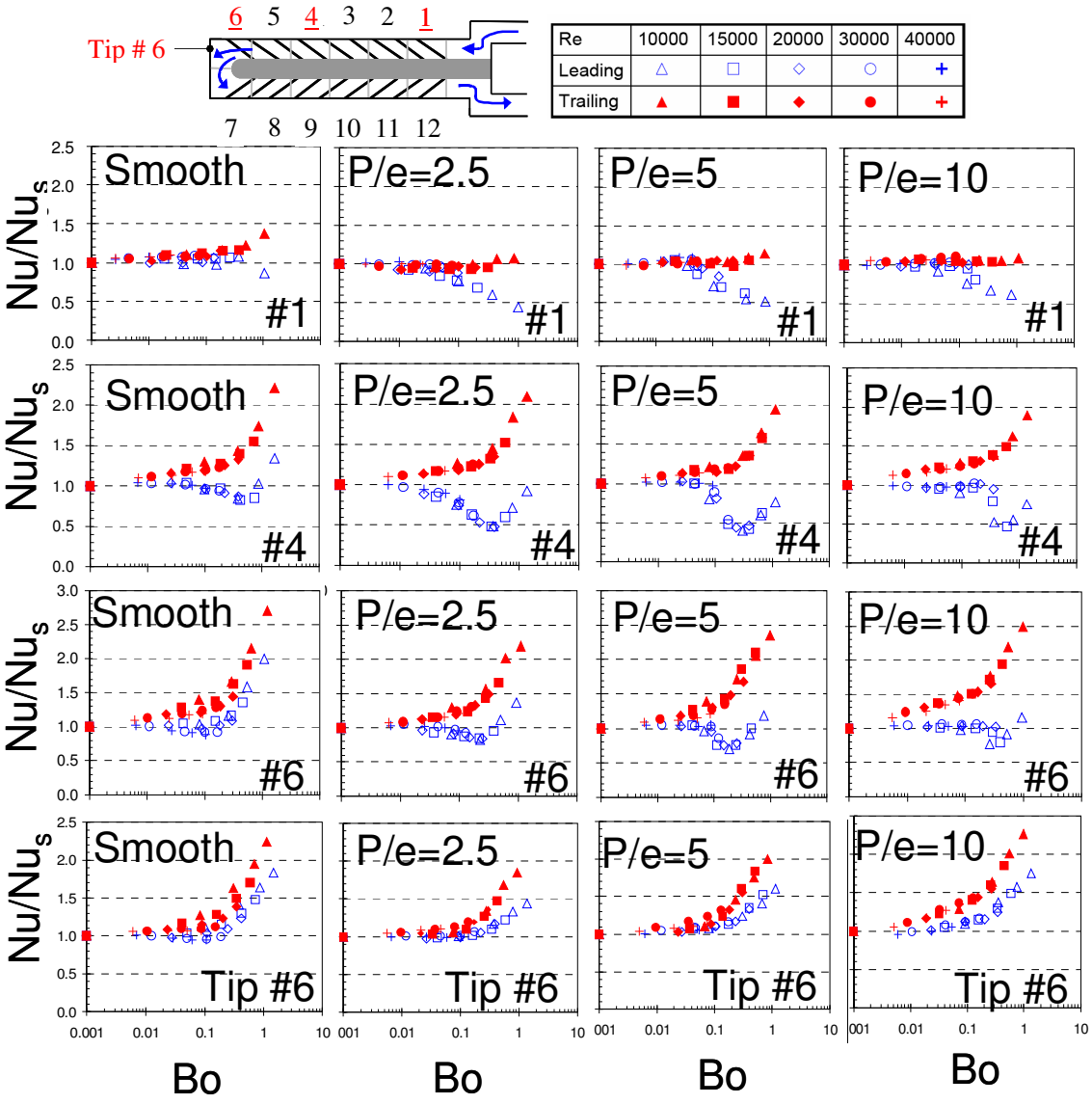

Figure 32: Nu/Nu_s ratio distribution as a function of local buoyancy parameter in first pass for smooth and ribbed cases.

Figure 32 also shows the effect of Bo at region four. Region four is the location at which the effect of the entrance and the turn are the smallest in the first pass. The trailing surface Nu/Nu_s ratios for all P/e ratios and the smooth case show similar trends. As Bo increases the Nu/Nu_s ratios increase. Although effect of rotation is clearly less for the larger rib spacing of P/e = 10 when compared to the tight rib spacing of P/e = 2.5.

On the leading surface, for P/e = 2.5, the Nu/Nu_s ratios show a decrease starting at a small Bo of 0.02 whereas the P/e=5 case shows a decrease on the leading surface Nu/Nu_s ratios at a Bo of 0.1. The P/e=10 case does not show a decrease until a Bo of 0.3. All P/e cases show that the leading surface Nu/Nu_s ratios decrease until a critical Bo value is reached, after which the Nu/Nu_s ratios begin to increase. As mentioned previously this is due to the development of large-scale reverse flow cells. This trend is also observed in the smooth channel. However, note that for none of the ribbed cases does the leading surface Nu/Nu_s ratios increase above 1 at the highest Bo values, as is the case for the smooth channel.

In region 6, the trailing surface heat transfer is similar for the smooth case and ribbed cases. However, now the trend is reversed in regards to rotation effects. As P/e increases the effect of rotation also increases. For the P/e = 2.5 case, at the maximum Bo of 1, Nu/Nus ratio is approximately 2.2. For the P/e = 10 case the Nu/Nus ratio is 2.5.

The leading surface heat transfer enhancement for the smooth case is constant at 1 and then begins to increase. However, for the ribbed cases the leading surface heat transfer enhancement decreases to value of 0.6-0.8 and then increase.

In the first pass, tip region 6 (**Figure 32**), and in the second pass, tip region 7 (**Figure 33**), the flow is very turbulent due to the sharp 180^o turn. Direct impingement of the mainstream flow occurs on tip region 6. Heat transfer in this region is high due to this impingement. Although no ribs were placed on the tip region copper plates, only on the adjacent leading and trailing walls in the first and second pass, there seems to be a slight influence on tip cap heat transfer with change in P/e ratios. The effect of rotation on the tip 6 increases as the P/e ratio on the adjacent leading and trailing increases. For the P/e = 2.5 case, the Nu/Nus ratio is approximately 1.8. For the P/e = 10 case, the Nu/Nus ratio is more similar to the smooth case at 2.3. A similar argument can be made for the tip 6 leading surface as well.

Figure 33 shows the effect of the buoyancy parameter in second pass. In region 7, the heat transfer for the trailing surface and leading surface is similar for all ribbed cases. This may be due to the strong turbulence mixing that occurs as the flow changes direction around the turn. In region 9, the Nu/Nu_s ratios on the trailing surface for all ribbed cases and smooth case, are similar. The leading surface Nu/Nu_s ratios increase with an increase in Bo, for the smooth case. For all ribbed cases, the increase in Nu/Nu_s ratios due to rotation, on the leading surface is less than the smooth case in region 9.

Figure 33 also shows the Nu/Nu_s ratios in region 12. The trailing surface heat transfer for all cases, is very similar. On the leading surface, there is little difference between Nu/Nu_s ratios of the ribbed cases. However, all ribbed cases show much lower Nu/Nu_s ratios than the smooth case on the leading surface in region 12. In region 12 for P/e = 5 & 10, the leading surface heat transfer is always higher than the trailing surface

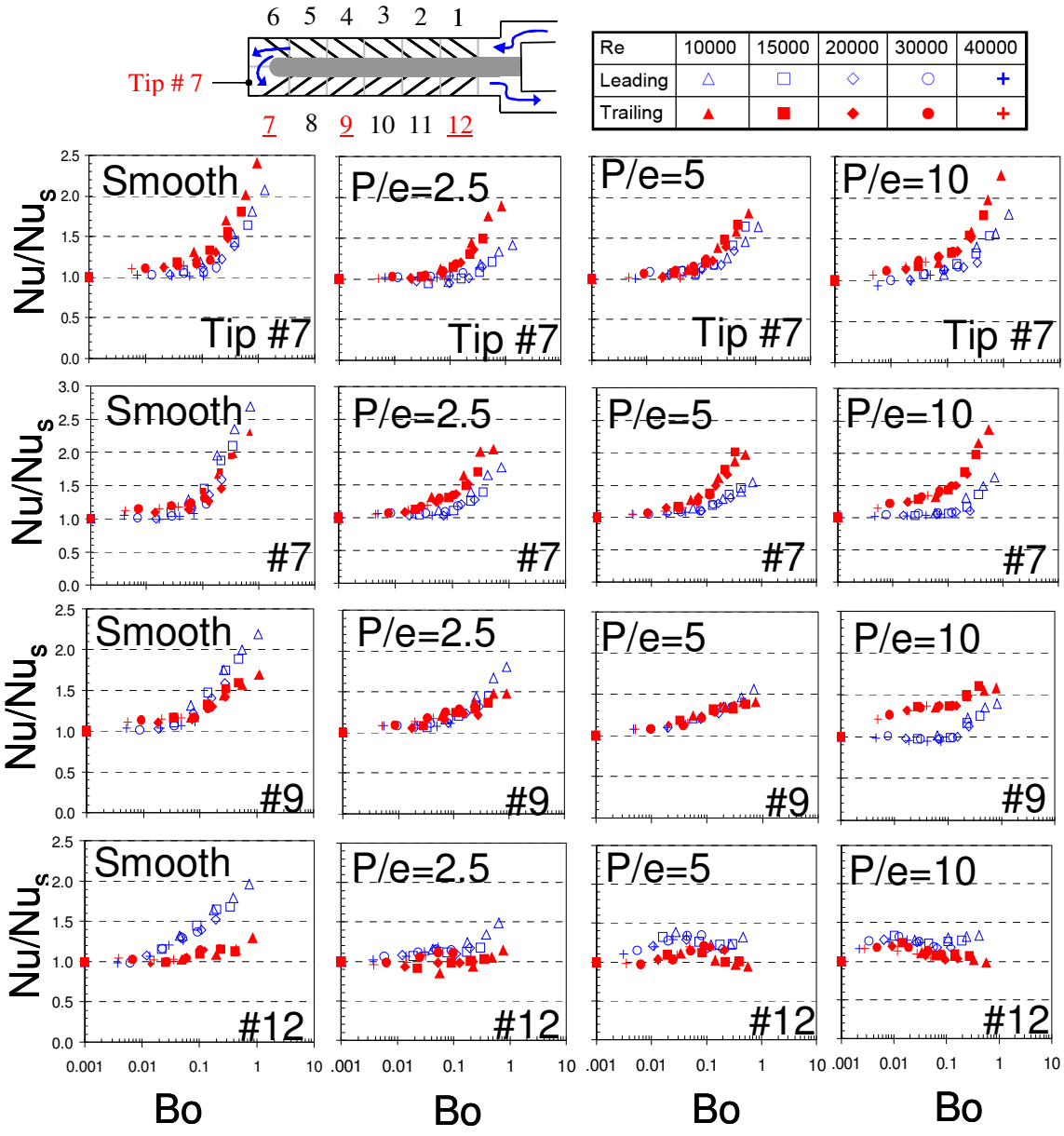

Figure 33: Nu/Nu$_s$ ratio distribution as a function of local buoyancy parameter in second pass for smooth and ribbed cases.

heat transfer. It appears that the data crosses, but actually the data converges slightly, but then diverges significantly.

4.1.2.7 *Pass Averaged Nusselt Number Ratios with Buoyancy Parameter Correlations*

In **Figure 34**, the average Nu/Nu_s ratios on the leading and trailing surface in the first pass and second pass, as a function of Bo, for the smooth and ribbed cases, are presented. The average Nu/Nu_s ratios are for the six copper plates on each surface (leading, trailing) in each pass (1^{st} & 2^{nd}). For the P/e = 10 case, the current study is compared to that of Fu et al. [13], which had a fully developed entrance condition. The strong entrance condition of the current study dominates over the effects of rotation as can be seen on the leading surface average Nu/Nu_s ratios for the P/e = 10 case. A decrease in Nu/Nu_s ratios is not observed until a Bo of 0.3 for the current study, whereas the fully developed case (Fu et al. [13]) shows a decrease earlier at a Bo of 0.1. For the trailing surface, there is not much difference in Nu/Nu_s ratios between the fully developed case and the sharp bend entrance for the P/e = 10 case. For the smooth case, a clear difference is seen on the trailing surface between the fully developed condition Fu et al. [13] and the sharp bend entrance condition.

The second pass averaged Nu/Nu_s ratios for the smooth and ribbed cases are also shown in **Figure 34.** Comparing the P/e = 10 case to that of Fu et al. [13] shows that not much difference is seen. First of all, this shows that the entrance condition is not impacting the heat transfer in the second pass. Secondly, the data from the current study are reliable because the P/e = 10 data for the current study agrees with that of Fu et al. [13]. The data should agree because the same sharp 180^o turn is present in both studies.

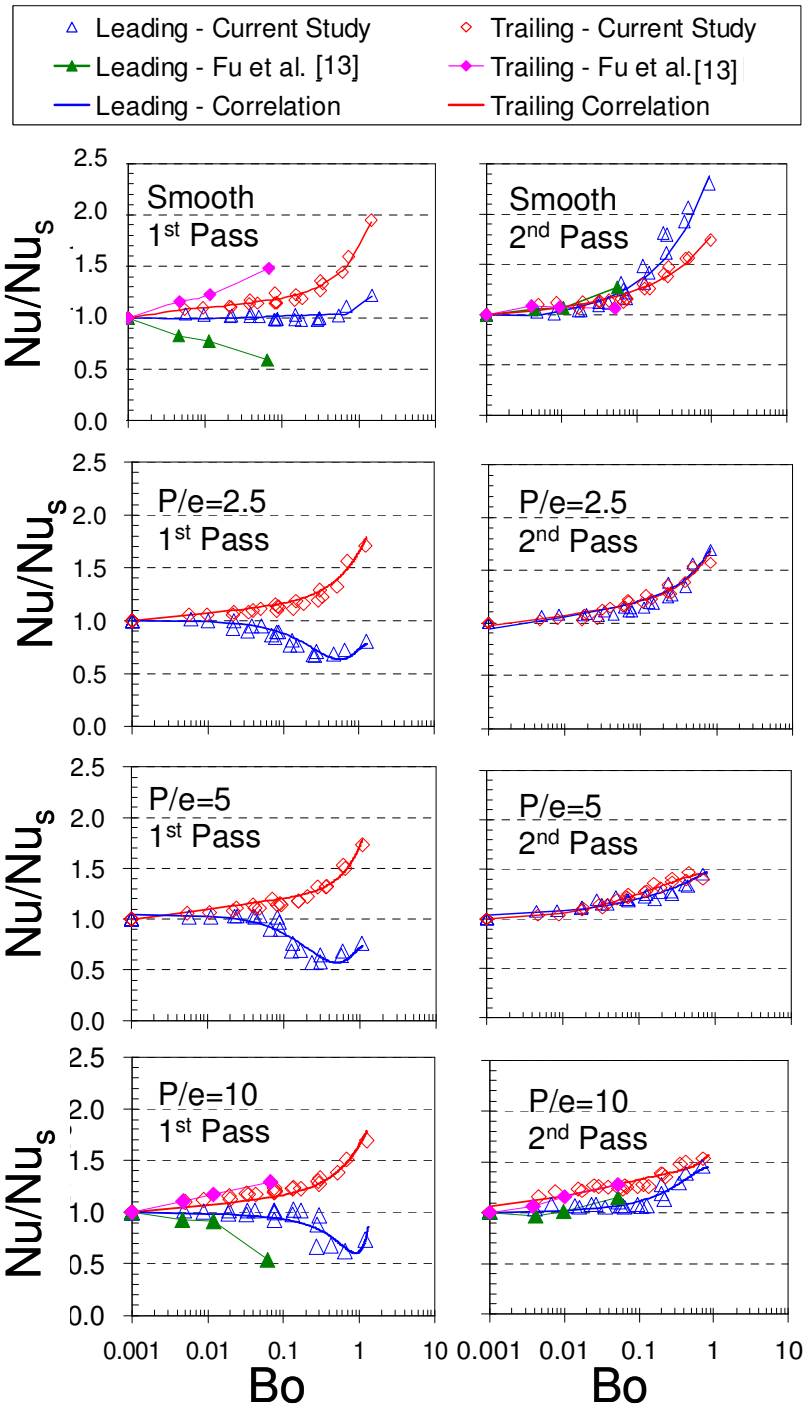

Figure 34: Average Nu/Nu_s ratios (6 points) on the leading and trailing walls in the first and second pass for smooth and ribbed cases.

The data in the current study have been correlated using a power law function as shown in equation (12).

$$Nu/Nu_s = A \cdot Bo^a + B \cdot Bo^b + C \cdot Bo^c + D \quad (12)$$

There is a discrepancy of +/-10% for P/e = 2.5 and +/- 7% for P/ e= 5 between the experimental data and the correlation on the leading surface in the first pass. For the P/e = 10 case, the correlation for the leading surface in the first pass has a discrepancy of +/-17%. However, the trailing surface in the first pass and both the leading and trailing surfaces in the second pass correlate very well and are within +/-9%. In **Table 3**, the coefficients and exponents that correspond to Eq. 12, for the smooth case and ribbed cases, are shown.

4.1.2.8 *Conclusions*

This study experimentally investigated the heat transfer in a rotating (90^o orientation) two pass, 1:4 AR channel, with parallel ribs on the leading and trailing surfaces in the first pass and second pass. The rib angle was held constant at 45^o. Square ribs with a height (e) of 1.59 mm were used and the e/D_h ratio was 0.078. The exhaustive testing matrix consisted of three P/e ratios: P/e = 2.5, 5, and 10. For each P/e ratio the Reynolds numbers tested were 10000, 15000, 20000, 30000, and 40000. For each Reynolds number, five rotational speeds were considered: 0,100, 200, 300, and 400 rpm. The test section had a sharp bend entrance and thus the flow at the test section entrance was not fully developed. Comparisons have been made to a smooth case 1:4 AR channel with a fully developed entrance and a sharp bend entrance. From the research work

Table 3: Coefficients and Exponents for Nu/Nu_s Correlations for Rib Spacing

(T=Trailing, L=Leading, 1=first pass, 2=second pass)

Smooth	**T2**	**T1**	**L2**	**L1**
A	1.21	1.23	1.20	1.04
B	0.57	0.44	1.25	0.19
C	0.00	0.00	0.00	0.00
D	0.00	0.00	0.00	0.00
a	0.03	0.03	0.04	0.01
b	0.69	1.20	0.75	5.60
c	0.00	0.00	0.00	0.00
P/e=2.5	**T2**	**T1**	**L2**	**L1**
A	1.29	1.30	1.33	-1.75
B	0.50	0.48	0.50	3.48
C	0.00	-0.19	0.00	-2.00
D	0.00	0.06	0.00	1.00
a	0.04	0.04	0.05	2.69
b	1.20	1.10	1.30	2.09
c	0.00	0.21	0.00	1.14
P/e=5	**T2**	**T1**	**L2**	**L1**
A	1.55	1.37	1.10	-2.21
B	-0.15	0.47	0.40	4.58
C	0.11	-0.20	0.14	-2.70
D	-0.07	0.09	-0.11	1.05
a	0.13	0.06	0.04	2.71
b	2.00	1.60	0.49	1.99
c	-0.20	0.30	-0.11	1.06
P/e=10	**T2**	**T1**	**L2**	**L1**
A	3.30	1.30	-1.60	1.42
B	-5.00	0.48	1.51	-1.55
C	2.34	-0.19	0.52	-0.25
D	1.00	0.06	1.00	1.00
a	1.15	0.04	2.10	2.80
b	0.90	1.10	1.85	2.30
c	0.51	0.21	0.70	0.60

performed in this study, the following observations and conclusions were made:

1. For the stationary case, the channel averaged Nu_s/Nu_o ratio is highest for the P/e = 2.5 case based on the projected area. When the channel averaged Nu_s/Nu_o ratio is based on the total area, the P/e = 10 case has the highest Nu_s/Nu_o ratios.

2. Near the entrance (region 1), the effect of the sharp bend entrance dominates over the rotation effects on the trailing surface regardless of whether the wall is ribbed or smooth. However, for the leading surface, for all P/e ratios, the effects of rotation dominate over the entrance condition when Bo is greater than 0.1.

3. The heat transfer, for all P/e ratios and the smooth case, on the trailing wall in the first pass, increases with an increase of Ro. For the ribbed cases, the leading surface in the first pass, initially shows a decrease in Nu/Nu_s ratios to a value of 0.5 until a critical Ro value of 0.3 is reached. Afterwards, the heat transfer begins to increase on the leading surface.

4. In the second pass, the trailing surface Nu/Nu_s ratios increase by approximately 50% at the highest Ro for all P/e ratios. For the leading surface, increasing the rib spacing causes the effect of rotation to decrease.

5. In the tip portion, the Nu/Nu_s ratios increase with Ro and Bo. Little difference is seen between the smooth case and all ribbed cases.

6. The rotation number and buoyancy parameter have been extended to values of 0.65 and 1.5 respectively. Bo correlations developed in this study show that the buoyancy parameter can be used in the higher range to satisfactory levels of accuracy to predict the effects of rotation (Nu/Nu_s).

4.1.3 Rib Height Effects

The ratio of rib height (e) to channel height (H) is called the blockage ratio (e/H). Kim et al. [41] explained that by increasing the ratio, flow is accelerated over the ribs, producing higher heat transfer levels. In that study, the blockage ratio was changed by decreasing the channel height H. The channel hydraulic diameter D_h was kept constant. In the current study, the channel height is kept constant along with the channel hydraulic diameter. The blockage ratio is increased by increasing the rib height (e). What is not clear yet, is if the doubling of the blockage ratio, in the narrow aspect ratio channel, will alter the heat transfer.

4.1.3.1 *Stationary Streamwise Nusselt Number Ratios*

When the channel is not rotating, the flow complexity is reduced because of the absence of the Coriolis force and rotational buoyancy effect. However, the rib effects are still present. These effects were previously stated to be mainstream flow separation, recirculation, reattachment, turbulent mixing, and angled secondary flow. To investigate the effects of the ribs on heat transfer in the stationary channel, comparisons are made to the smooth results as shown in **Figure 35**. The stationary Nusselt number (Nu_s) is normalized by the Nusselt number for smooth, fully developed, stationary round pipe (Nu_o). From this figure, a few important observations are made.

The heat transfer is greatly enhanced by the strong entrance condition for the smooth case and the ribbed cases. This is seen by the large Nu_s/Nu_o ratios for $x/D_h=0.625$. These high Nu_s/Nu_o ratios are a result of a very thin boundary layer. The

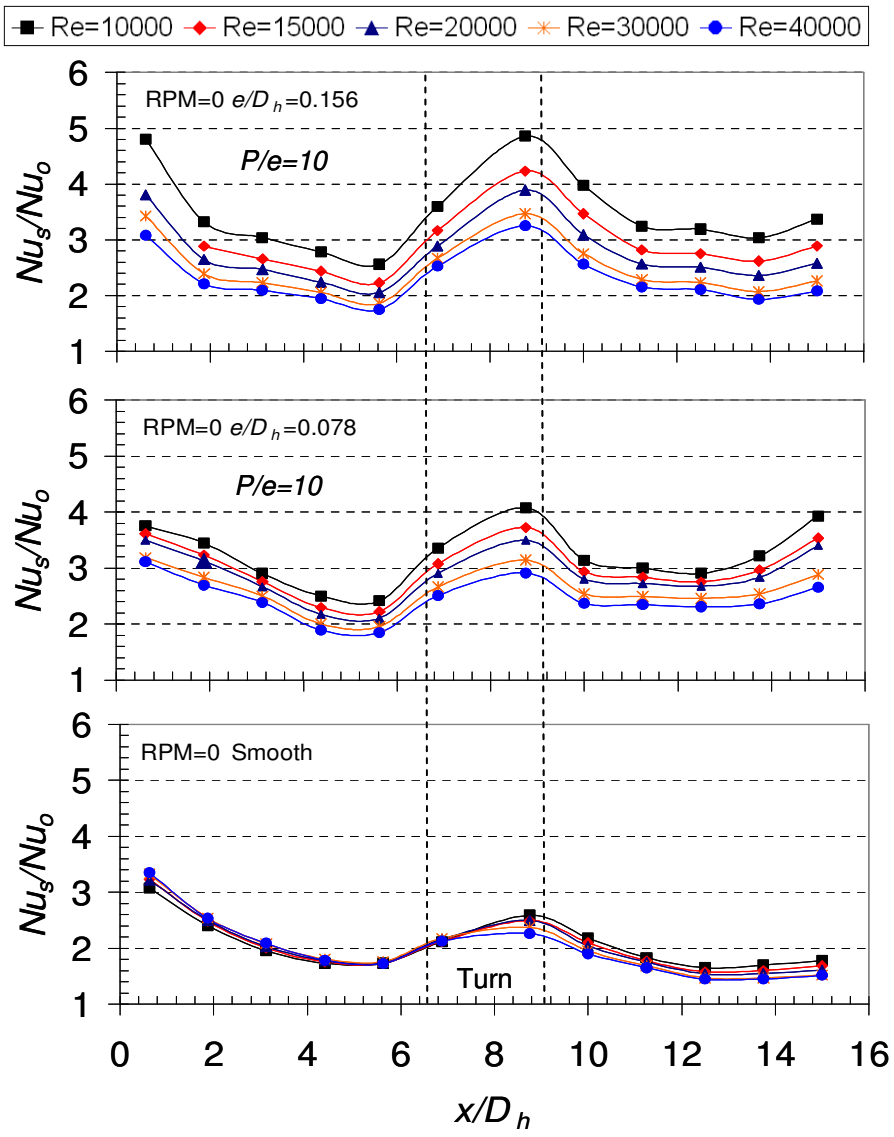

Figure 35: Stationary streamwise Nu ratio (Nu_S/Nu_o) distribution at different Reynolds numbers for the ribbed cases (e/D_h=0.156, e/D_h=0.078) and smooth.

e/D_h=0.156 case shows the highest Nu_s/Nu_o of 4.8 at the entrance for a Reynolds number of 10000. One point to focus on is the effect of the ribs on the entrance effect. At a Reynolds number of 40000, the smooth case and the e/D_h=0.078 case have remarkably similar values between x/D_h=1.9 and x/D_h=4.375. The Nu_s/Nu_o ratios continually decrease until x/D_h=4.375. For the e/D_h=0.156 case (at Re=40000) the Nu_s/Nu_o ratios are nearly constant at 2.0. From these observations one can conclude that the effect of the entrance is stronger in the smooth channel when compared to the larger blockage ratio of 15.6%.

Another interesting observation is the large effect of the Reynolds number on the Nu_s/Nu_o ratios for the ribbed cases. As the Reynolds number increases, the heat transfer enhancement (Nu_s/Nu_o) continually decreases for a fixed x/D_h. Although the Reynolds number effect seems to be stronger for the e/D_h=0.156 case.

In the turn portion of the channel, the Nu_s/Nu_o ratios are high due to the turn effect. The flow is also increasing in turbulence in the turn portion as described by Liou and Chen [9] . In their 1.25 aspect ratio channel the turbulent kinetic energy increased from 1% in the region prior to the turn to 24% just after the turn in the second pass. The Nu_s/Nu_o ratios for the ribbed case is clearly greater than the smooth channel in the turn region. Once again, the e/D_h=0.156 case shows the highest Nu_s/Nu_o ratio of about 4.9 in the turn at a Reynolds number of 10000. At a Reynolds number of 40000, both ribbed cases have very similar Nu_s/Nu_o ratios of about 3 at x/D_h=8.9. The smooth case has an Nu_s/Nu_o ratio of about 2.2 at the same location.

In the second pass, when x/D_h is greater than (or equal to) 11.25, the Nu_s/Nu_o ratios remain mostly constant for both the ribbed cases and smooth case, until the exit of the channel is reached at x/D_h=15. The mostly constant Nu_s/Nu_o ratios are due to the re-development of the boundary layer.

4.1.3.2 *Rotating Streamwise Nusselt Number Ratios*

The flow in the heated rotating ribbed channel is quite complex. The Coriolis induced secondary flow along with the rotation induced buoyancy force, combined with the presence of angled rib induced secondary flow, are what make the flow in the channel so interesting. The combined influence on the Nu/Nu_o ratios, from all of the aforementioned effects, is presented in **Figure 36** for the e/D_h=0.156 case. In this figure, the rotational speed is increased systematically and the streamwise Nu/Nu_o ratio distribution for the leading and trailing surfaces, with ribbed walls, at a Reynolds number of 10000 and 20000 is shown.

One observation made immediately is the interesting occurrence on the leading surface, in the first pass (x/D_h<6.875), at a Reynolds number of 10000. No difference is seen in the Nu/Nu_o ratios for the stationary case and the 100 rpm case. However, for the case of 200 rpm, the Nu/Nu_o ratio is reduced significantly. Furthermore, as the rotational speed is increased to 300 rpm and 400 rpm, an interesting phenomenon occurs. The Nu/Nu_o ratios begin to increase in the streamwise direction for x/D_h>1.9. It is worth noting that at a Reynolds number of 20000, no decrease is seen in the heat transfer levels until the rotational speed is greater than 300 rpm. Also noted is that the heat transfer levels decrease in the streamwise direction for all rotational speeds.

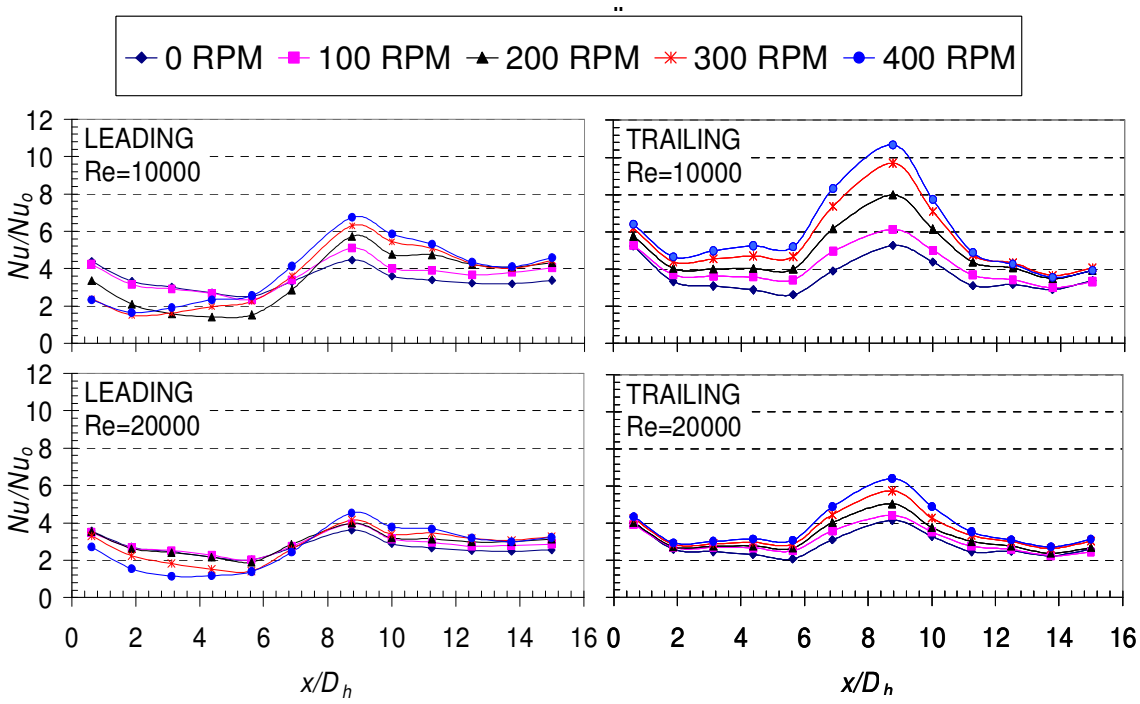

Figure 36: Streamwise Nu ratios (Nu/Nu_o) distribution at Re=10000 and Re=20000 for the leading and trailing wall at different rotational speeds for e/D_h=0.156.

The trend of the Nu/Nu_o ratios on the trailing surface in the first pass is very different compared to that of the leading surface. For a given x/D_h value, as the rotational speed is increased, (for both Reynolds numbers) the Nu/Nu_o ratios increase. However, this increase is much smaller for the larger Reynolds number case. Of note is also the large heat transfer enhancement in the turn portion on the trailing surface at x/D_h=8.9. The Nu/Nu_o ratio increases from about 4.9 (stationary) to nearly 11 at 400 rpm.

In the second pass, for an $x/D_h > 11.25$, and a fixed Reynolds number and rpm, little difference is seen in the Nu/Nu_o ratios levels between the leading and trailing surfaces. This was not the case for the smooth channel (see **Figure 30**, smooth case) in which a clear difference was observed.

4.1.3.3 *Rotation Number Effects*

The rotation number (Ro) is the ratio of the Coriolis force to the bulk inertial force. From the definition of the rotation number, the same rotation number can be reached by various combinations of rotational speed and fluid bulk velocity. It is vital to show that the rotation number holds valid and can be used to predict heat transfer over an extended range. In **Figure 37**, the effect of rotation on heat transfer (Nu/Nu_s) is shown as a function of the rotation number in various regions in the first pass and second pass. The stationary Nusselt number (Nu_s) was chosen as the denominator so that the effects of rotation can be clearly visible.

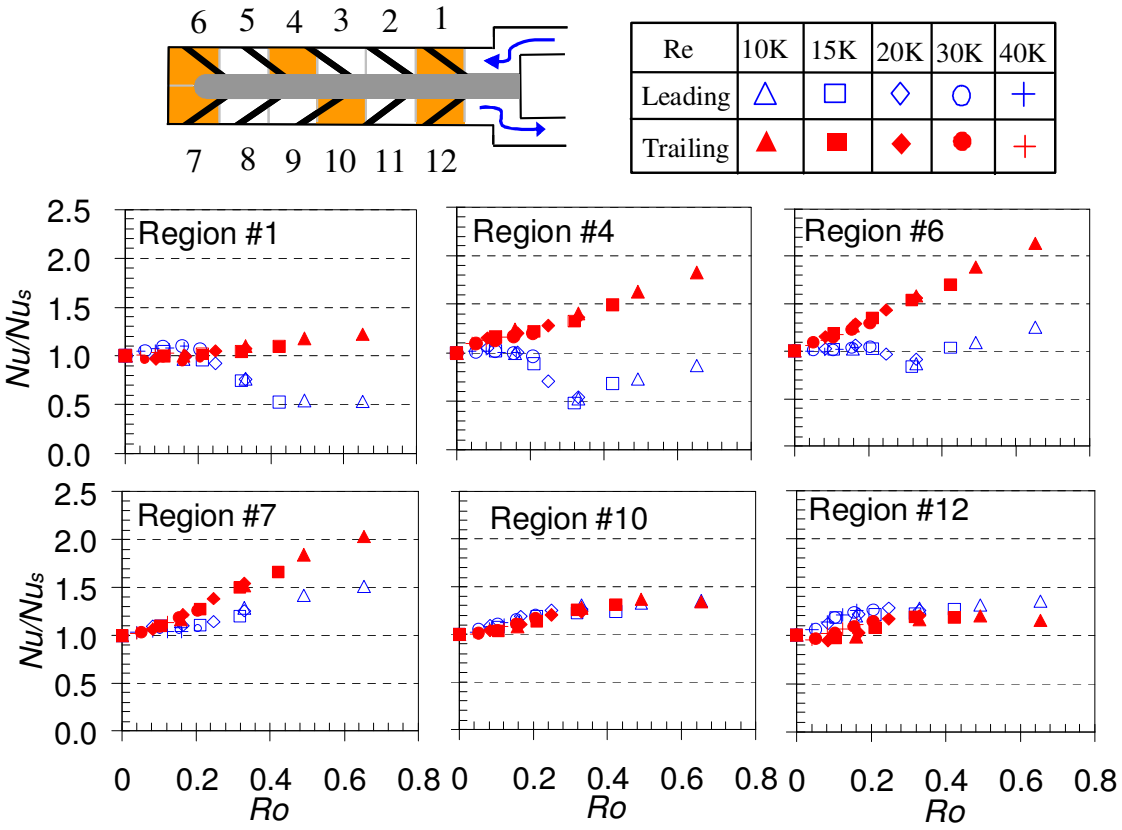

Figure 37: Regional leading and trailing surface Nu ratios (Nu/Nu_s) as a function of rotation number (Ro) for e/D_h=0.156.

In the first pass, the Coriolis force skews the mainstream flow towards the trailing wall because the flow is radially outward. Thus, higher velocities are experienced near the trailing wall region. The velocity of the fluid near the leading surface is reduced. One observation that stands out is how the Nu/Nu_s ratios on the trailing surface in region 1 are essentially not affected by rotation. This is due to the strong entrance condition which already serves to provide a high level of heat transfer. However, the leading surface in region 1, experiences a severe degradation in heat transfer enhancement levels (Nu/Nu_s=0.5) with an increase in the rotation number. This finding is extremely important for the gas turbine designer. A 50% reduction of heat transfer in the rotating frame is important because so much of the cooling passage design is based upon stationary measurements. In regions 4 and 6, it is clear that the entrance condition is no longer dominating the heat transfer on the trailing surface. Rather, as the rotation number increases, the trailing surface experiences great heat transfer enhancement due to rotation and reach values of around Nu/Nu_s=2.0.

The leading surface Nu/Nu_s ratio trend is quite different from the trailing in regions 4 and 6. In region 4, the leading surface Nu/Nu_s ratios decrease to Nu/Nu_s=0.5 with an increase in rotation number until a critical rotation number of 0.3 is reached. The Nu/Nu_s ratios then begin to increase due to the development of large-scale reverse flow cells as reported by Wagner et al.. [6] and Su et al. [33]. In region 6, the decrease in Nu/Nu_s ratios on the leading surface is not as severe and only slightly falls below the stationary case. This is mostly due to the high turbulent mixing which occurs in the turn portion.

In region 7, both the leading and trailing surfaces experience an increase in Nu/Nu_s ratios as the rotation number increases. The trailing surface heat transfer enhancement occurs at a more rapid rate compared to the leading. Little difference is observed in the Nu/Nu_s ratios between the trailing and leading surfaces in region 10. The effect of rotation in this region is reduced and an increase in Nu/Nu_s ratios on both surfaces is about 30% for the highest rotation number reached. When considering these results for gas turbine applications, the reader is reminded that for gas turbines, an increase of 30% in heat transfer is a large amount. In region 12, the Nu/Nu_s ratios on the trailing surface still increase slightly with rotation, but the effect of rotation is even less when compared to region 10. On the leading surface in the region 12, rotation again increases the heat transfer by about 30%. Thus there is little difference between the effect of rotation in region 10 and region 12 on the leading surface.

Although ribs are not placed on the tip cap of the channel, it is interesting to determine how the effects of rotation impact the heat transfer levels in this region. Furthermore, a question that arises is if the adjacent ribbed walls will have an impact on the Nu/Nu_s ratios in the tip region. **Figure 38** compares the heat transfer enhancement due to rotation for two different blockage ratios and the smooth channel condition. From this figure, the effect of rotation seems to be quite similar for all three cases in tip region 6 for both the leading and trailing surfaces. For all three cases, the trailing surface Nu/Nu_s ratios are higher than the leading surface. Also, for all three cases the maximum trailing Nu/Nu_s ratios are 2.25 and the leading Nu/Nu_s ratios are about 1.75 to 1.85. That is to say, the heat transfer in the rotating frame is about 75% to 125% of the stationary

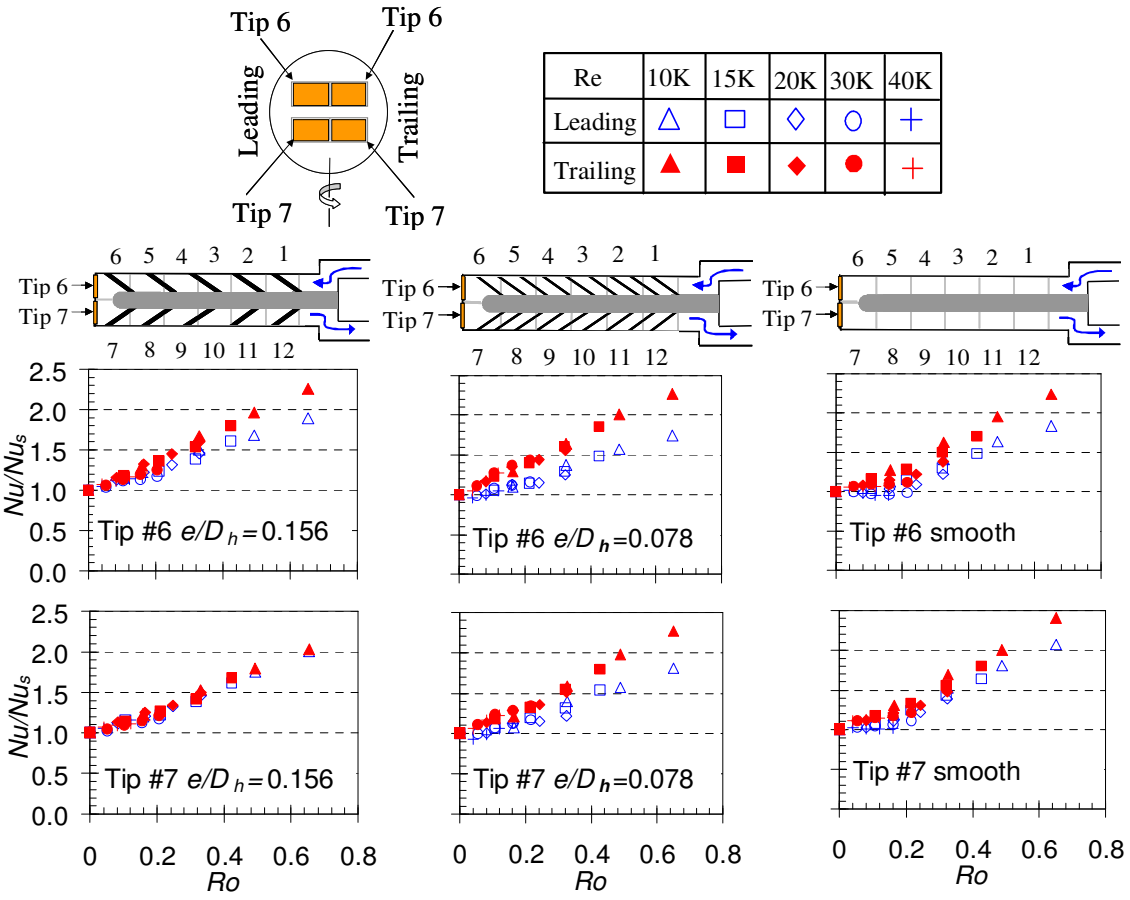

Figure 38: Comparison of regional tip Nu ratios (Nu/Nu_s) as a function of rotation number (Ro) for e/D_h=0.156, e/D_h=0.078 and smooth adjacent leading and trailing walls.

case. In tip region 7, the smooth channel and the e/D_h=0.078 case again show very similar trends and the effect of rotation is nearly the same for theses two cases. The maximum Nu/Nu_s ratio for the trailing surface in these two cases again reaches to about 2.25 to 2.4 or nearly 140% of the stationary case. The leading surface maximum Nu/Nu_s ratio for the e/D_h=0.078 case is lower than the smooth case. However, when the blockage ratio is increased to e/D_h=0.156, it is seen that the leading and trailing tip cap surfaces exhibit nearly identical Nu/Nu_s ratios for both the leading and trailing tip cap surfaces. These high Nu/Nu_s ratios in tip region show the gas turbine designer that rotational heat transfer enhancement is large at the tip portion.

4.1.3.4 *Buoyancy Parameter Effects*

By heating the walls of the test section, a temperature gradient develops in the fluid from the fluid core to near the wall surface. This temperature gradient results in a variation of the density in the fluid. This density difference and the centrifugal force induced by rotation, result in a rotation induced buoyancy force. The combined effects of temperature and rotation on the heat transfer are realized by investigating how the Nu/Nu_s ratios vary with a change in the buoyancy parameter. In **Figure 39**, the effects of the buoyancy parameter on the leading and trailing surfaces Nu/Nu_s ratios in the first pass are shown. The first thing to notice is the behavior of the Nu/Nu_s ratios on the trailing surface. At the entrance (region 1) the heat transfer levels on the trailing surface are only so slightly affected by an increase in the buoyancy parameter. However, notice how the trend of the Nu/Nu_s ratios on the trailing surface becomes more and more dependant on the buoyancy parameter in the streamwise direction. This is observed by

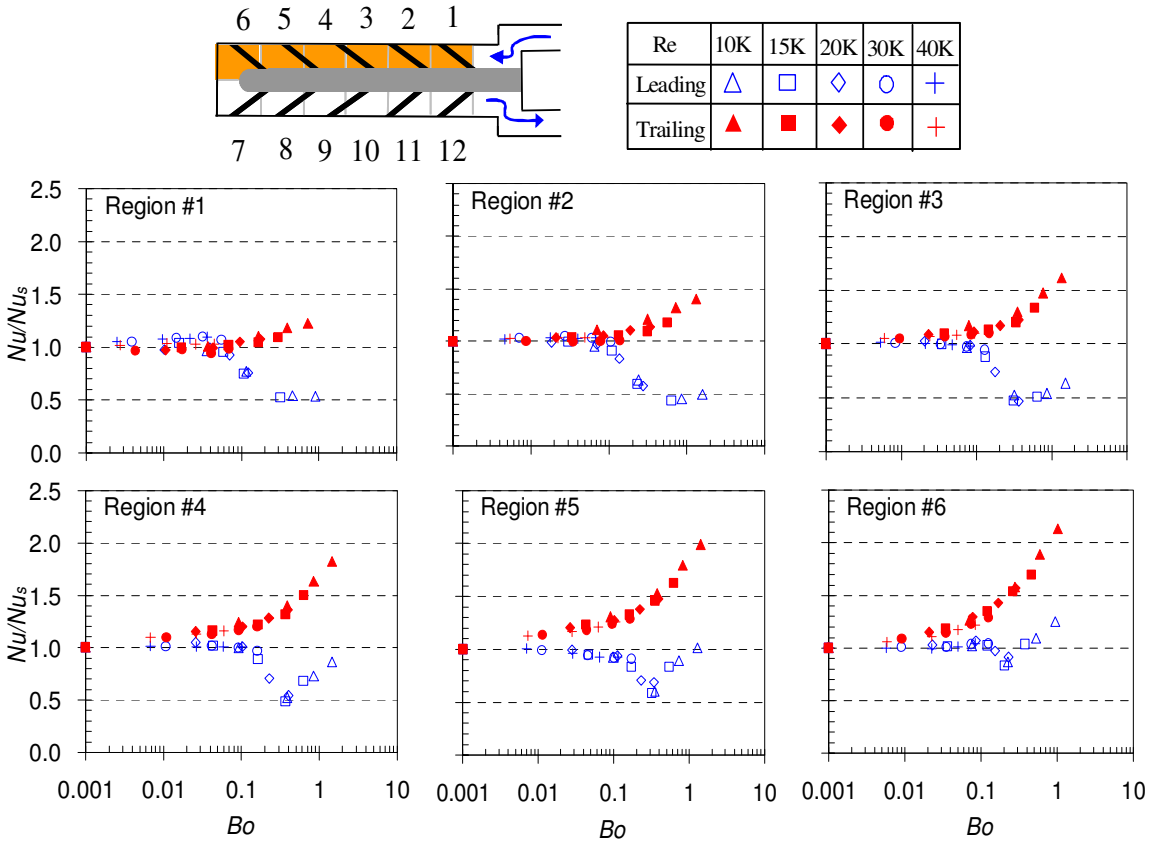

Figure 39: Regional leading and trailing surface Nu ratios (Nu/Nu_s) in the first pass as a function of buoyancy parameter (Bo) for e/D_h=0.156.

noticing that an increase in Nu/Nu_s ratios begins to occur at smaller and smaller buoyancy parameter values as you move along in the streamwise direction. The heat transfer on the leading surface also exhibits an interesting behavior. First of all, a decrease in Nu/Nu_s ratios on the leading surface does not occur until a buoyancy parameter value great than 0.1. The Nu/Nu_s ratios on the leading surface decrease to a very low level of 0.5 from region 1 to region 5. That is to say, heat transfer is reduced by 50%, which is significant in gas turbine applications since mostly stationary experimental values are used in gas turbine cooling passage design. In regions 3 through 6, it is seen that a critical buoyancy parameter value is reached (Bo=0.2-0.3) when the Nu/Nu_s ratios begin to increase with an increase of the buoyancy parameter. This is due to the development of large scale reverse flow cells as mentioned previously.

In the second pass of the test section, the mainstream flow direction is reversed. Because the flow is radially inward, the centrifugal force and the inertial force of the flow are counteracting. Due to this, the velocity profile in the second pass becomes more uniform as compared to the first pass velocity profile. In the first pass, the velocity profile is skewed towards the trailing surface. This is why such a stark difference was observed in heat transfer levels on the leading and trailing surfaces. With this in mind, it is expected that there would not be such a stark contrast in Nu/Nu_s ratios between the leading and trailing surfaces in the second pass, especially after the turn region. In fact, this is the case as seen in **Figure 40**. In this figure, the second pass regional heat transfer enhancement levels on the leading and trailing surfaces are shown as a function of the buoyancy parameter. The first thing that is noticed is that indeed in the turn portion

(region 7), a noticeable difference in Nu/Nu_s ratios is seen between the leading and trailing surfaces. Both the leading and trailing surfaces increase in heat transfer with an increase in the buoyancy parameter. The increase is greater on the trailing surface with Nu/Nu_s ratios of about 2.0, compared to Nu/Nu_s ratios of 1.5 for the leading surface. This is not to be misunderstood as insignificant since an increase of 50% to 100% is large for gas turbine applications.

However, moving along in the steamwise direction downstream from turn, clearly the difference between the leading and trailing surface Nu/Nu_s ratios becomes less and less. From region 7 through region 9, the leading surface Nu/Nu_s ratios remain constant at approximately 1.5 at the maximum buoyancy parameter value of 1.5. On the other hand, the trailing Nu/Nu_s ratios show a continual decrease from region 7 (Nu/Nu_s=2.0) through region 9 (Nu/Nu_s=1.5), at which point both the leading and trailing surface exhibit nearly identical levels of Nu/Nu_s ratios. In regions 10 through 12, the leading surface Nu/Nu_s ratios have fallen to about 1.25 at the maximum buoyancy parameter value. The trailing surface Nu/Nu_s ratios continue to drop from region 10 through region 12. In region 12, the Nu/Nu_s ratios of the trailing surface have fallen below the leading surface Nu/Nu_s ratios; albeit, the difference is small.

One important distinction to make about the heat transfer in the second pass for both the leading and trailing surfaces is that at no point does rotation reduce heat transfer. Rather, rotation is always increasing heat transfer over the stationary case. Whereas, in the first pass, the leading surface heat transfer was reduced by 50% and the trailing surface heat transfer was doubled due to rotation in certain regions.

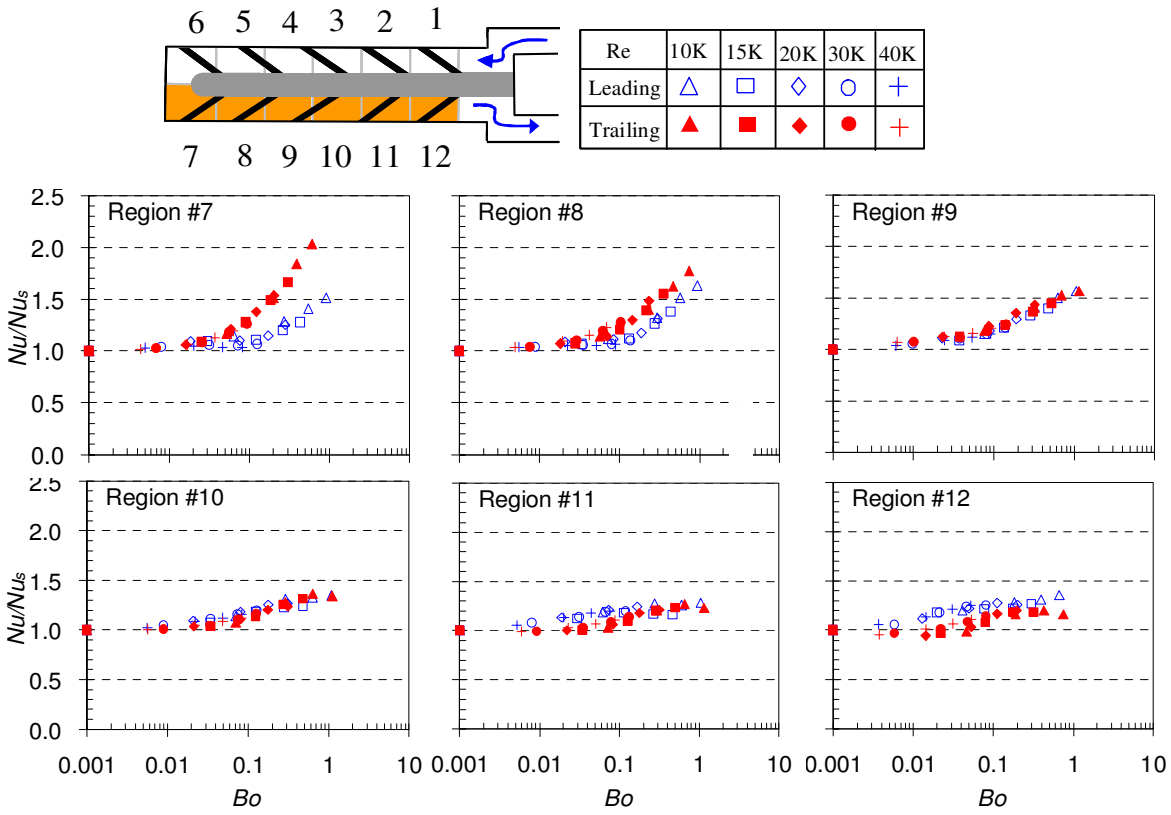

Figure 40: Regional leading and trailing surface Nu ratios (Nu/Nu_s) in the second pass as a function of buoyancy parameter (Bo) for e/D_h=0.156.

4.1.3.5 *Pass Averaged Nusselt Number Ratios with Buoyancy Parameter Correlations*

It is advantageous for designers of gas turbine blades to have a trustworthy method by which the internal heat transfer in rotating blades can be predicted within an acceptable margin of error. The buoyancy parameter has been the preferred method to predict heat transfer levels for rotating conditions. However, to fully depend on the buoyancy parameter, it must be shown that this parameter is not limited to only a small range of values and that it is applicable to smooth and ribbed channels. For this reason, the buoyancy parameter has been extended into a larger domain in this study. The maximum buoyancy parameter reached in this study was Bo=1.5. Not only was the range of the buoyancy parameter extended, but to prove that this parameter is useful to predict the effect of rotation on heat transfer, correlations have been developed in the extended range. To generate these correlations, the leading surface average and the trailing surface average of the Nu/Nu_s ratios in each pass was plotted as a function of the buoyancy parameter as shown in **Figure 41**. The stationary Nusslet number (Nu_s) was chosen as the denominator so that the effects of rotation can be seen.

The importance of this figure is clear when considering the averaged Nu/Nu_s ratios on the leading surface in the first pass. The two ribbed cases show a very different trend when compared to the smooth case. The averaged Nu/Nu_s ratios on the leading surface for the smooth case are not affected by the buoyancy parameter until the maximum buoyancy parameter value of almost 2.0. This is due to the strong entrance effect. The two ribbed cases show nearly similar Nu/Nu_s ratios trends on both the leading

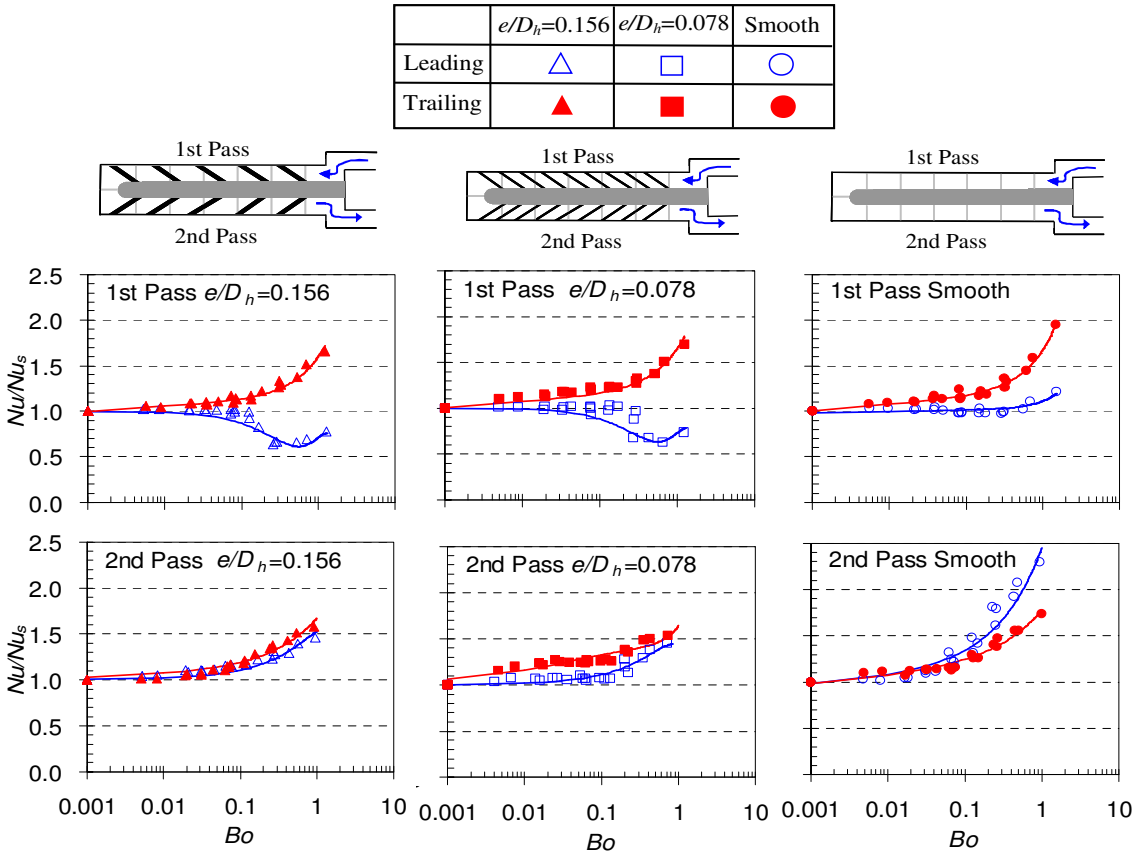

Figure 41: Comparison of first pass and second pass average leading and trailing surface Nu ratios (Nu/Nu_s) as a function of buoyancy parameter (Bo) for e/D_h=0.156, e/D_h=0.078), and smooth cases.

and trailing surfaces in the first pass. This implies that the effect of rotation for both blockage ratios (e/D_h) compared in this study is the same; this lack of difference may be due to the large distance between the leading and trailing surfaces in the 1:4 aspect ratio channel.

Another point to make is that the presence of the ribs on the leading surface in the first pass diminish the effect of the entrance. This statement is drawn from the observation that the averaged Nu/Nu_s ratios drop to a value of nearly 0.5 for the ribbed cases, whereas the averaged Nu/Nu_s ratios for the smooth case stay nearly constant at 1.0 and actually increase at the highest buoyancy parameter value. Contrarily, the averaged Nu/Nu_s ratios on the trailing surface in the first pass do not seem to be altered by the presence of the ribs.

In the second pass, the averaged Nu/Nu_s ratios for the ribbed cases again are similar to each other in that the effect of rotation is reduced when compared to the smooth channel. For both ribbed cases, the averaged Nu/Nu_s ratios on the leading and trailing surfaces are about 1.5 at the maximum buoyancy parameter. However, the smooth case, the leading surface shows a stronger dependence on rotation and a maxi-

mum averaged Nu/Nu_s ratio of 2.25 is reached at the highest buoyancy parameter. Also notice that a clear difference in averaged Nu/Nu_s ratios on the leading and trailing surfaces is seen for the smooth channel. For the e/D_h=0.078 case the difference in averaged Nu/Nu_s ratios between the trailing and leading surface decreases. Finally, for the e/D_h=0.156 case, it is seen that the averaged Nu/Nu_s ratios for the leading and trailing surfaces is nearly identical. **Figure 41** also shows the correlations for each ribbed case and the smooth case. The power law function used to correlate the data is shown in equation (13). The corresponding coefficients and exponents for the three different cases are listed in **Table 4**.

$$Nu/Nu_s = A \cdot Bo^a + B \cdot Bo^b + C \cdot Bo^c + D \tag{13}$$

The discrepancy between experimental and predict values of averaged Nu/Nu_s ratios for the current study was +/-12% for the leading surface and +/-7% for the trailing surface in the first pass. In the second pass the leading surface had a discrepancy of +/-7% and the trailing +/-6%. The discrepancy for the other two cases are also shown in **Table 4**.

Table 4: Coefficients, Exponents and Discrepancy Values for Nu/Nu_s Correlations for Rib Height

(T=Trailing, L=Leading, 1=first pass, 2=second pass)

e/D_h=0.156	L1	T1	L2	T2
Discrepancy	**+/-12%**	**+/- 7%**	**+/- 7%**	**+/- 6%**
A	-1.73	1.25	-1.50	1.10
B	3.49	0.48	1.51	0.57
C	-2.05	-0.19	0.52	0.00
D	1.00	0.06	1.00	0.00
a	2.65	0.04	2.10	0.01
b	2.04	1.10	2.00	0.69
c	1.10	0.21	0.70	0.00
e/D_h=0.078	L1	T1	L2	T2
Discrepancy	**+/-16%**	**+/- 9%**	**+/- 8%**	**+/- 8%**
A	-1.75	1.30	-1.60	3.30
B	3.48	0.48	1.51	-5.00
C	-2.00	-0.19	0.52	2.34
D	1.00	0.06	1.00	1.00
a	2.69	0.04	2.10	1.15
b	2.09	1.10	1.85	0.90
c	1.14	0.21	0.70	0.51
Smooth	**L1**	**T1**	**L2**	**T2**
Discrepancy	**+/-5%**	**+/- 6%**	**+/- 15%**	**+/- 9%**
A	1.00	1.23	1.20	1.21
B	0.04	0.44	1.25	0.57
C	0.05	0.00	0.00	0.00
D	0.02	0.00	0.00	0.00
a	0.01	0.03	0.03	0.03
b	2.00	1.20	0.75	0.69
c	1.20	0.00	0.00	0.00

4.1.3.6 *Stationary Pass Averaged Results*

To further investigate the differences between the two ribbed cases and the smooth channel, the pass averaged stationary Nu_s/Nu_o ratios are plotted as a function of the Reynolds number as shown in **Figure 42**. In the first pass and second pass, it is seen that the Nu_s/Nu_o ratios for both blockage ratio cases decrease with an increase in Reynolds number. At a Reynolds number of 10K, the e/D_h=0.156 case has the highest Nu_s/Nu_o ratio in both the first pass and second pass. It seems then that at the low Reynolds number of 10K, the secondary flow of the taller rib (e/D_h=0.156) may be stronger compared to the shorter rib (e/D_h=0.078). In the first pass, for a Reynolds number of 15K or more, the two blockage ratios have nearly identical Nu_s/Nu_o ratios. This is due to the entrance of the channel. At a Reynolds number of 40000, all cases (both ribbed and smooth) show identical heat transfer levels. This further illustrates that the Reynolds number effect in ribbed channels. In the second pass, for a Reynolds number of 15K or more, the Nu_s/Nu_o ratios for the e/D_h=0.156 case are slightly less than the e/D_h=0.078 case.

Figure 42 also shows how the surface condition (smooth or ribbed) of the adjacent leading and trailing walls affects the Nu_s/Nu_o ratios on the tip cap. Tip 6, which is in the first pass, shows similar Nu_s/Nu_o ratios for all ribbed cases and smooth case for a Reynolds number of 15K or less. However, at the larger Reynolds numbers (20K-40K) the Nu_s/Nu_o ratios for the ribbed cases are below the smooth case. However, no difference in Nu_s/Nu_o ratios is seen between the two blockage ratios tested. A similar pattern is seen for tip 7 for a Reynolds number of 20K to 40K.

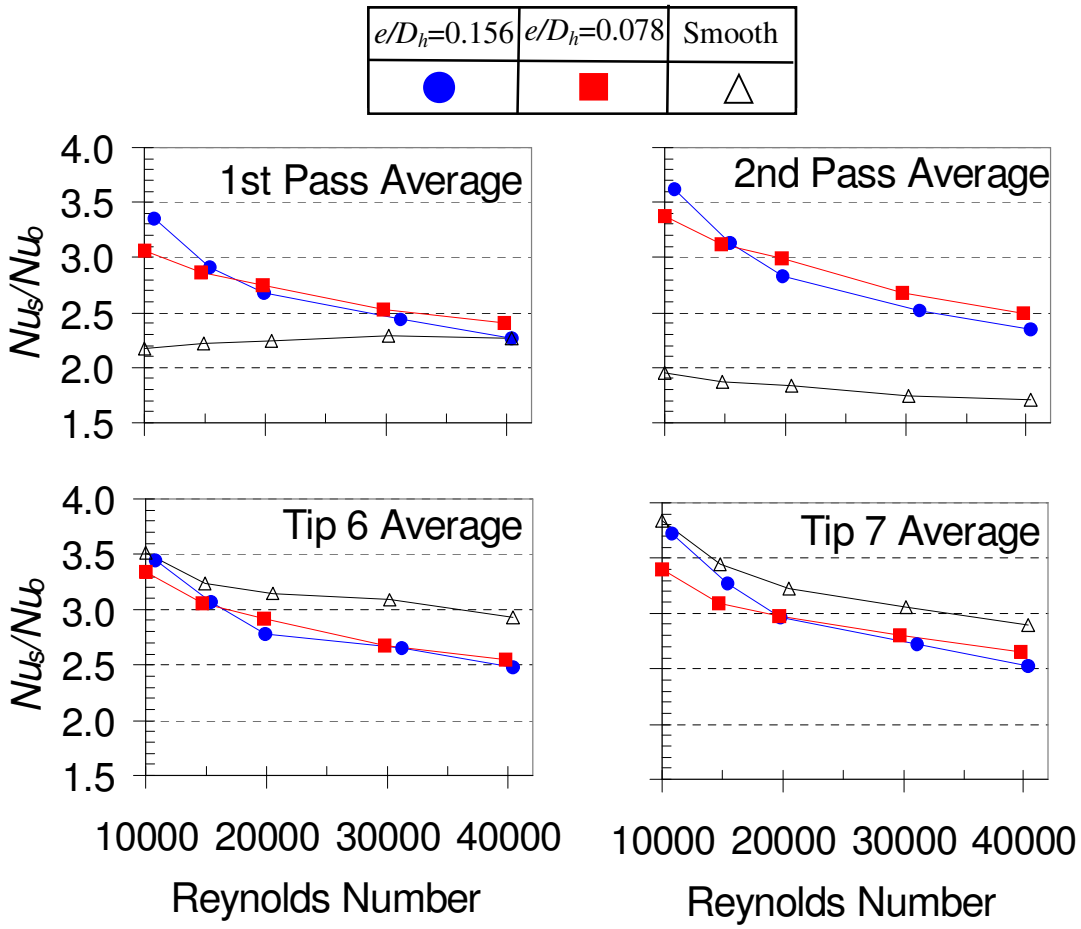

Figure 42: Comparison of stationary first pass, second pass and tip cap average Nu ratios (Nu_s/Nu_o) as a function of Reynolds number for e/D_h=0.156), e/D_h=0.078, and smooth cases.

4.1.3.7 *Conclusions*

In the current study, experimental heat transfer tests were performed in a 1:4 aspect ratio channel. Ribs were placed on the leading and trailing walls of the channel in both the first pass and second pass. Two different blockage ratios were tested. From this research, the following conclusions have been made:

1. The entrance effect dominates over the rotation effect on the trailing surface at the entrance region while the opposite is true for the leading surface.

2. The effect of rotation in the first pass (downstream from the entrance), serves to increase the heat transfer on the trailing surface significantly (Nu/Nu_s=2.0), and decrease the heat transfer on the leading surface significantly to values of Nu/Nu_s=0.5. A critical rotation number exists (Ro=0.3) after which an increase in heat transfer occurs on the leading surface.

3. The effect of rotation in the second pass (downstream of the turn) decreases. Only slight increases in the heat transfer on both surfaces are observed. The difference in Nu/Nu_s ratios between the leading and trailing surfaces is very small.

4. In the tip portion, the effect of rotation is to increase heat transfer for both the leading and trailing tip cap surfaces. In the stationary case, the adjacent ribbed walls caused a decrease in heat transfer compared to smooth.

5. The effect of rotation and stationary pass averaged results are very similar for both blockage ratios (e/D_h) compared in this study. This is due to the large distance between the leading and trailing surfaces, the sharp entrance and sharp 180^o turn.

6. The rotation number and buoyancy parameter have been extended to values of 0.65 and 1.5 respectively. The correlations developed in this study show that the buoyancy parameter can be used in the higher range to satisfactory levels of accuracy to predict the effects of rotation (Nu/Nu_s).

4.2 Heat Transfer in Smooth and Ribbed 2:1 Aspect Ratio Channels

4.2.1 Smooth Surface

4.2.1.1 *Stationary Nusselt Numbers and Entrance Geometry Effects*

The 2:1 aspect ratio test section consists of a sudden expansion from a circular tube to the rectangular cross section of the channel. As such, the heat transfer at the channel entrance is high since the hydrodynamic and thermal boundary layers are thin. **Figure 43** shows the stationary Nusselt number in every region of the test section as a function of the Reynolds number. The Nusselt numbers shown in this figure are the average of the leading and trailing Nusselt numbers. The stationary smooth tube Nusselt number for fully developed flow (Dittus/Boelter correlation) is also shown. In region 1, the effect of the strong entrance is clearly seen. At the highest Reynolds number is approximately 275. As the flow proceeds through the channel, the boundary layer grows and the heat transfer levels begin to decrease. This is clearly seen in **Figure 43**, for a fixed Reynolds number, the Nusselt number decreases in the streamwise direction from region 1 to region 4. In the first pass, near the turn region, the heat transfer levels are similar as seen in **Figure 43**. In the second pass, it is evident that the strong turn effect is dominating the heat transfer. Tip cap 7 and regions 7 through 9 all show nearly identical Nusselt number values for a given Reynolds number. At the highest Reynolds number,

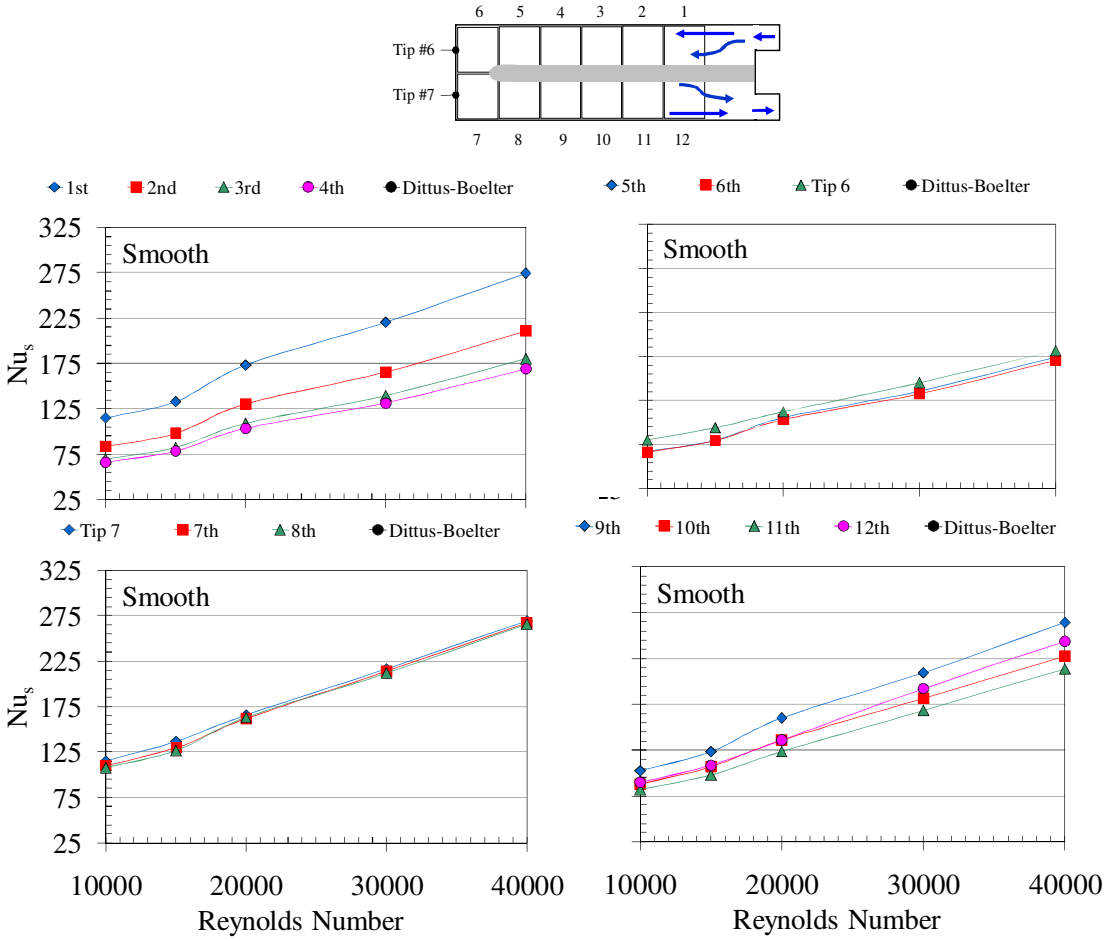

Figure 43: Stationary Nusselt numbers in the regions of the 2:1 aspect ratio channel.

the maximum Nusselt number is approximately 260. The heat transfer in region 10 and 11 begins to decrease due to the dissipation of the turn vortices and boundary layer growth as see in **Figure 43**. However, in region 12, the heat transfer once again increases due to the exit effect.

As previously shown, the entrance configuration of the 2:1 aspect ratio channel significantly enhances the heat transfer. This is especially the case in the regions near the entrance because the entry length is short. In the current study, the flow does not achieve the fully-developed flow behavior in the first passage (L/D_h=12). **Figure 44** shows the Nu_s/Nu_o ratio comparisons inside a smooth stationary channel from several open literature sources. Only the first few data points of the current study in the first passage were compared to eliminate the effects from the 180° turn. In the re-directed sharp bend entrance for 1:4 aspect ratio channel, the cooling air enters a plenum and then is re-directed into the 1:4 test region. The flow in that channel did not achieve the fully-developed flow behavior in the first passage either. The passage is short with a channel length to hydraulic diameter ratio of L/D_h=7.6. The sharp-bend geometry presented by Kays et al. [32] in the circular tube and the redirection geometry by Wright et al. [20] in the 4:1 channel clearly show that the entrance geometry significantly augments the Nu_s/Nu_o ratio, especially when x/D_h is small. The fully-developed flow inside the AR=2:1 stationary channel by Fu et al. [14] shows the lowest Nu_s/Nu_o ratio as expected. As x/D_h increases, the Nu_s/Nu_o ratios of the five curves converge along the streamwise direction.

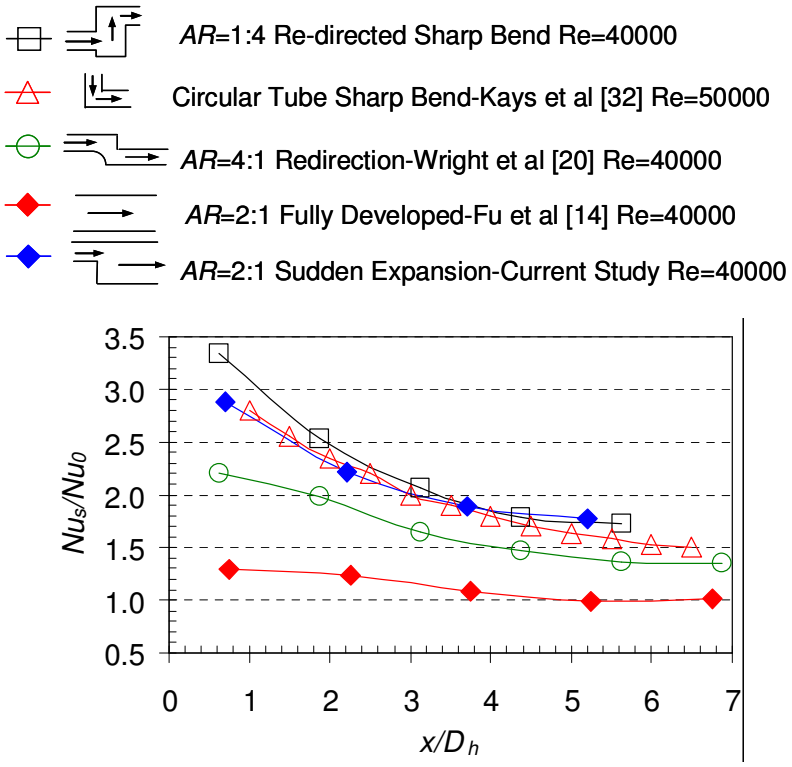

Figure 44: Comparison of stationary streamwise averaged Nu_s/Nu_o ratios for different entrance geometries and the 2:1 channel.

4.2.1.2 *Rotating Streamwise Nusselt Number Ratios*

Figure 45 and **Figure 46** show the streamwise Nu/Nu_o ratio distribution in the 2:1 channel under stationary and rotating conditions for Re=10K to 40K. In general, in the first passage, the heat transfer enhancement is high at the inlet (small x/D_h) and then begins to decrease in the streamwise direction due to the boundary layer growth. For Re=10K, increasing the rotational speed from 0 to 400 rpm reduces the Nu/Nu_o ratio by about 15% on the leading surface for x/D_h <5.2. In the turn region (7.5 < x/D_h *<11.4) the Nu/Nu_o ratios increase greatly with rotation and a maximum value Nu/Nu_o=4.4 is reached at x/D_h = 10.6. In the second pass, the heat transfer enhancement on the leading surface increases with rotation over the stationary case. The trailing surface at Re=10K in the first pass shows great heat transfer enhancement with increasing rotational speed. A maximum Nu/Nu_o ratio of 4.5 is reached at x/D_h = 8.3 and a rotational speed of 400 rpm. In the second pass, rotation causes the heat transfer enhancement on the trailing surface to decrease below the stationary case. At x/D_h = 18.2 and a rotational speed of 400 rpm, the Nu/Nu_o ratio is 35% lower than the stationary case. This trend is different from the AR=1:4 channel in which rotation increased the heat transfer enhancement on the trailing surface in the second pass. From **Figure 45 and Figure 46**, it is seen that as the Reynolds number is increased from 10K to 40K the effect of rotational speed decreases on both the leading surface and trailing surfaces in both passes.

Figure 47 shows the Nu/Nu_o ratios on tip cap 6 and 7 as a function of the Reynolds number at all rotational speeds tested. Rotating trends are similar for both tip cap 6 and 7. On tip cap 6, the highest Nu/Nu_o ratio is approximately 4.5 at a rotational